universität wien

Dissertation

Engineered Nanoparticles in the Environment

Behavior of Titanium Dioxide in Aquatic Systems

Verfasserin

Stephanie Ottofülling, M.Sc.

angestrebter akademischer Grad

Doktor der Naturwissenschaften (Dr. rer. nat.)

Wien, im August 2010

Studienkennzahl lt. Studienblatt: A 091 431

Dissertationsgebiet lt. Studienblatt: Geologie

Betreuer: Prof. Dr. Thilo Hofmann

1. Gutachter: Prof. Dr. M. F. Hochella Jr.
2. Gutachter: Dr. Jürgen Thieme

Wer, wenn nicht wir, wann, wenn nicht jetzt ?

Jeanne d'Arc

Acknowledgment

I would like to thank Thilo Hofmann for the opportunity to learn, work and write in his group. You challenged me a lot and asked questions when you knew I had no answer and pushed me further than I thought I could go. You also gave me the chance to proof my skills in organizing two terrific conferences at the University of Vienna. Thank you for your confidence!

Frank von der Kammer for his never ending ideas, technical and scientific knowledge and enthusiasm in everything he does. You were always positive and creative about my work. Thank you for all discussions, encouragement, guidance in the laboratory and patience!

I would like to thank Tom Battin who encouraged me many times. The laboratory work in the WasserCluster Lunz was most efficient and professional. Despite hard work I had a lot of fun and a terrific time in 'Lunz am See'. I would like to thank the WasserCluster Lunz team for fantastic support.

Thank to Anders Baun und Nanna Hartmann for the opportunity to learn about toxicity of TiO_2 and to contribute to their research.

Thanks to Bernhard Keppler for the opportunity to learn about clinical applications of nanoparticles and the financial support from the University of Vienna FSP project: *'Development and Optimization of Multifunctional Nanoparticles for Clinical Molecular Imaging and Therapy'*.

I would like to thank the Environmental Geosciences Team for support in the laboratory, solving daily life crisis and overcoming bureaucracy. Thank you Wilfried and Petra Körner, Andreas Doll, Wolfgang Obermaier and Sabine Kranzl.

Also I would like to thank my friends and colleagues Susanne Laumann, Christian Müllegger and Lisa Neubauer. They had a universal map when I was lost, gave hope when I was stranded and enriched my days when I was most hungry.

Abstract

Engineered nanomaterials and, in particular, engineered nanoparticles, are already being released into the environment. The growing production and application of engineered nanoparticles will inevitably lead to an increasing discharge into the environment. Nanoparticles can be indirectly emitted into the environment by passing trough wastewater treatment plants or can be directly introduced into the environment by emission to soil and aquatic systems. The release of nanoparticles into the environment raises concerns about contamination, both by the nanoparticles themselves and also by the co-transport of contaminants into surface water and groundwater. Engineered nanoparticles can pose a toxicological risk to organisms within the aquatic environment. It is generally accepted that understanding nanoparticle behavior in the aquatic environment is crucial to assessing the related risks. A full characterization is therefore needed in order to understand and compare results from toxicological tests as well as to elucidate their impact and fate within natural systems.

The potential effects of nanoparticles with respect to their environmental behavior can then be identified and minimized before they cause risk to humans, and also to biota. The behavior and transport of nanoparticles within aqueous systems are controlled by their surface properties as well as by the chemistry of the particular aqueous system involved. Factors such as ionic strength, pH, or the presence of organic matter, will cause either aggregation or stabilization of nanoparticles. Stable nanoparticles have the potential to be transported further than aggregated particles, which are more likely to settle and be retained in the sediment. Depending on the stability the potentially effected organisms such as pelagic species in the water column or the benthic species in the sediment will change.

The objective of this thesis is to describe the behavior of nanoparticles, both in synthetic water and in natural water. Commercially available titanium dioxide, as nano-TiO_2 dry powder, is used as a model compound. The transport behavior of TiO_2 nanoparticles is extrapolated from experiments in an open water-channel microcosm experiment. The toxicological effects of nano-TiO_2 on pelagic species such as algae, and on floating microorganisms and organisms embedded in biofilm, are also tested under near-natural conditions. The thesis therefore summarizes the environmental behavior, transport, and toxicity of a model nanoparticle, namely TiO_2.

Kurzfassung

Die steigende Produktion und Anwendung technischer Nanomaterialen, im speziellen Nanopartikel, erhöht das Risiko einer Emission in die Umwelt. Nanopartikel können indirekt in die Umwelt emittiert werden, indem sie Wasseraufbereitungsanlagen passieren oder über direkte Emission in terrestrische oder aquatische Systeme gelangen. Nanopartikel stellen eine potentielle toxikologische Gefährdung für die Umwelt dar. Einerseits können diese selbst toxische Eigenschaften aufweisen und andererseits können andere Kontaminanten an Nanopartikel gebunden sein. Für eine Risikoabschätzung ist es unerläßlich das Verhalten von Nanopartikeln zu verstehen. Eine umfassende Charakterisierung ist daher notwendig, um Ergebnisse von toxikologischen Versuchen auszuwerten und die Auswirkungen und den Verbleib von Nanopartikeln in der Umwelt zu erfassen. Mögliche negative Effekte für Menschen und andere Lebewesen können so identifiziert und minimiert werden.

Das Verhalten und der Transport von Nanopartikel wird vor allem durch deren Oberflächeneigenschaften sowie die umgebende Wasserchemie geprägt. Faktoren wie Ionenstärke, pH und das Vorkommen organischer Substanzen führen entweder zu Aggregation oder erhöhter Stabilität der Nanopartikel. Aggregierte Partikel sinken zu Boden, wo sie im Sediment akkumulieren können, während stabilisierte Nanopartikel in der Wassersäule verbleiben und somit über weitere Distanzen transportiert werden. Davon ausgehend sind entweder pelagische oder benthale Organismen von den toxikologischen Effekten betroffen.

Das Ziel dieser Doktorarbeit ist das Verhalten von technisch hergestellten Nanopartikeln in synthetischen und natürlichen Gewässern zu untersuchen. Dafür wurde kommerziell erhältliches Titandioxid (TiO_2) als Modellsubstanz verwendet. Dessen Transportverhalten wurde ausgehend von Experimenten in offenen Fließrinnen im Mikrokosmen-Maßstab extrapoliert. Die toxikologischen Effekte auf pelagische Spezies, wie zum Beispiel Algen und schwebende Mikroorganismen sowie Organismen im Biofilm wurden unter naturnahen Bedingungen getestet. Die vorliegende Arbeit faßt das Umweltverhalten, den Transport und die Toxikologie von TiO_2 Nanopartikeln zusammen.

Contribution to the Studies

Study I

Assessment of the physico-chemical behavior of titanium dioxide nanoparticles in aquatic environments using multi-dimensional parameter testing

F. v.d. Kammer, S. Ottofuelling, T. Hofmann

Environmental Pollution Volume (2010), in press (doi:10.1016/j.envpol.2010.05.007)

F. v.d. Kammer	30%	Concept; discussion of results; data interpretation; manuscript preparation
S. Ottofuelling	60%	Concept; laboratory work; data analysis; data interpretation; manuscript preparation
T. Hofmann	10%	Concept; discussion of results; manuscript preparation

Study II

Information on the stability of TiO_2 in synthetic and natural waters

S. Ottofuelling, F. v.d. Kammer, T. Hofmann

To be submitted to Environmental Science & Technology (2010)

S. Ottofuelling	80%	Concept; laboratory work; data analysis; data interpretation; manuscript preparation
F. v.d. Kammer	10%	Concept; discussion of results; manuscripts preparation
T. Hofmann	10%	Concept; discussion of results; manuscript preparation

Study III

Nanostructured TiO_2: Transport behavior and effects on aquatic microbial communities under environmental conditions

T. J. Battin, F. v.d. Kammer, A. Weilhartner, S. Ottofuelling, T. Hofmann

Environmental Science & Technology 43 (2009), 8098-8104

T.J. Battin	15%	Concept; discussion of results; data interpretation; manuscript preparation
F. v.d. Kammer	10%	Discussion of results; manuscript preparation
A. Weilhartner	30%	Concept, Laboratory; data analysis
S. Ottofuelling	30%	Concept; laboratory; data analysis; data interpretation; manuscript preparation
T. Hofmann	15%	Concept; discussion of results; data interpretation, manuscript preparation

Study IV

Algal testing of titanium dioxide nanoparticles - Testing considerations, inhibitory effects and modification of cadmium bioavailability

N.B. Hartmann, F. v.d. Kammer, T. Hofmann, M. Baalousha, S. Ottofuelling, A. Baun

Toxicology 269 (2010), 190-197

N.B. Hartmann	60%	Concept; laboratory; data analysis; data interpretation; discussion of results; manuscript preparation
F. v.d. Kammer	5%	Discussion of results; data interpretation; manuscript preparation
T. Hofmann	5%	Discussion of results; proof reading
M. Baalousha	5%	Laboratory; data analysis; proof reading
S. Ottofuelling	5%	Laboratory; data analysis; discussion of results; proof reading
A. Baun	20%	Concept; discussion of results; manuscript preparation

Study V (appendix)

Preparation of gadolinium chelate coated HSA-lectin nanoparticles for magnetic resonance imaging

A. Kundu, S. Ottofuelling, M. Krssak, F. v.d. Kammer, T. Hofmann, T.H. Helbich, B. Keppler

To be submitted to Journal of Pharmaceutics (2010)

A. Kundu	50%	concept; laboratory syntheses; data analysis, data interpretation; discussion of results; manuscript preparation
S. Ottofuelling	20%	Laboratory; data analysis; discussion of results; proof reading
M. Krssak	10%	data analysis; discussion of results
F. v.d. Kammer	5%	Discussion of results; manuscript preparation
T. Hofmann	5%	Discussion of results; proof reading
T. H. Helbich	5%	Discussion of results; proof reading
B. Keppler	5%	Concept; discussion of results; manuscript preparation

Table of Content

1 General Introduction

1.1 Nanotechnology

By giving a talk entitled "There is plenty of room at the bottom" in 1959 at the California Institute of Technology, Richard Feynman sowed the seeds for a new era in science and technology (*1*). The physicist and Nobel laureate challenged the scientific community by asking "What would the properties of material be if we could really arrange the atoms the way we want them?". The answers have come during the last decades, with the rapid technological development in this sector. Professor Norio Taniguchi (1974) from the Tokyo Science University defined nanotechnology in the following way: "Nano-technology mainly consists of the processing, separation, consolidation, and deformation of materials by one atom or by one molecule" (*2*). In 2004 the Royal Society, together with the Royal Academy of Engineering, expanded this definition as follows: "Nanotechnology is the design, characterization, production and application of structures, devices and systems by controlling their shape and size at the nanometer scale" (*3*).

Small particles, or colloids, have been in the focus of research for some decades (e.g. polymers and natural oxides, organic or clay particles), but it is only in recent years that the sophisticated tools are available to make nanoscale materials and devices visible. Scanning tunneling microscopes (STMs) and atomic force microscopes (AFMs) are two instruments that enable techniques in nanotechnology to be used for the investigation and manipulation of matter on a nanoscale (*4*). There are generally two procedures used in the construction or manipulation of material on a nanoscale, the ‘top-down’ technique or the ‘bottom-up’ technique. The Eigler & Schweizer team (1990) at IBM demonstrated the ‘bottom-up’ technique, which involves the assembly of atoms or molecules to make larger structures (e.g., xenon atoms assembled around a nickel surface) (*5*). ‘Bottom-up’ techniques include chemical synthesis (e.g. cosmetics), self-assembly (displays) and positional assembly. The ‘top-down’ technique comprises lithography (e.g. computer chips) and etching, and cutting or grinding a block of material into smaller entities (e.g. optical mirrors).

1.2 Nanomaterials

1.2.1 Properties and applications

Nanomaterials are defined as particulate matter with at least one dimension less than 100 nm, where one nanometer is equal to one-billionth of a meter (i.e. 10^{-9} m) (*6*). Material that is <100 nm in one dimension and extended in the other two are thin films or surface coatings. Materials that are nanoscale in two dimensions include nanorods, nanowires and nanotubes. Materials that are nanoscale in three dimensions are particles, such as precipitates, colloids and quantum dots. Since colloids are, by definition, particles in the range of 1 nm to 1 µm, nanoparticles can be considered to be a subfraction of colloids (Figure 1) and fundamental knowledge from the classical colloid sciences may also be applicable to research on nanomaterials (*7*). Airborne particles and particulate matter are excluded from our definition for the purpose of this thesis since, in this particular context, only the aquatic (and soil) system is of interest.

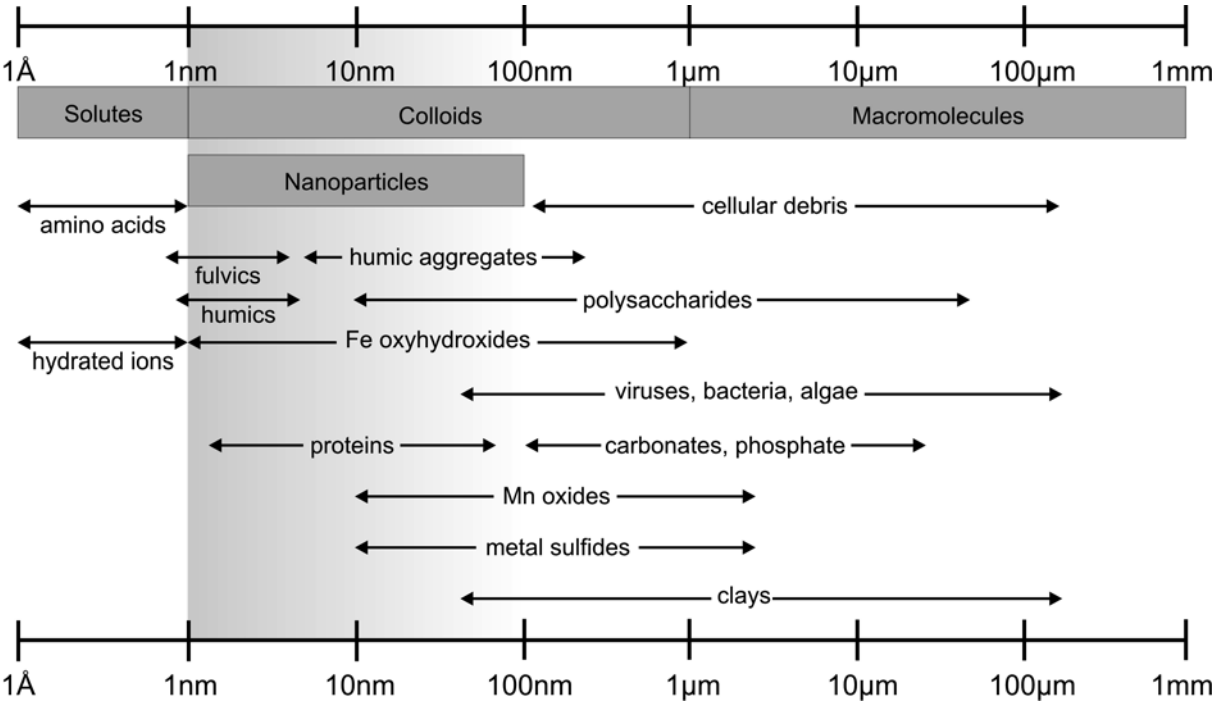

Figure 1. Size domains of various types of environmental colloids and nanoparticles; adapted from (*8-9*).

Nanomaterials are abundant in the environment and can be of either anthropogenic or natural in their origin (*10-11*). Natural nanomaterials are divided into inorganic and organic materials. Examples of inorganic materials are silicates (e.g. clay), kaolinite,

oxides and hydroxides (e.g. Fe-hydroxides), carbonates, phosphates and metal sulfides. Macromolecules such as humic and fulvic acids, polysaccharides and proteins, as well as bio-particles (e.g. bacteria, viruses and fungi) and coal, soot and black carbon are all representatives of organic materials. Anthropogenic nanomaterials are, either intentionally or unintentionally, produced from wear and corrosion, for example from tyres, brakes, catalysts, or from waste and combustion (e.g. soot and fly ash). For our purposes we define nanomaterials as intentionally produced materials and we distinguish between engineered nanoparticles in carbon-based materials, and those in metal and metal oxides or in hybrid structures.

Carbon-based nanoparticles

Fullerenes are molecules with at least 60 atoms of carbon, of which the C_{60} molecule (Buckminsterfullerene) is the most widely studied (*12*). The discovery of C_{60} led to the subsequent discovery of other fullerenes such as carbon nanotubes or CNT (*13*). There are a number of different types of manufactured carbon nanotubes, including single-walled (SWCNT) and multi-walled (MWCNT). SWCNT are made up of graphene sheets rolled-up into cylindrical shapes, while MWCNT are made up of two or more concentric layers (*14*). Carbon nanotubes can also be open or capped. CNTs are synthesized by arc evaporation, pyrolysis, electronic methods and laser ablation, generally followed by purification methods (*15*). Chemical interests have focused in further development of CNTs with the aim of producing stable dispersions of nanoparticles with dimensions of less than 200 nm. (*16-18*). The techniques favored for this include ‘solvent exchange’ including toluene (*19*), ethanol (*20*) or the ‘top-down’ approach involving breaking down aggregates by rigorous stirring (*21*) or ultrasonication (*22*). The relative insolubility of carbon-based nanoparticles and the possibility of producing a variety of materials with different mechanical, thermal, photochemical and electrical properties makes them interesting for biological/medical, electronic and optical applications (*23*). However, engineered carbon nanotubes have close relatives in the natural environment that have formed from polycyclic aromatic hydrocarbons (PAHs) by natural combustion processes, or were brought to earth by comets or asteroids (*24-25*).

Metal nanoparticles

In 1857, Faraday observed a shift in the color of a colloidal gold suspension due to aggregation processes, and although gold had been the subject of chemical investigation for centuries it now came under a renewed focus of scientific investigation. Gold and silver nanoparticles are synthesized either physically (e.g. by laser ablation) or chemically. Chemical methods form Ag and Au aggregates by reducing a metal salt in the presence of a stabilizer (e.g. citrate); the particles then tend to coalesce into large aggregates (*26*). Ag and Au nanoparticles are industrially produced because of their special, size-related, magnetic, optical, and electronic properties (*27*). These nanoparticles, as well as silver ions (Ag^+) or related silver species, are known to have significant antibacterial properties and are hence used in medical applications and various consumer products such as disinfectant sprays and textiles (*28*). Among other important metal nanoparticles zero-valent iron has attracted attention in the scientific community because it has the promising ability to transform or sorb common environmental contaminants, including chlorinated organic solvents, nitro aromatic compounds, organic dyes and some inorganic compounds (*29*).

Metal oxide nanoparticles

Bulk metal oxide materials have been extensively produced for many years. Only recently has the nanoparticulate form of this material been introduced into consumer products (*11*). Among others (e.g. ZnO, CeO_2 and SiO_2), nano-TiO_2 is manufactured for application in cosmetics, food, pigments and photocatalysis (*30*). Titanium dioxide occurs naturally in three types of crystal structure: as rutile, anatase, or brookite. All three are expressed with the chemical formula TiO_2 although they are significantly different in their structure; rutile and anatase are considered the most important. The industrial production of TiO_2 involves reduction by sulfur or chloride. The size, shape and crystalline modification are dependent on the desired application and the production process (e.g. Evonik, TiO_2 P25 and Sachtleben, TiO_2 Hombikat UV-100). TiO_2 is generally considered to be an excellent band-gap semiconductor. By irradiation with light of $\leq$413 nm (rutile) and $\leq$388 nm (anatase) the valence band electrons move up to the conduction band (Figure 2). In the case of a semiconductor such as TiO_2 electrons cannot jump to the conduction band unless they are excited by external energy (e.g. by light). The photoexcited state of a semiconductor is

generally unstable, but this is not the case for TiO_2 which makes the material an excellent photocatalyst (*31*). Despite the fact that rutile can also absorb rays close to the visible light range, anatase exhibits even higher photocatalytic activity (*32*). Even though certain nanoparticles have positive side-effects, including the potential to remediate contaminated groundwater (e.g. zero-valent iron) and disinfect or sterilize drinking water (e.g. TiO_2), their fate, behavior, and potential risk to humans and the environment has not yet been adequately investigated (*33*).

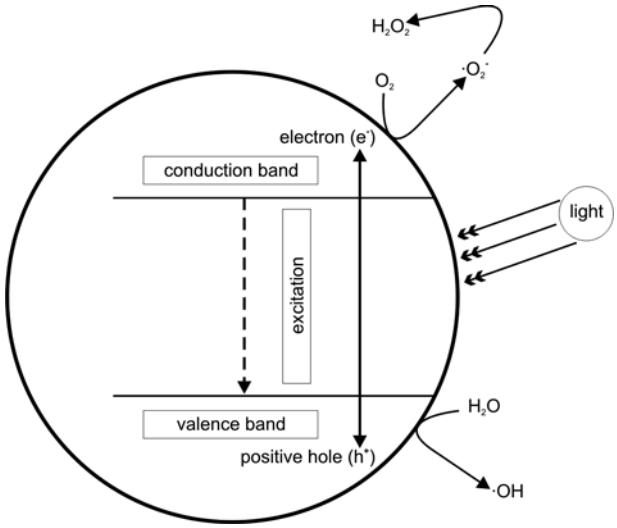

Figure 2. Electron structure, reduction and oxidation mechanism of TiO_2. When TiO_2 is exposed to light, electrons (e^-) and positive holes (h^+) are formed inside the crystal. Positive holes cause oxidative reaction and hydroxyl radical are formed which have strong oxidative power. Electrons form oxygen which is associated with photocatalytic reduction.

1.2.2 Environmental relevance

Nanomaterials are abundant in the environment as airborne particles, as well making up a considerable proportion of the solid matter in the lithosphere (both oceanic and continental) (*10; 34*). Murr et al. even found natural nanocrystals in melt water from a 10,000 year-old ice core (*35*). In aquatic systems the amount of total suspended solids (TSS) is usually less than 20 mg L^{-1}, but there are exceptions, especially after heavy rainfall when rivers carry larger quantities of particulate matter. At present concentrations of engineered nanoparticles in the environment are low but their increasing production and use means that environmental exposure to these particles is likely to increase in the future (*36-37*). Nanoparticles are likely to enter the environment as a result of both unintentional and intentional release, with the latter

including their use in soil remediation (*38*). Unintentional release comprises atmospheric emission and soil or liquid waste streams from production facilities (*39*). Depending on their dispersion state, nanoparticles may be transported within and between the different environmental compartments (Figure 3).

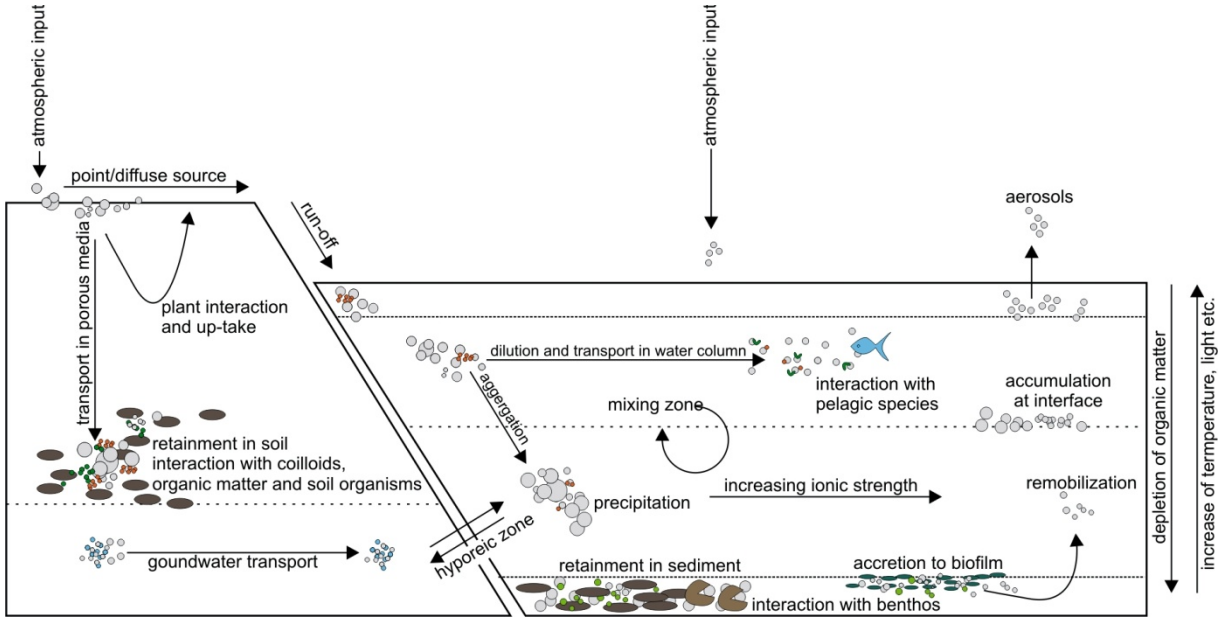

Figure 3. Schematic diagram of the possible fate of nanoparticles in the environment, exchange between compartments and potential interaction with organisms and solids.

Within the soil plants can take up nanoparticles through their roots (*40*) or they can be transported into the groundwater (*41*). From the groundwater particles can then pass through the hyporheic zone and then enter either into fresh water or into the sea. Depending on their dispersion state nanoparticles may remain in the water column, increasing their transportation distances and rates. Aggregation leads to settling onto the sediment floor and benthic organisms are therefore the key receptors for nanoparticles. The sediment is not an ultimate sink, however, and nanoparticles can be disaggregated, resuspended and remobilized (*8*). Within the different environmental compartments nanoparticles may interact with other engineered or natural particles, with contaminants (*42-43*), and with organisms (*40; 44*). The extent to which nanoparticles are mobile or interact with solids, sediments, and organisms is dependent on their behavior within aquatic systems.

1.2.3 Behavior of nanoparticles

The behavior of engineered nanoparticles within an aquatic environment is rather complex and involves several processes that may influence their dispersion and aggregation (*8; 45*). The dispersion of nanoparticles is controlled by their surface properties and the hydrochemistry that they encounter. Dispersion is one phase (solid) homogenously distributed in another (liquid) and therefore, by definition, dispersion is distinct from the process of dissolution (*46*). Particles diffuse during dispersion and will collide with other particles, potentially resulting in aggregation with particles of the same type (homoaggregation) or with other solid matter (heteroaggregation). Single particles are often referred to as primary particles. Agglomerates are primary particles held together by weak van der Waals forces, while aggregates are particles held together by strong chemical bonds (Figure 4).

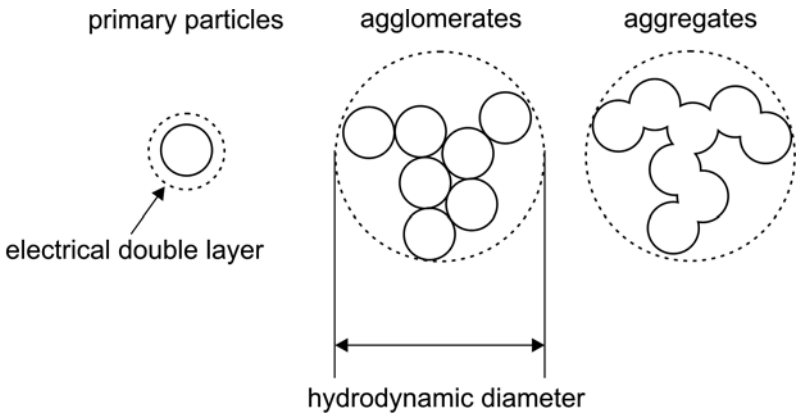

Figure 4. The state of dispersed nanoparticles in aqueous media. The electrical double layer thickness depends on the solution chemistry. The hydrodynamic diameter is depending on the fractal dimension of the particles and is important for size measurements based on light scattering; adapted from (*47*).

Particle-particle collision is controlled by three processes: Brownian motion (perikinetic aggregation), shear flow (orthokinetic aggregation) and differential settling due to differences in size, shape and density of the particles (*48*). The collision rate is dependant on the particle size and the homogeneity of the dispersion; monodisperions are more stable than polydispersions. Furthermore, Brownian motion, temperature and the particle number concentration determine the frequency of particle-particle collisions (*49*). Stabilizing effects can also occur within a colloidal system, as a result of forces between the particles. These forces are described as Borne repulsion, diffuse double layer potential, and van der Waals attraction, and are

taken into account in the extended DLVO theory developed by Derjaguin, Landau, Verwey and Overbeck (*46*). The DLVO theory is however limited by factors such as particle shape, charge heterogeneity, and surface roughness (*50-51*). Van der Waals forces are always attractive, whereas the electrostatic double layer can have either a net negative or a net positive charge, generally resulting in repulsion. A simplified potential energy diagram for the interaction of particles is depicted in Figure 5.

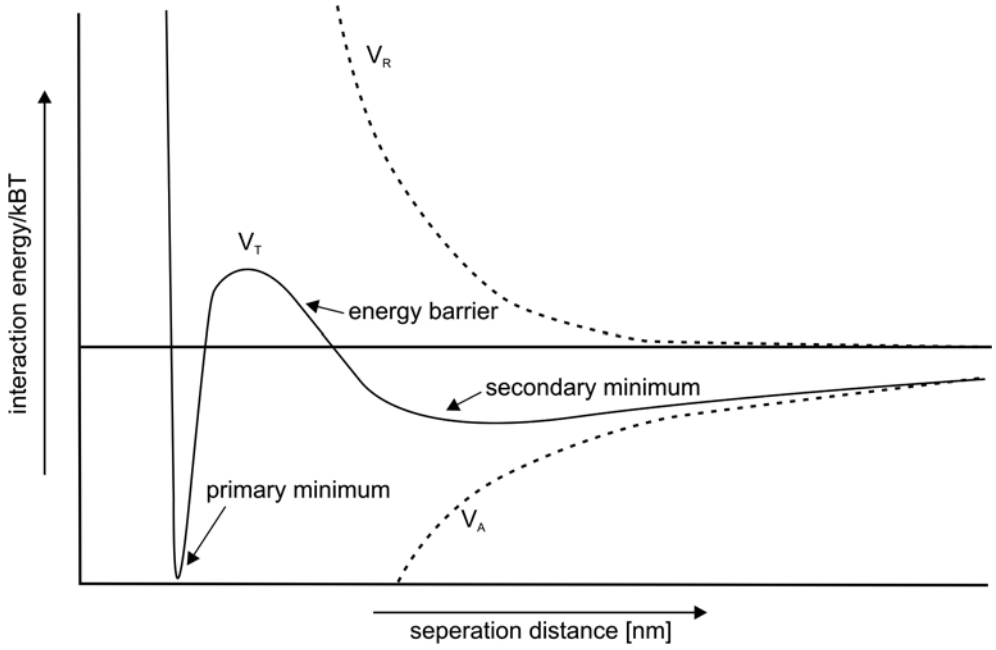

Figure 5. Simplified graph of the DLVO interaction energies and the resulting sum function (V_T). The repulsive forces (V_R) are working against the attractive van der Waals forces (V_A). Particle-particle attachment is achieved in wither the primary or secondary minimum; adapted from (*8*).

By adding salts to the dispersion the thickness and length of the double layer will be reduced (*52*). The valence of an ion determines the compression efficiency where bi- or trivalent ions effectively screen the surface charge of the particle or specifically sorb to the particle's surface. The addition of salts and compression of the double layer promote the attachment efficiency because attractive forces (van der Waals, hydrophobic, and electrostatic interaction) overcome the repulsive forces. Particles can also be sterically stabilized by, for example, the binding of molecules and polymers, which can even occur at high ionic strengths (*53*). The opposite effect can be achieved through the bridging effects of multi-charged polymer reagents or multiply charged ions (*54*). The surface charge of a particle is difficult to measure directly and therefore scientists measure the electrophoretic mobility, that is, the ratio

of the velocity of particles to the field strength. The surface charge can be deduced from the electrophoretic mobility measurement by calculating the zeta potential described by the Smoluchowski equation:

$$\zeta = \frac{4\pi\eta}{\varepsilon} * U \quad with\ U = \frac{v}{VL} \qquad \textbf{Equation 1}$$

in which ζ is the zeta potential, η is the viscosity of the solution, ε is the dielectric constant, *U* is the electrophoretic mobility for particle speed *v*, *V* is the voltage, and *L* is the distance between the electrodes. The zeta potential is therefore the voltage reflecting the effects of surface charge and flow dynamics close to the surface (Figure 6).

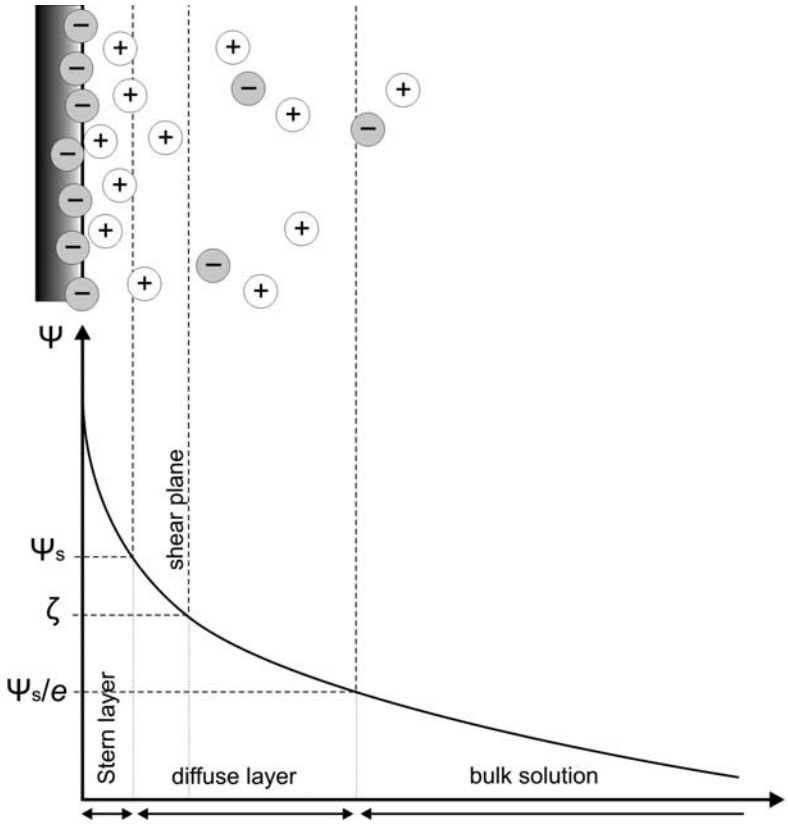

Figure 6. Schematic diagram of the Stern-Gouy-Chapman model for the electrical double layer on the surface of particles. Abbreviation: zeta potential (ζ), electrostatic potential (Ψ), electrostatic potential at the Stern layer (Ψs), Euler's number (*e*) and the x-axis describing the distance from the surface. The shear plane is the distance of from the surface where ions and molecules are mobile, the potential at the shear plane is measured as the zeta potential. The diffusion layer is a layer of water adjacent to the surface and the bulk solution is the surrounding media (e.g. sea water, freshwater); adapted from (*55*).

The stability of nanoparticles in aqueous systems is also regulated by the pH of the dispersion. Particles such as clay minerals have a net negative charge over a wide pH range (*56*). Other particles, such as many oxides, have a positive charge at an acidic pH and a negative charge at a basic pH (*57-58*). The point of zero charge (pzc) is given when the net surface charge density is equal zero and the point of zero net proton charge (pznpc) is given when the pzc is established only by H^+ and OH^- binding on the particle surface. In the presence of ions the isoelectric point (iep) is referred to situation when the surfaces of solids carry no net electrical charge. This is the condition where particles do not move in an electric field. The iep is also affected by, for example, surface-sorbed organic or inorganic matter (*56; 59*). By varying the substances in the aqueous dispersion (e.g., the humic acids, carbonates, and mono- or divalent ions), titration provides information on the stability of nanoparticles in rather complex media. Defining the iep therefore has practical implications, such as determining the dispersion and aggregation state of nanoparticles in natural water. Additionally, the point of zero salt effect (pzse) is given when the surface charge is not affected by a change in concentration of an 'inert' background electrolyte (*60*).

1.2.4 Transport of nanoparticles

The dispersion state determines the mobility and transportation range of nanoparticles in the aquatic environment. The travel distance is also governed by the hydrology of the system and the morphology of the sediment surface. Aggregates will deposited as a results of gravitational settling or interaction with the existing sediments, while the stable fraction of particles will remain in the water column and travel downstream. However, it has been shown that a variety of suspended particles are transferred across the sediment-water interface (*61*). This process is called hyporheic exchange and leads to suspended particles being deposited in the sediment, and filtration and settling mechanisms result in the retention of particles in the subsurface (*62*). The hyporheic exchange can be influenced by interactions with surface-attached microbial communities, generally referred to as biofilms (*63*). Biofilms are ubiquitous in the aquatic environment and consists of microorganisms enclosed by a heterogeneous matrix of extracellular polymeric substances (EPS) composed of polysaccharides, lipids, proteins and nucleic acids (*64*). The chemistry and morphology of biofilms promote the deposition and retention of nanoparticles

and colloids (*65*). As a result the biofilms act as environmental reservoirs of nanoparticles from which they can be subsequently released back into the water column together with biofilm detaching from the substrate surface. This has major implications for organisms and for the receiving surface-waters downstream from such a nanoparticle source (*66*). If nanoparticles are not retained in the substrate, they are predicted to travel extremely long distances in river water. However, their stability can be drastically altered if the water chemistry changes. For example, sea water mixing with river water has been shown to remove almost all inorganic nanoparticles from the suspended load as a result of salt-induced aggregation (*67*). In the aquatic environment nanoparticles can also undergo modification and degradation processes that will alter their surfaces, mobility and toxicity (*33*).

1.2.5 Toxicity of nanoparticles

The environment contains many natural nanoscale colloids and, since they have existed for millions of years (*10*), organisms must have adapted to live in the presence of these materials. However, nanoparticles from anthropogenic sources present a potential hazard to humans and to the environment (*55*), and it is generally accepted that nanoparticles can, in theory, pose risks to biota as well as humans. An example of the damage that can be caused by nonoparticles is provided by the lung damage that results from the inhalation of asbestos fibers, as shown by Maynard et al. 2004 and Oberdörster et al. 1992 (*68-69*). The unique physico-chemical properties and reactivities of engineered nanoparticles as opposed to natural nanoparticles, are considered to be potentially very harmful. However, recent studies have shown that the toxic effects of nanoparticles are related to their size, shape, surface area and surface chemistry (*70-72*). Their unique properties make engineered nanoparticles powerful adsorbents. As with black carbon (*73*), multiwalled carbon nanotubes adsorb a wide variety of organic compounds such as pyrene, phenanthrene and naphthalene (*74*). The interaction of nanoparticles with toxic compounds can both amplify and reduce their toxicity by carrier effects (*75-76*), or by decreasing their bioavailability through complexation of metals, for example Cd^{2+} complexation on the TiO_2 surface (*77*).

1.3 Research Objectives

The objectives of this study were, firstly, to describe the behavior of nano-TiO_2 as a model compound in synthetic water (study 1). The driving parameters causing stabilization or promoting aggregation were identified by varying the water chemical situation the nanoparticles encounter. We chose an experimental approach of low complexity; meaning particles were allowed to settle within a defined time and varied the pH from 4 to 8 at various ionic strength or organic matter content. The graphical representation as interpolated contour plots allowed an interpretation extending the experimental limitations.

Secondly, we extended the previously explained simplified approach to a more complex system. In the framework of a second study (study 2) we proposed the hypothesis to predict the behavior of nanoparticles in natural water by investigating their behavior in a large set of synthetic and natural water. We therefore introduced the nano-TiO_2 in synthetic well defined water. Further, we suspended nano-TiO_2 in natural water classified according to their water chemistry. The experimental approach remained as described in the first study. The information gained from this second study complemented the understanding of nanoparticle behavior in aqueous systems and further allowed prediction and generalization of nanoparticle behavior in the aquatic environment.

The third objective of this study was to investigate the transport behavior of TiO_2 nanoparticles in natural water. Therefore we suspended nano-TiO_2 in already well described natural water (study 2) and monitored the deposition rate in a microcosm flume experiment (study 3). The deposition was strongly depending on the presence of biofilm which was naturally grown in the flumes. This study was in cooperation with T. Battin's group, who in detail investigated the toxicological effects of the nano-TiO_2 to floating microorganisms in the pelagic zone and microorganisms embedded in protective biofilm matrix (study 3).

The fourth objective of this study was to elucidate the size dependent toxicological effects of various TiO_2 nanoparticles. The nanoparticle size is determined by the algae growth media and the presence of algae themselves. A. Baun's group in detail

investigated the inhibitory effects of various TiO_2 nanoparticles on algae and the bioavailability of cadmium in the presence of TiO_2 nanoparticles (study 4).

In another study (study 5, appendix) we tested nanoparticles behavior in media relevant for medical applications. We tested the possible application of a nanoparticle (gadolinium complex) in medical applications (magnetic resonance therapy). We performed a full characterization for each synthesis step of the nano-Gd complexation in order to identify the most adequate complex which is defined by the relaxation time relevant for the medical application.

2 The Stability of Titanium Dioxide in Synthetic Water

Assessment of the physico-chemical behavior of titanium dioxide nanoparticles in aquatic environments using multi-dimensional parameter testing

F. v.d. Kammer, S. Ottofuelling, T. Hofmann

2.1 Abstract

Assessment of the behavior and fate of engineered nanoparticles (ENPs) in natural aquatic media is crucial for the identification of environmentally critical properties of the ENPs. Here we present a methodology for testing the dispersion stability, zeta potential and particle size of engineered nanoparticles as a function of pH and water composition. The results obtained from already widely used titanium dioxide nanoparticles (Evonik P25 and Hombikat UV-100) serve as a proof-of-concept for the proposed testing scheme. In most cases the behavior of the particles in the tested settings follows the expectations derived from classical DLVO theory for metal oxide particles with variable charge and an isoelectric point at around pH 5, but deviations also occur. Regardless of a 5-fold difference in BET specific surface area particles composed of the same core material behave in an overall comparable manner. The presented methodology can act as a basis for the development of standardized methods for comparing the behavior of different nanoparticles within aquatic systems.

2.2 Introduction

The current and future production and use of engineered nanoparticles (ENPs) results in their release into the environment, and ENPs such as titanium dioxide have already been identified in surface run-off and waste waters (*36-37; 78*). There is also clear evidence that ENPs have adverse effects on algae, fish, and higher organisms (*72; 79-80*), as well as on human health (*81-82*). Even at low concentrations TiO_2 nanoparticles and their aggregates can compromise microorganisms in natural aquatic systems (*83*). The relevance of toxic effects which were identified in test

systems will however scale with the future real world concentrations and accumulation rates of ENPs in the environment. In this respect the fate and behavior of ENPs in the environment, and especially in the aquatic environment, are important factors determining the distribution of ENPs between different environmental compartments, their appearance and concentration. Whether an insoluble ENP accumulates in river sediments close to the outlet of waste-water treatment plant, or ends up in soil that has been fertilized with sewage sludge from that plant, or resists attachment and travels long distances to finally reach the open ocean, is mainly controlled by the tendency of this particle to aggregate or attach to other surfaces. Due to the substantial absence of analytical methodology for the quantification of ENPs in environmental media, reports on real environmental concentrations of ENPs are still rare (*36-37; 84*). As an alternative, the development of environmental exposure models enables us to at least assess realistic concentration ranges of ENP in environmental media. These models are making rapid progress but there is still a critical lack of knowledge concerning how ENPs will behave in aquatic media and during transition from one model compartment to another (e.g. from waste-water to surface waters) (*78; 85-86*).

It can be anticipated from investigations on natural colloids that the future environmental concentrations and the accumulation rates of ENPs in soil, sediment and biota depend on a multitude of processes, most of which are currently only partially understood or missing critical information such as, for example, their release from consumer products (*42; 85; 87*). Similar to colloids and nanoparticles of natural origin, and apart from the mere dissolution of physically non-persistent particles, it can be expected that aggregation, attachment to suspended particulate matter, settling and deposition in sediments, are the major processes limiting the mobility of ENPs in natural waters (*8; 55; 88*). These processes also determine which organisms will be most exposed to the ENPs. For example fast aggregation under freshwater conditions will result in exposure of benthic, rather than pelagic organisms, while steric stabilization may allow the ENPs to even cross the estuarine mixing zone, in which case exposure of marine organisms then needs to be considered.

Aggregation (or dispersion stability) is controlled by the structure, composition and surface chemistry of the particles on one hand and the water chemistry i.e. pH,

concentration of ions, redox chemistry, type and concentration of natural organic matter (NOM), and temperature, on the other hand (*89-91*). Particularly in natural waters, the presence of calcium as a divalent cation and NOM can have a significant effect on the aggregation of both natural colloids (*56*) and ENPs (*53; 92-93*) in aquatic systems. From current literature different approaches to elucidate the behavior of ENPs in natural waters can be identified. Overall the studies try to either reassemble complex natural conditions as good as possible or perform experiments of highly reduced complexity to gain process understanding. The first approach is represented by the use of test media commonly applied in toxicological testing, near-natural synthetic waters or real waters from sources representative of a certain type of surface water (*90; 94*). The second approach is represented by mechanistic studies which are conducted in ultrapure water containing only a single, or at the most two, components at any one time (i.e. NaCl, $CaCl_2$, NOM or Na_2HPO_4). With a comparably small set of different hydrochemical conditions these studies are aiming to gain quantitative data and identify factors controlling the aggregation process (*89; 95-96*).

There are also two different approaches to reporting the characteristics of ENPs in aquatic media. On one hand there is investigation of the dynamic (kinetic) of the aggregation process by (1) determining quantitative aggregation rate constants as doublet formation rates (*97*), (2) determining coagulation rate constants (*56*), (3) determining particle growth rate constants (*98*), (4) measuring the evolution of particles sizes or size distributions over time (*89; 92*) or (5) determining the sedimentation of ENPs due to aggregation as a function of the transparency of the supernatant over time (*92*). Approaches (1) to (3) provide quantitative and universal parameters such as the critical coagulation concentration (CCC), and (5) can, in principle, provide sedimentation rate constants, but these are only valid for the individual test set-ups. On the other hand are studies that concentrate on the particle sizes or size distributions and ζ-potentials/electrophoretic mobilities, obtained under different hydrochemical conditions after a defined reaction period (*16; 95-96; 99*).

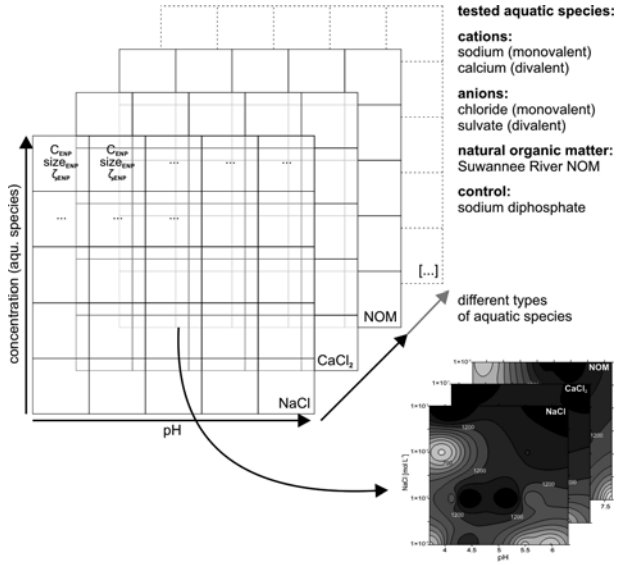

Figure 7. Concept of the multi-dimensional test matrix as employed in the present study.

While the studies employing near-natural or real surface waters are highly relevant and may be closest to reality, they are only valid for the exact system tested. Since the composition of natural waters show seasonal and local variations the results will not be generally transferable to other conditions and rarely allow detailed understanding of the underlying processes. On the other hand, mechanistic studies performed under simplified conditions are valuable for investigating the underlying processes, but are only valid for a limited set of hydrochemical conditions and are hence not applicable to most natural waters. To complement the existing studies a test system was designed (Figure 7 and Figure 8) that covers a broad but realistic range of different water compositions and pH conditions, while still offering insight into the processes taking place.

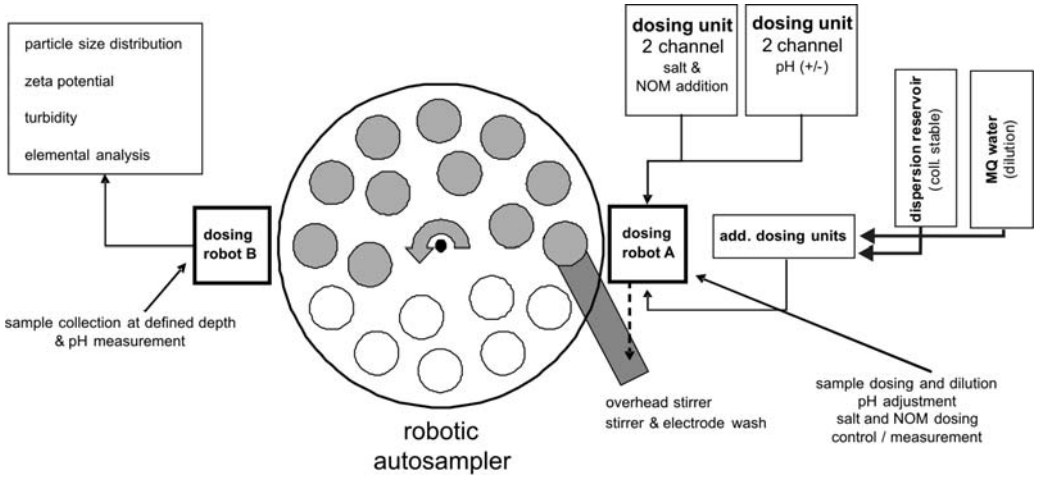

Figure 8. Graphical representation of the autotitrator set-up.

In the experiment an environmentally relevant electrolyte (NaCl, $CaCl_2$, Na_2SO_4) or NOM is dosed to dispersions of the ENPs and the pH adjusted to different levels between 4 and 8. The dispersion stability of the ENPs is then assessed by a classical sedimentation method where the transmittance of the supernatant serves as a criterion for the non-settled particle concentration (Figure 9) (*46*).

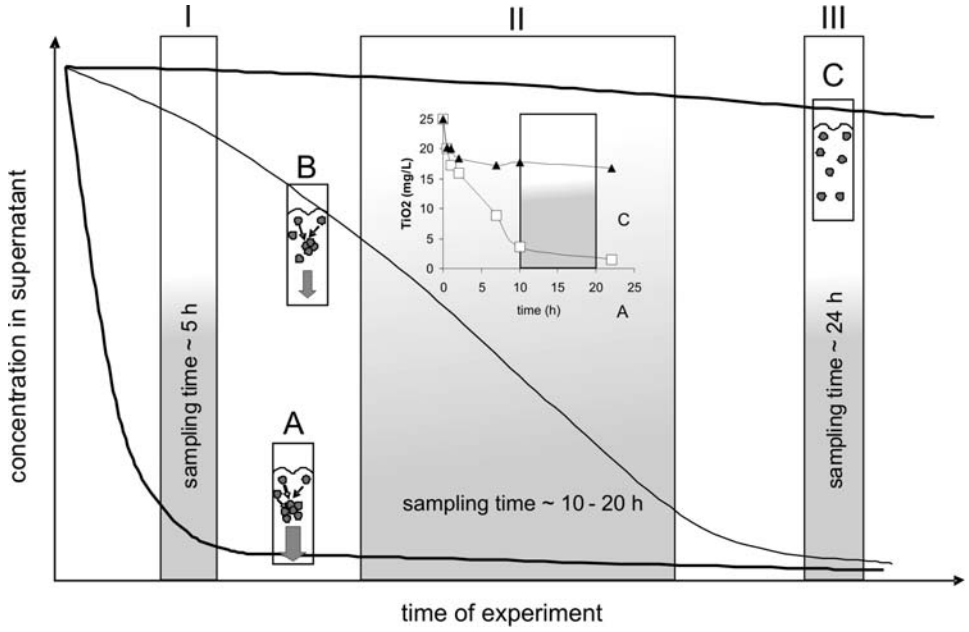

Figure 9. Graphical representation on how the reaction period was selected for the experiments. The inset in region II shows data determined for P25 in Milli-Q water at pH 4 (black pyramids) and 100 mmol L^{-1} NaCl solution at pH 4 (open squares), representing stable and unstable conditions respectively. The reaction period (sampling time) should be situated after the fast aggregation reaction has leveled out and before the most stable dispersion starts to settle.

Following a specified aggregation/settling period the particle size, ζ-potential, and ENP concentrations in the supernatant are determined. By not only measuring the remaining particle concentration in the supernatant but also determining important particle properties, such as the particle size and ζ-potential, it is possible to evaluate the concentration data for the underlying process (electrostatic stabilization, charge reversal, shift of the isoelectric point). We are aware, however, that for the sake of covering this larger dataset we are sacrificing details of the dynamic sedimentation behavior (*92*) or aggregation rates (*100*). The residual concentration of ENPs in the supernatant after a certain time is, however, a function of the aggregation rate, hence, when the period until sampling is correctly chosen, the test also reflects kinetic aspects of the aggregation (Figure 9). The principle of this multi-parameter test matrix is shown in Figure 7 and the set-up of the auto titration unit is shown in Figure

8. The results of the different datasets (i.e. ENP concentrations a function of pH and sodium concentration, Figure 14) are plotted as contour graphs, each supported by 60 individual measurements.

2.3 Material and methods

To perform this proof-of-concept study we used two different commercially relevant titanium dioxide particles, Degussa P25 and Hombikat UV-100. As the aquatic species we selected Na^+ and Ca^{2+} as cations (chloride salts), Cl^- and SO_4^{2-} as anions (sodium salts), Suwannee River Natural Organic Matter as a surrogate for NOM and sodium diphosphate as a classical dispersant and positive control.

2.3.1 Suspensions and solutions

We used Evonik Aeroxide P25 and Sachtleben Hombikat UV-100 as supplied by the manufacturers. A detailed description of the material is included in the table below (Table 1) together with representative TEM micrographs (Figure 10).

Table 1. Characteristics of TiO_2 nanoparticles.

	TiO_2 P25 Evonik	**TiO_2 Hombikat UV-100 Sachtleben**	
Characteristic			**Reference**
Primary particle diameter [nm]	~ 21	< 10	Ettlinger (*101*), Sachtleben (*102*)
Hydrodynamic diameter (as z-average) [nm][1)]	293 ± 16	302 ± 43	this study
Zeta potential [mV][1)]	20 ± 3.2	19.1 ± 0.7	this study
SSA BET [$m^2\ g^{-1}$]	50 ± 15	> 250	Ettlinger (*101*), Sachtleben (*102*)
Point of zero charge[2)]	pH 5.6	pH 4.8	this study
Density [g mL^{-1}]	3.7	3.9	Ettlinger (*101*), Sachtleben (*102*)
Purity [%]	99.5	-	Ettlinger (*101*)
Pore volume [mL g^{-1}]	0.15	0.34	Colón (*103*)
Pore size distribution	little porosity, peak at 31.5 nm	heterogeneous, peak at 3.5 nm; mesopores ~5.6 nm	Colón (*103*)

[1)] MQ water
[2)] 10 mM NaCl

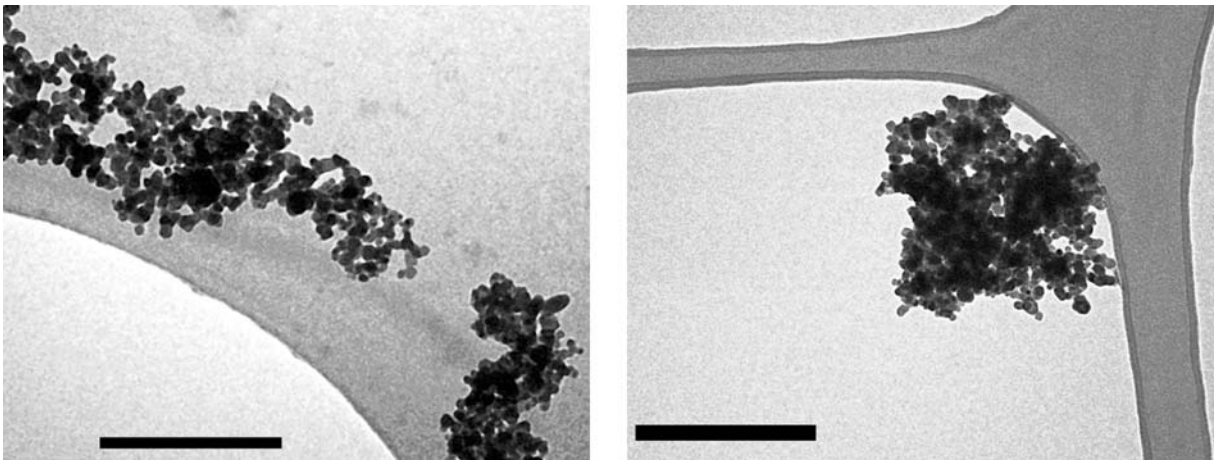

Figure 10. TEM images of TiO_2 P25 (left) and TiO_2 Hombikat UV-100 (right). The scale bar represents 500 nm.

It should be noted that both materials are aggregates of strongly bound (sintered) primary particles, and hence we were studying the aggregation (or agglomeration) of these aggregates (cluster-cluster aggregation). The TiO_2 stock dispersions were prepared by suspending TiO_2 particles (50 mg L^{-1}) in Milli-Q water followed by 30 min of sonication in an ultrasonic bath (2×60 W indicated power, Sonorex RK 106, Bandelin, Germany). The water used throughout the study was prepared by a Millipore Advantage A10 system (Millipore, Billerica, US) equipped with a Bio-Pak-ultrafilter (5000 g mol^{-1} molecular weight cut-off) for final clean-up. The pH was adjusted using NaOH and HCl at 0.001 mol L^{-1} diluted from 0.1 mol L^{-1} stock solutions (Titrisol, Merck, Austria). All other reagents used were analytical grade purchased from Fisher Scientific, Austria. Suwannee River natural organic matter (SR NOM, International Humic Substances Society) was used as a NOM surrogate (stock 50 mg L^{-1}).

2.3.2 Titration of TiO_2 suspension

An auto titration system (Metrohm Titrando 836) equipped with four individual dosing units (Metrohm Dosino 807) and 20 mL burettes (Metrohm Dosino 800) was used, together with a robotic sample processor (Robotic sample Processor XL 815) and a fast reaction pH electrode (Metrohm Aquatrode Plus), all devices from Metrohm, Switzerland (Figure 8). Each of the 125 mL polyethylene titration vessels were dosed with 25 mL of the stock suspension. The electrolyte or NOM solutions were then added automatically, followed by Milli-Q water to reach the desired concentration at a

total volume of 50 mL. NaOH and HCl were used to adjust the pH. To consistently reach a total volume of 50 mL (Vol_{tot}) in each sample the system calculates the amount of H_2O (Vol_{H2O}) needed by the following equation:

$$Vol_{tot} - Vol_{TiO2} - Vol_{El} - Vol_{ET} = Vol_{H2O} \qquad \textbf{Equation 2}$$

The pH was measured after the addition of electrolyte solution and H_2O and determined the decision of titrant following the rules a) use NaOH if measured pH < target pH and b) use HCl if measured pH > target pH. Titration was carried out with a fixed endpoint determination. The volume that has been added when the endpoint is reached gives the calculable reagent consumption. The dosing of titrants follows three stages: initial, continuous phase and control range. In the initial phase the dosing rate increases constantly (from min. to max. value) whereas in the continuous phase the rate is set to max. volume. Close to the endpoint the titration is carried out at the minimum rate. The maximum and minimum rate is defined with 2 mL and 50 µL, respectively. The termination of the titration at the endpoint is after a waiting period of 180 s. Electrode calibration (buffers used were pH 4, 7 and 10, Fisher Scientific, Austria) was performed before commencement, after half of the samples, and at the end of each experimental set. The drift was below ±0.1 pH units. All vessels were sealed with plastic lids once the parameters had been adjusted. Aggregation/sedimentation was allowed to occur together with equilibration of the sample with atmospheric CO_2 for 15 h in non-stirred vessels until a constant pH had been reached (< ±0.1 pH units h^{-1}). After 15 h 10 mL was sampled trough a Ø 1mm hole in the lid of the vessel at a depth of exactly 2 cm using a stainless steel needle and a syringe. The reason for choosing a 15 h reaction period can be seen in Fig. S1. Sampling should occur after the fast aggregation reaction has leveled out to a nearly constant low concentration in the supernatant before the slowly aggregating dispersion has left its stable plateau. We decided to choose a period in between both limits in order to resolve intermediate aggregation rates, and also because of practical concerns of sampling and measurements to be performed during the following day. The pH of the remaining sample (pH_{t15}) was measured again after 15 h; this pH was further used for data visualization. Here, we worked deliberately on un-buffered systems due to concerns of buffer induced reactions through elevated ionic strength and possible specific adsorption of buffer components to the particle surface.

The possible impact of an added buffer on experimental results is shown by the well-buffered sodium diphosphate set, where adsorption of the diphosphate leads to strong stabilization under all applied conditions.

2.3.3 Nanoparticle analysis

The supernatant was analyzed for ENP concentration, particle size and electrophoretic mobility. Particle size and electrophoretic mobility were determined using a Zetasizer Nano ZS (Malvern Instruments, UK). The method of cumulants was used for derivation of the intensity-weighted diffusion coefficient (z-average, 1st cumulant) and the polydispersity index (PDI, 2nd cumulant), while CONTIN (*104*) was used for the particle size distribution and for derivation of the 1st peak (mode) of the distribution (*105*). Each measurement consisted of 10 stacked individual measurements of 10 s. The particle hydrodynamic diameter was calculated from the diffusion coefficient using the Stokes equation. The ζ-potential was calculated from the electrophoretic mobility using the Smoluchowski approximation (with F(κa) = 1.5 or medium sized particles at an ionic strength of greater than 1 mmol L^{-1}). This was done for greater clarity in the presentation. The possibility of an error being introduced with this simple linear transformation is acknowledged but does not change the general picture. Each data point is the average of 20 repeated measurements. The concentration of nano-TiO_2 was determined by measuring the nephelometric turbidity (Hach 2100 N IS Turbidity meter). The turbidity meter applies a LED light source with a wavelength in the near IR with λ=870 nm. Detection is performed at 90° angle in a glass cell with 25 mL volume. The NTU values were calibrated against known concentrations in a TiO_2 dispersion stabilized by 5 mmol L^{-1} $Na_4P_2O_7$. The resulting calibration is shown below (Figure 11).

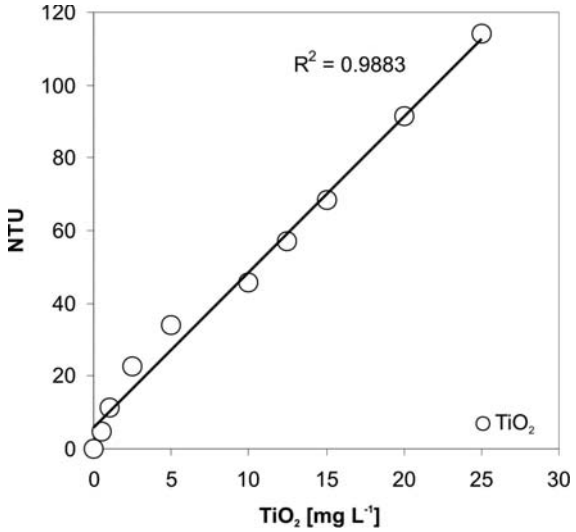

Figure 11. TiO_2 concentration (mg L^{-1}) versus turbidity (NTU) (n=3, 1SD <1.7 NTU).

The addition of NOM does not increase the turbidity in the sample as the NOM is far smaller than the average particle size of measured dispersions. Although problems can arise from the fact that turbidity is also a function of particle size (*106*), turbidity is a valid approximation of particle concentration under the conditions of these experiments, where the size distributions are broad and the average particle diameter is in the range of the incident light wavelength. Electrical conductivity (mS cm^{-1}) was measured within the Zetasizer Nano ZS folded capillary cell and cross-checked with a portable conductivity meter (TetraCon 325 probe,WTW, Germany).

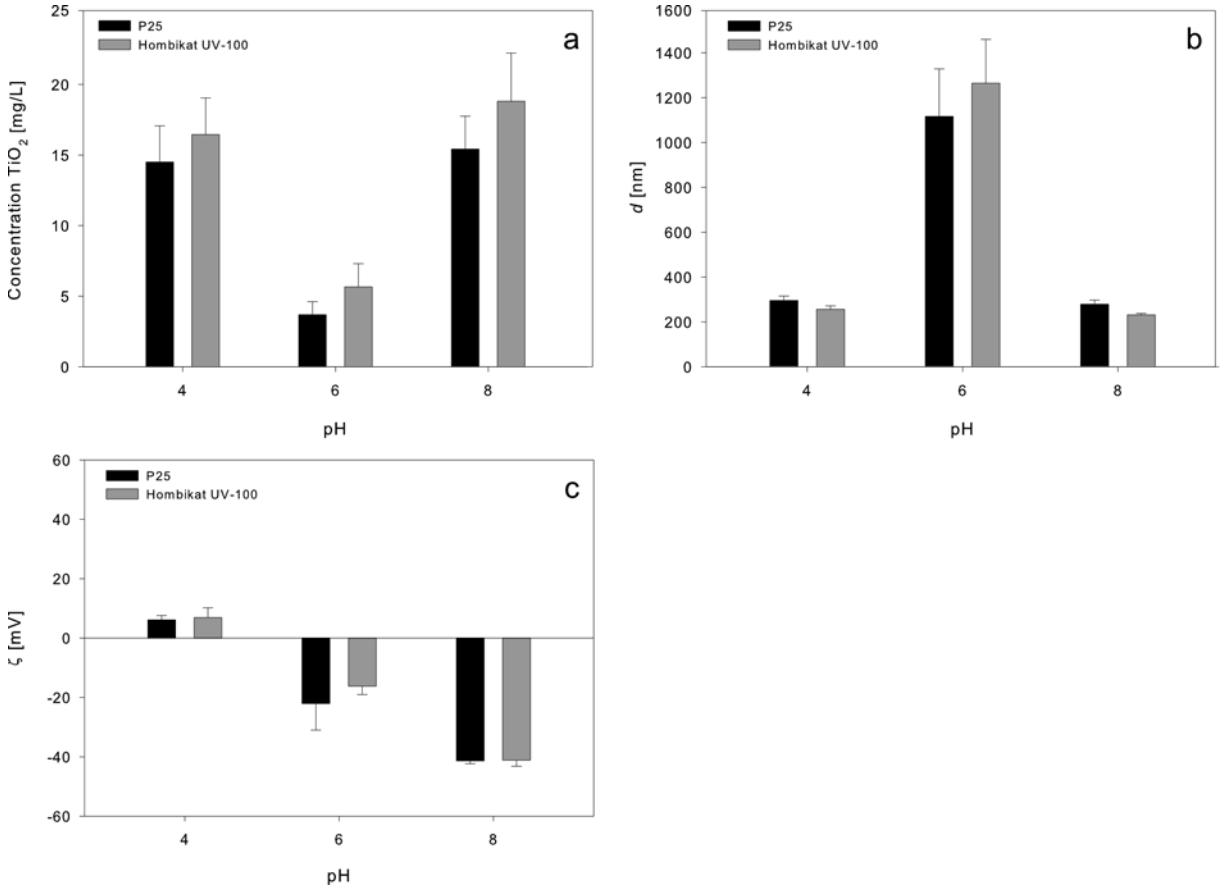

Figure 12. Concentration (a), hydrodynamic diameter as z-average (b) and zeta potential (c) of TiO_2 P25 and Hombikat UV-100 (25 mg L^{-1}) in Milli-Q water at pH 4, 6 and 8 (n=5, ±1SD).

The titrations for determining the isoelectric point (IEP) were performed with the same autotitrator as described in section method & materials. Individual samples were titrated to the desired values, allowed to equilibrate for 2 hours and then measured in the Malvern Zetasizer ZS. The start and end values for the zeta-potential match well with values found by i.e. Dutta et al. (2005). Also in our analysis the Hombikat UV-100 particles show a IEP shifted towards lower pH values compared to P25, what is identical to what Dutta et al. (2005) observed. The lower IEP values in our study compared to Dutta et al. (2005) can not be fully explained on the basis of the available information (*107*). Different equilibration times with atmospheric CO_2 or different batches of the materials tested could be the reason for the observed deviations. Method reproducibility for nanoparticle concentration, hydrodynamic diameter and z-potential obtained in Milli-Q water at pH 4, 6 and 8, are shown in (Figure 12), Supplementing Material. The IEP was determined for both materials in 10 mmol L^{-1} NaCl (Figure 13).

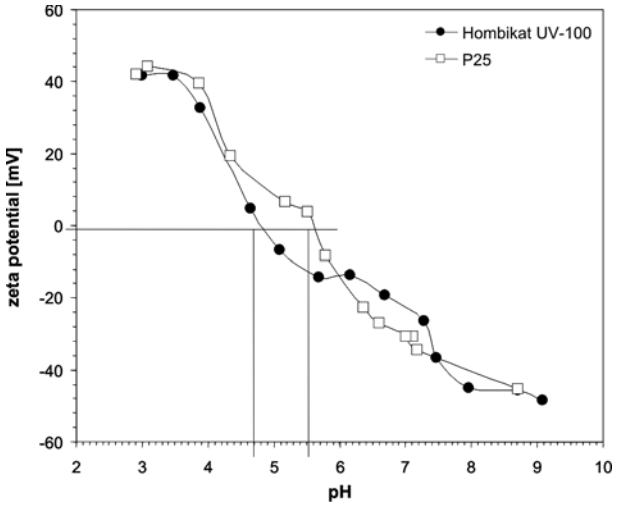

Figure 13. Plot of the zeta potential over pH of 25 mg L^{-1} ENP dispersions with resulting isoelectric points (IEP) for P25 (at pH 5.6) and Hombikat UV-100 (at pH 4.8) Titrations were performed in 10 mM NaCl from pH 3 to pH 9.

2.3.4 Data interpolation

We used the Inverse Distance Weighting (IDW) algorithm with the Surfer 7.0 software (Golden Software, Inc.) to interpolate data. The interpolated surface (contour plot) is a distance weighted average of the observed parameters, i.e. with increasing distance between data points their relative contribution to the interpolation declines with distance from the grid node according to equations (3) and (4):

$$Z_i = \frac{\sum_i^n 1 \frac{Z_i}{h_{ij}^{\beta}}}{\sum_i^n 1 \frac{1}{h_{ij}^{\beta}}} \qquad \textbf{Equation 3}$$

with

$$h_{ij} = \sqrt{d_{ij}^2} + \delta^2 \qquad \textbf{Equation 4}$$

where *hij* is the effective separation distance between grid node *j* and the neighboring point *i*. *Zj* is the interpolated value for grid node *j*; *Zi* are the neighboring points; *dij* is the distance between the grid node *j* and the neighboring point *i*; *δ* is the weighting power and *d* is the smoothing parameter.

2.4 Results and discussion

The experimental sets deliver the particle concentration, the average ζ-potential and the z-average particle size of ENPs still in the supernatant. In the following figures concentration and ζ-potential are given for each ENP and as a function of the concentration of an environmentally relevant electrolyte or NOM and the pH. Particle size plots are given below (Figure 14). To facilitate the interpretation and identify correlations between the sets we chose interpolated contour plots in which the base grid is made up from the controlling parameters, namely the electrolyte or NOM concentration and the pH while the z-axis relates to ENP concentration, ζ-potential or size. Each contour plot is supported by 60 individual stability experiments (data points). High particle concentrations are shown in bright shades and low concentrations in dark shades. Similarly, small particle sizes are shown in bright shades and large aggregates in dark shades (Figure 14). The grayscale shading of the ζ-potential plot has been set to emphasize the magnitude of the ζ-potential rather than its polarity. It has been assumed that, under pure electrostatic interaction, within ±15 mV the system would be inherently unstable and tend to aggregate, up to ±30 mV it would be in a transitional state, from ±30 mV it would be predominantly stable and above ±40 mV it would be well stabilized. The value and polarity of the z-potential is plotted on the iso-lines. Both particles tested (P25 and Hombikat UV-100) were composed of the same core material and behaved in a relatively similar manner, even though their production methods, as well as parameters such as mineralogy, surface area and crystallinity, all differ considerably (Table 1). Due to the un-buffered dispersions and the desired equilibration with CO_2 from the ambient air, deviations of the pH from the initially set values were observed for pH values of 6 and 8, as has also been described (*89*).

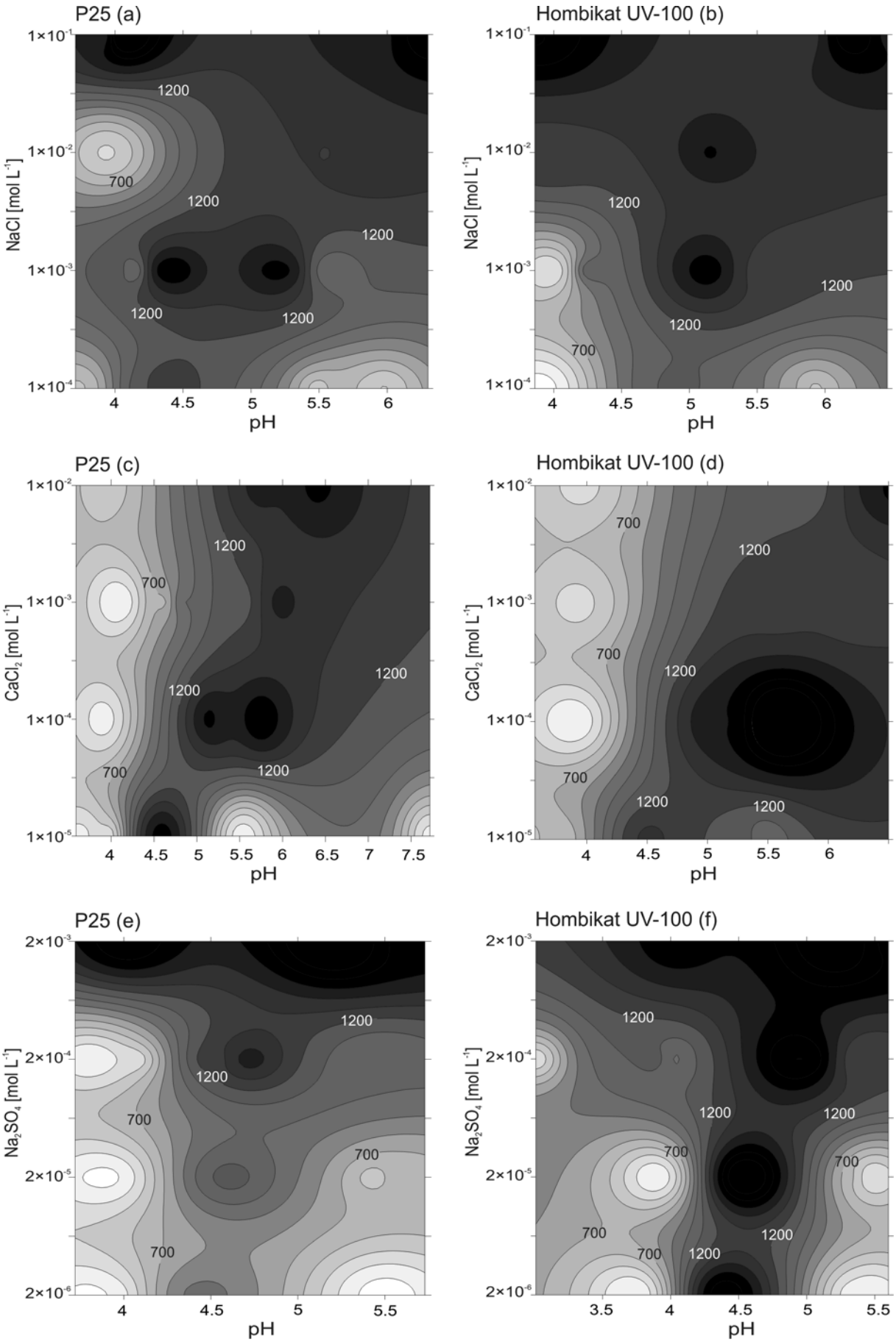
P25 (a)
Hombikat UV-100 (b)
P25 (c)
Hombikat UV-100 (d)
P25 (e)
Hombikat UV-100 (f)
NaCl [mol L-1]
CaCl2 [mol L-1]
Na2SO4 [mol L-1]
pH
700
1200

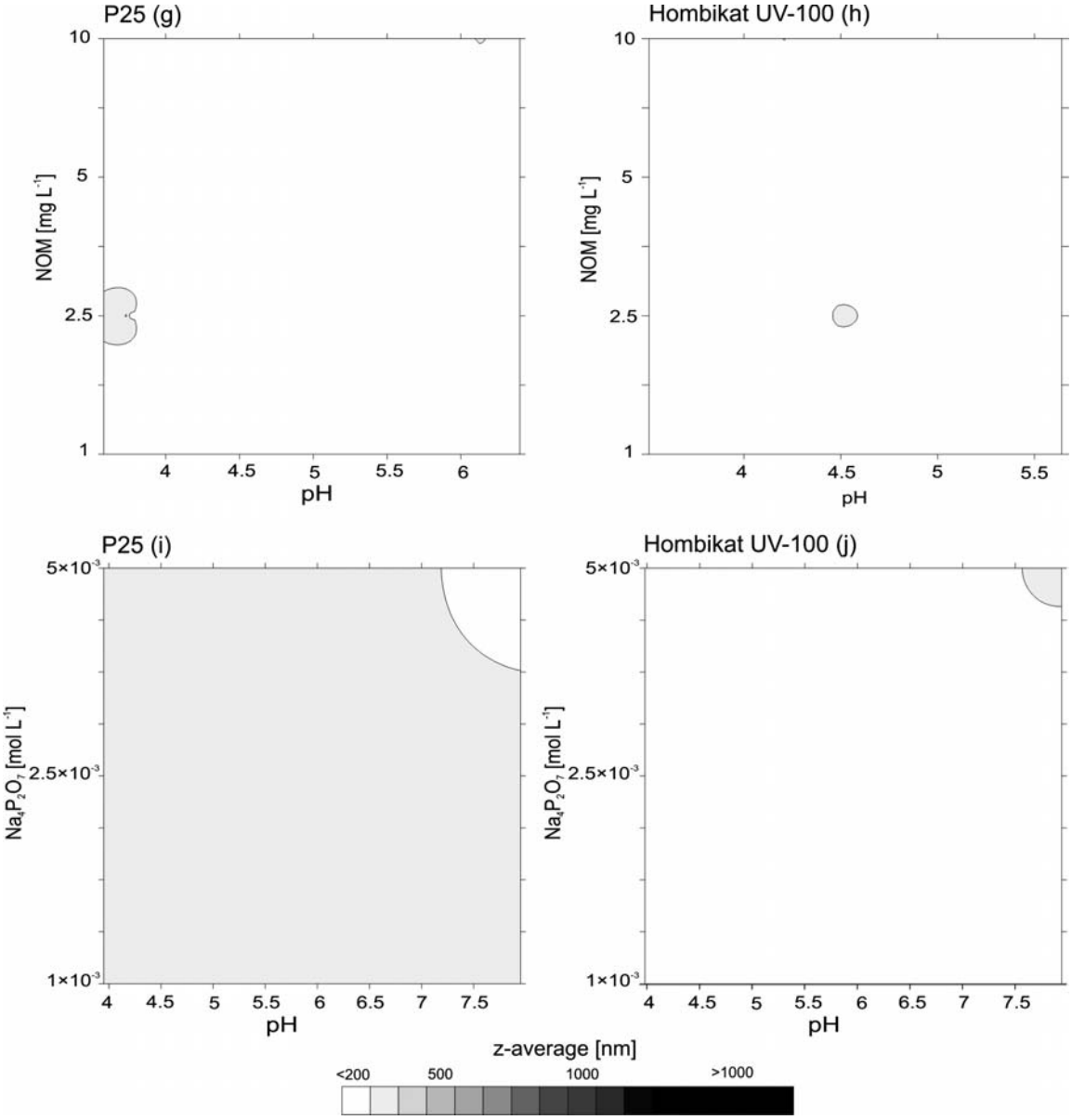

Figure 14. Z-average of TiO_2 P25 and Hombikat UV-100 in the presence of NaCl (a, b), $CaCl_2$ (c, d), Na_2SO_4 (e, f), NOM (g, h), and $Na_4P_2O_7$ (i, j) at different pH values. The plots for the NOM and $Na_4P_2O_7$ additions show nearly no features (flat planes) since under all conditions only small clusters of the materials prevail.

2.4.1 NOM and sodium diphosphate sets

Both NOM and diphosphate anions adsorb to the surface of the TiO_2 and induce charge reversal at pH< IEP and an elevated negative surface charge at pH ≥ IEP. Figure 15 shows the result matrix of particle concentrations and ζ-potential for P25 (a, b) and Hombikat UV-100 (c, d) for the NOM additions. It can be seen that, under all of the investigated conditions, the addition of NOM generates a well stabilized

dispersion under all conditions tested. This was to be expected since the interaction of NOM with the surfaces of clays (*56*) and iron oxides (*108-109*) results in a shift in the isoelectric point (IEP) towards a lower pH, and can even cause charge reversal if the ratio of NOM to positively charged surface sites is sufficiently high. The same general behavior was found for zero valent iron (*110*), has been observed for carbon nanotubes (*111*) and quantitatively described for fullerenes (*97*). It can also be shown that the modification of aquifer material by NOM even enhances the transport of E.coli bacteria (*112*) and NOM deactivates potential attachment sites on heterogeneously charged collector grains (*113*). There are indications that certain ratios of NOM-to-particle concentrations can destabilize particle dispersions through charge neutralization, or even by bridging flocculation (*96*). The concentrations of ENP for the NOM addition ranged from 20.5 to 25.5 mg L^{-1} and 15 to 20.5 mg L^{-1} for Hombikat UV-100 and P25, respectively. Although the distribution of particle concentrations is highly uniform over the parameter set, minimum concentrations for P25 occurred at high pH with low NOM concentrations, and for Hombikat UV-100 at low pH with high NOM concentrations. The distribution of the ζ-potential again reveals similarities in both cases for NOM addition from about 2 mg L^{-1} NOM decreasing with higher NOM concentrations. Interestingly, at low NOM concentrations and around pH 4 the ζ-potential of both materials peaks towards less negative values and is most extreme for P25. This observation is supported by the IEPs, which indicate that both bare materials should have (on average) a positive surface charge at this pH.

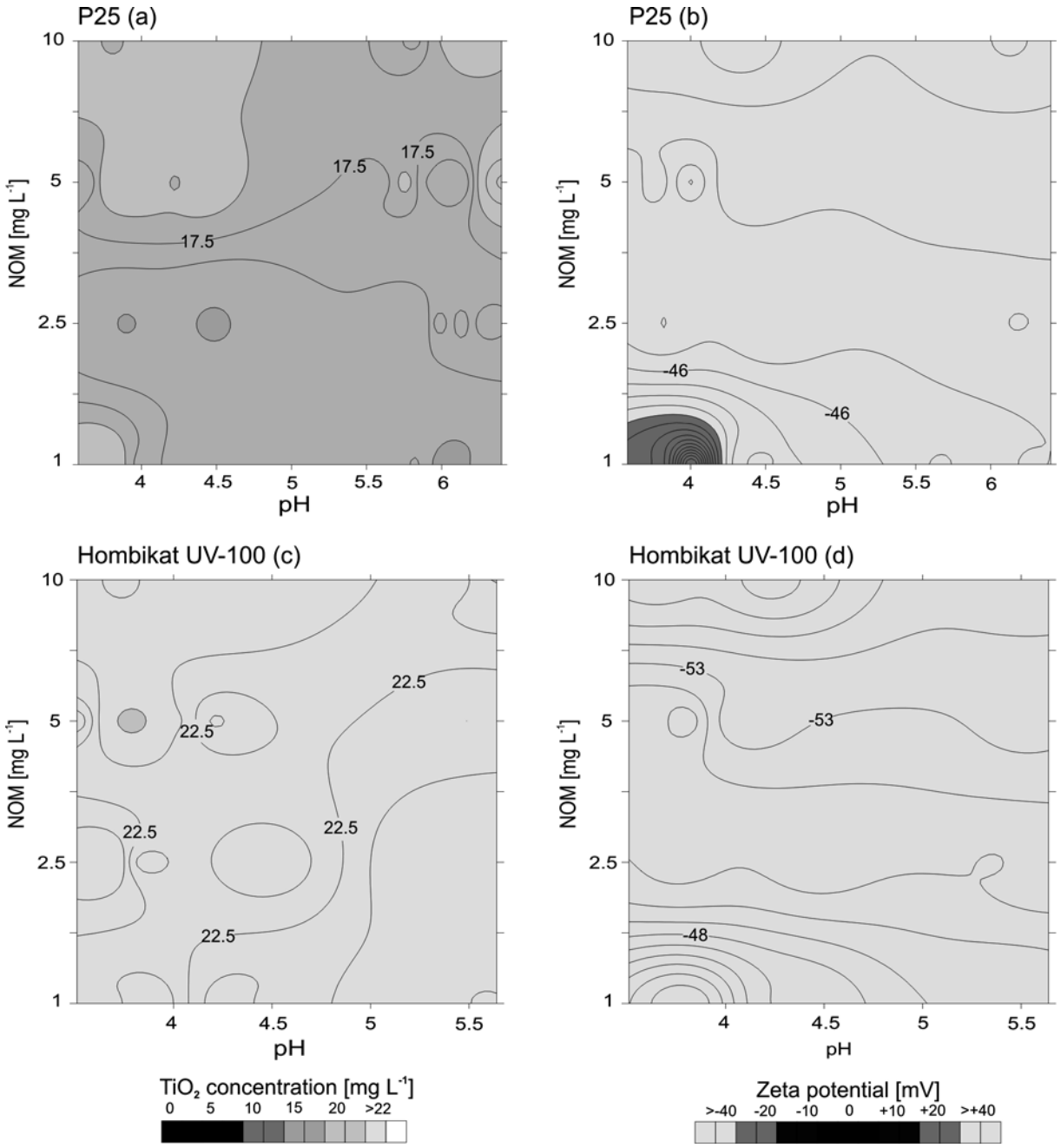

Figure 15. TiO_2 concentration (a, c) and z-potential (b, d) of P25 and Hombikat UV-100 in the presence of NOM at different pH values.

The low NOM concentration can only compensate for this to a limited extent, and in this case obviously compensates more for Hombikat UV-100, which has a lower IEP, than for P25. Figure 15 it is evident that the ratio of surface area to NOM concentration does play a much smaller role than the charge balance of the bare particle surface. We need to consider here that the Hombikat UV-100 particles have a 5-fold larger specific surface area compared to P25. Hence a much smaller proportion of the Hombikat UV-100 surface is coated by the NOM molecules, leading

to deactivation of the positive charge or even charge reversal. Figure 16 shows the result matrix for particle concentrations and ζ-potential of P25 (a, b) and Hombikat UV-100 (c, d) for $Na_4P_2O_7$ additions. Diphosphate was used as positive control because it is frequently used as a dispersing agent (food additive E 450c) showing here similar results as NOM with smaller effect on dispersion stability but similar magnitude of the ζ-potential. The diphosphate additions show an even more uniform pattern of behavior in terms of particle concentration and ζ-potential, between the two TiO_2 materials. Within a very low overall range of variability, the highest particle concentrations are found for low diphosphate additions at low pH values, and also for high diphosphate additions at high pH values. The lowest particle concentrations are found for low diphosphate concentrations at around the IEP of the materials. This behavior is not, however, mirrored in the ζ-potential plots, where the lowest ζ-potentials are found for the lowest diphosphate addition and low pH. The particle size plots also show little variability in the range of particle sizes found in this stabilizing environment, (see Figure 12).

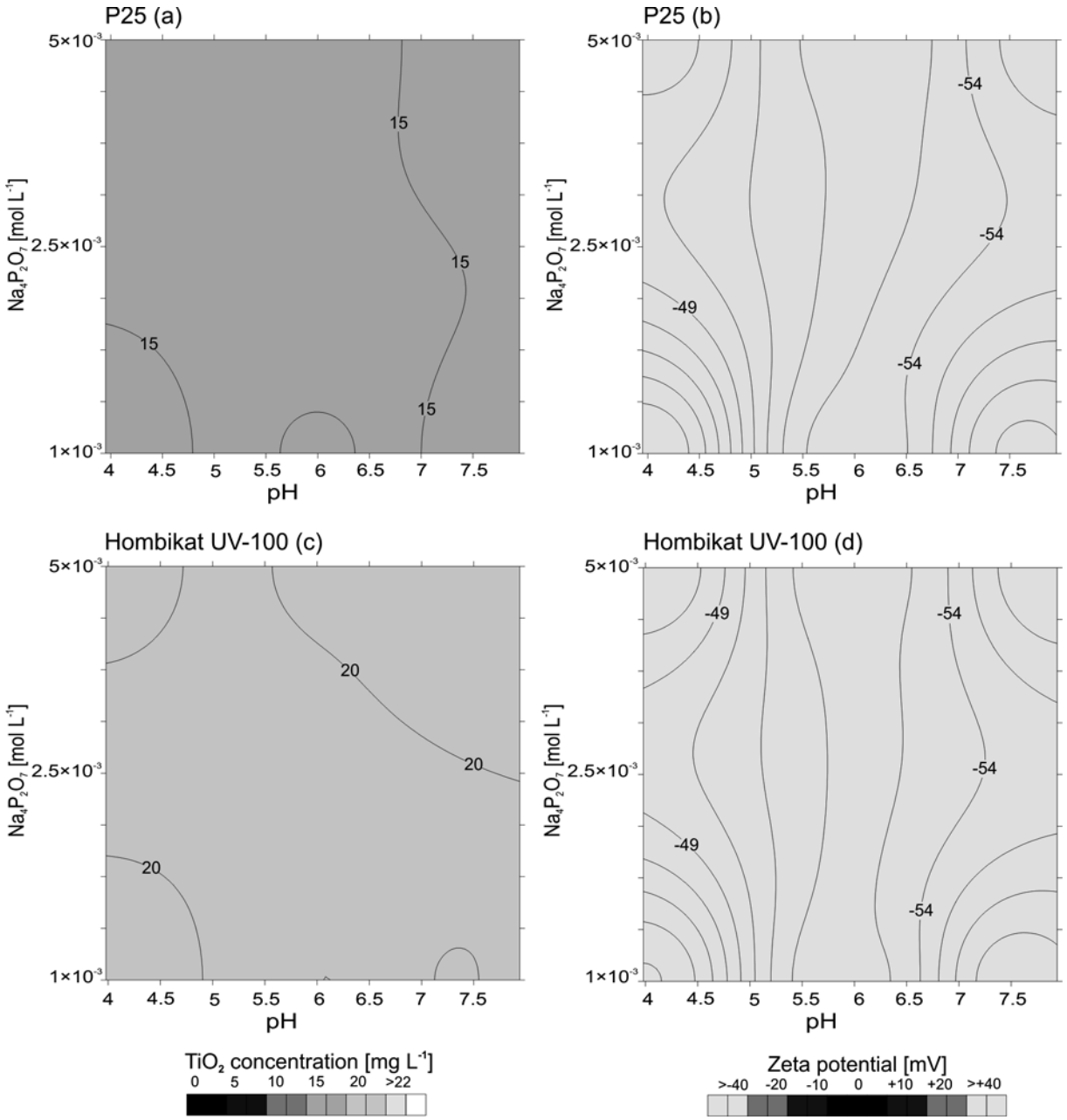

Figure 16. TiO_2 concentration (a, c) and z-potential (b, d) of P25 and Hombikat UV-100 in the presence of $Na_4P_2O_7$ at different pH values.

2.4.2 Sodium and calcium chloride sets

Figure 17 shows the result matrix of particle concentrations and zeta potential of P25 (a, b) and Hombikat UV-100 (c, d) for the $NaCl_2$ additions while Figure 18 shows the result matrix for the $CaCl_2$ additions. These experimental sets investigate the roles of the two major cations present in natural waters, and the different response to mono- and divalent cations. According to the Schulze-Hardy rule (*114*) the critical

coagulation concentration (CCC) of mono- , di- and trivalent cations for a given dispersion is approximately 1:0.033:0.0011. Considering purely electrostatic interactions and neglecting the effects of specific adsorption or steric stabilization (due to, e.g., NOM), the calcium concentration should accordingly dominate the behavior of nanoparticles in most freshwaters.

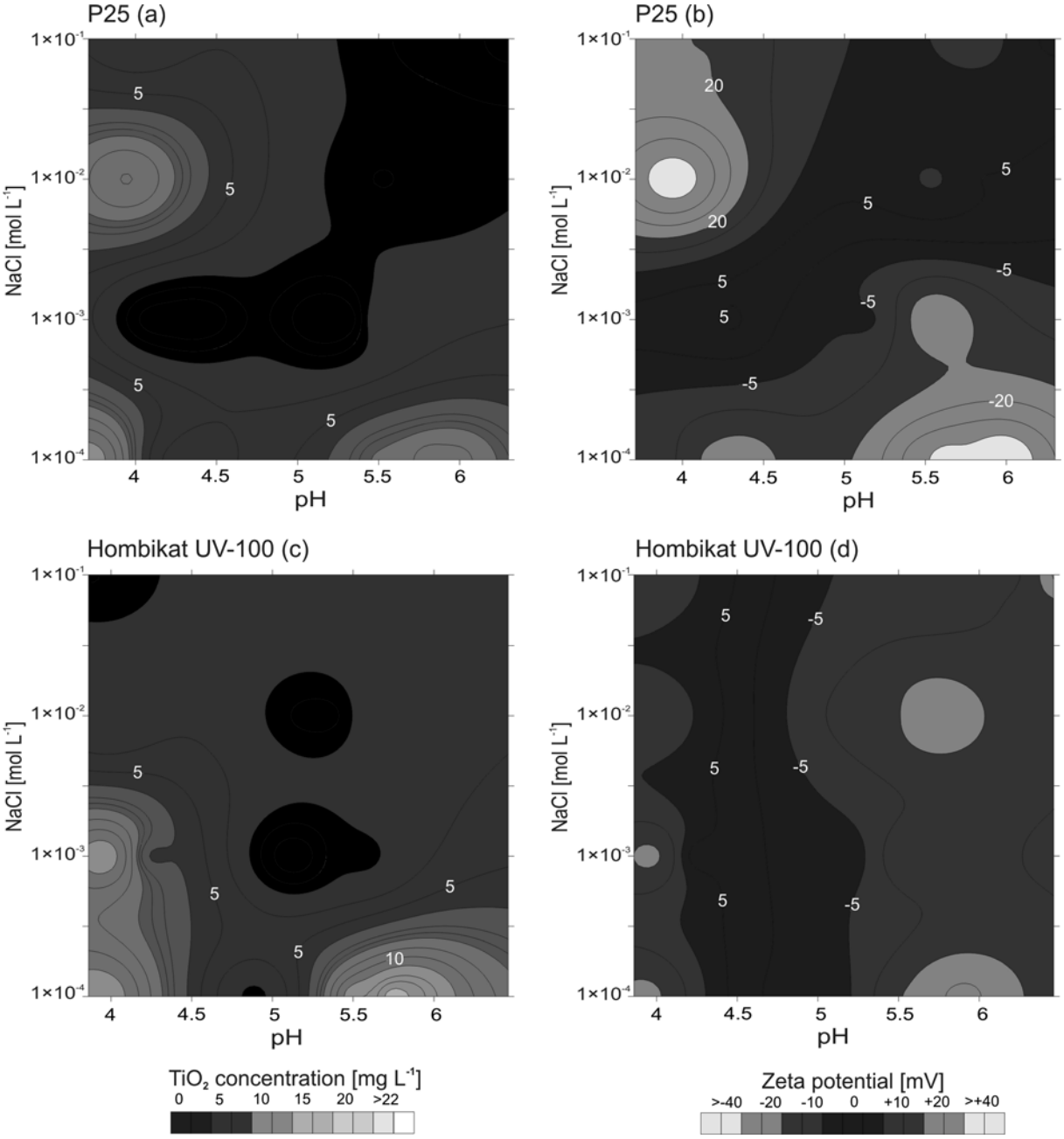

Figure 17. TiO_2 concentration (a, c) and z-potential (b, d) of P25 and Hombikat UV-100 in the presence of NaCl at different pH values.

The result matrix for sodium chloride shows quite similar behavior for both TiO_2 materials in terms of the dispersed particle concentration. At low particle

concentrations the ζ-potential always has a low magnitude. The lowest particle concentrations are found at pH values of 5 ±1, and towards higher electrolyte concentrations. This corresponds to the expected destabilization at higher ionic strengths and around the IEP. At low pH the relative stability of the dispersion reaches up to 1 mmol L^{-1} NaCl (Hombikat UV-100). For P25 stability peaks at 0.1 and 10 mmol L^{-1} NaCl, with a local minimum at 1 mmol L^{-1}. This observation for P25 is underpinned by the independent measurement of the ζ-potential which is in agreement with the concentration data. While for Hombikat UV-100 the ζ-potential reflects a titration of TiO_2 at different ionic strengths of a non-interacting electrolyte, for P25 we observe a charge reversal at pH 4 with increasing salt concentration. At pH 4 the maximum particle concentration for Hombikat UV-100 is accompanied by positive z-potential at all electrolyte concentrations; the maximum particle concentration for P25 is observed with ±35 mV at 10 mmol L^{-1} NaCl and -5 to -10 mV at 0.1 mmol L^{-1} NaCl. The relatively high stability of the P25 dispersion at such a low negative z-potential is unexpected but is additionally underpinned by the particle size data which also show small particles to be present in these samples. With variation in NaCl concentration the IEP behaves differently for P25 and Hombikat UV-100. While Hombikat UV-100 follows the classical Debye-Hückel theory (*115*) with an IEP nearly independent of the NaCl concentration, P25 shows an IEP ranging from high pH/high salt to low pH/low salt concentrations (see Figure 17). Figure 18 for calcium chloride shows a much higher degree of variation in the plots. The particle concentration plots are remarkably similar for both P25 and Hombikat UV-100, although for P25 a wider pH range was captured. This indicates that both react in a similar manner with $CaCl_2$. In contrast to the NaCl set, destabilization of the dispersion is only observed for intermediate $CaCl_2$ concentrations and around the IEP. The IEP for both particle types shows similar behavior, comparable to P25 with NaCl. Results in Figure 18 suggest a specific interaction of Ca^{2+} and TiO2 with a resulting charge reversal at higher calcium concentrations. This behavior has long been documented, e.g. for rutile particles (*116*) where calcium concentrations of 0.33 mmol L^{-1} caused a charge reversal to positive z-potentials at all tested pH values (except between the IEP and 1 pH unit above). The observed charge reversal is accompanied by elevated dispersion stability, whereas we would have expected complete and rapid aggregation due to absence of a repulsive energy barrier.

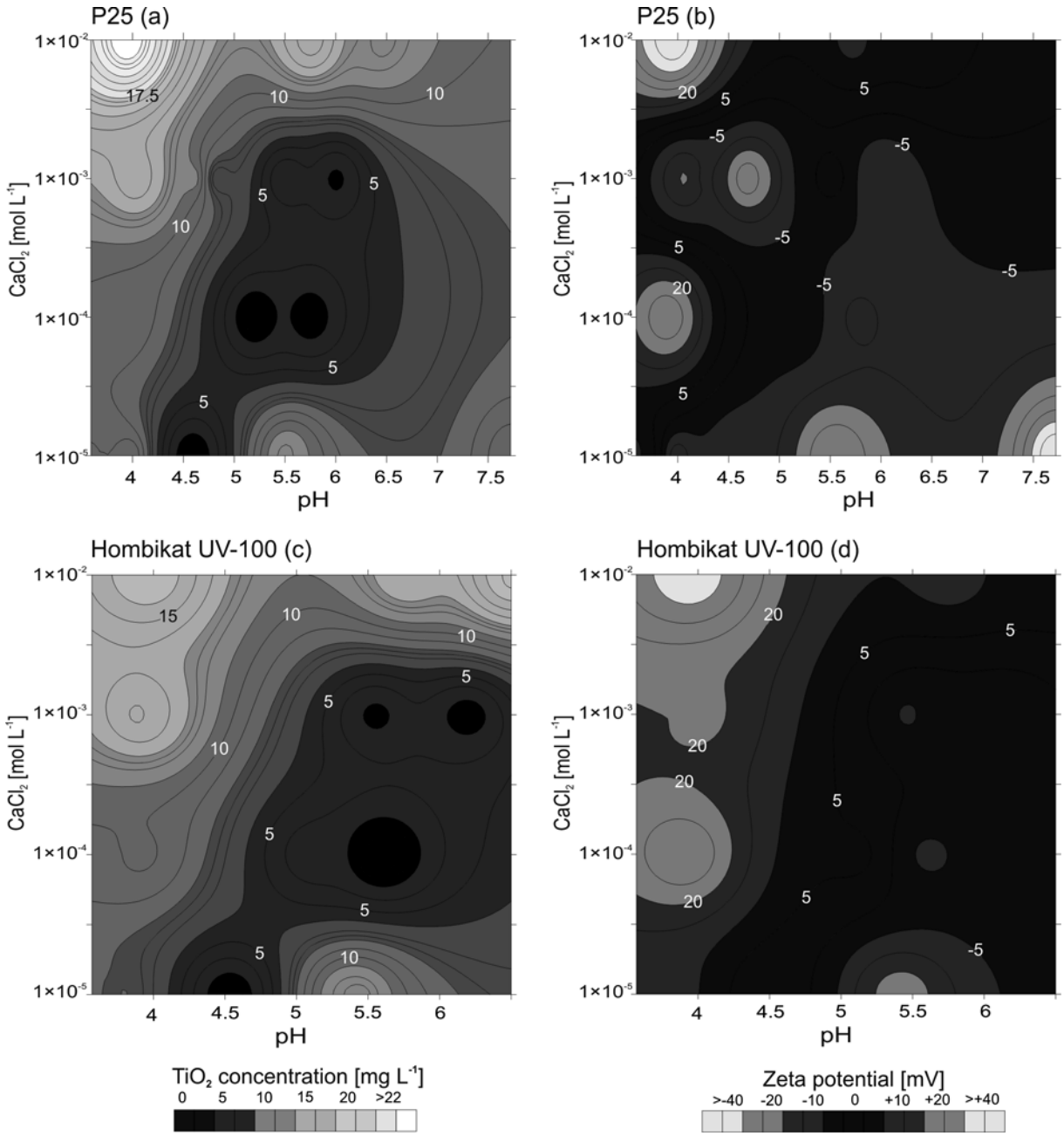

Figure 18. TiO_2 concentration (a, c) and z-potential (b, d) of P25 and Hombikat UV-100 in the presence of $CaCl_2$ at different pH values.

For a $CaCl_2$ concentration of 10 mmol L^{-1} the elevated dispersion stability at pH 5.5 to 6.5 for P25 and pH > 6 for Hombikat UV-100 is accompanied by z-potential values of below 10 mV. No stable dispersion would have been expected under these conditions. Despite the well known drawbacks of particle sizing by DLS (*117*), valuable information can be gathered from DLS at this point. The recorded particle sizes all peak at over 1000 nm in this region. The settling velocity for 1 mm particles would be around 6 mm h^{-1} and if rapid aggregation had occurred then all particles

should have been removed from the topmost 2 cm of the reaction vial, from where the samples were taken. This is an indication of a slow aggregation process under charge reversal caused by Ca^{2+}, at elevated particle and $CaCl_2$ concentrations. At a pH around 4 and at 0.1 and 10 mmol L^{-1} $CaCl_2$ concentrations, P25 shows positive ζ-potentials. In between, at a 1 mmol L^{-1} $CaCl_2$ concentration, a charge reversal from positive to negative values occurs, peaking at -17.1 mV accompanied by elevated particle concentrations and small particle sizes. It is not clear what might be the cause of this double reversal but it clearly shows that Figure 18 anomalies can exist. The situation for Hombikat UV-100 is more uniform, showing positive ζ-potentials and elevated particle concentrations for low pH and all $CaCl_2$ concentrations. The results indicate a stabilizing effect of calcium ions at concentrations > 1 mmol L^{-1}, but it should be noted that although such situations may be encountered in these pure electrolytes, they may not be directly transferable to more complex conditions. Brant et al. (2005), for example, noted a diversion of the ζ-potential for fullerenes towards positive values under low calcium concentrations, which vanished completely with the addition of 1 mmol L^{-1} NaCl. Under all tested conditions a correlation of calcium with a low particle concentration at low ζ-potential magnitudes is less obvious than in the other tests.

2.4.3 Sodium sulfate set

Figure 19 shows the result matrix of particle concentrations and ζ-potential of P25 (a, b) and Hombikat UV-100 (c, d) for the $Na_2SO_4^{2-}$ additions. Sodium sulfate was used to investigate the role of a divalent anion present in natural waters at low concentrations ≤2 mmol L^{-1}.

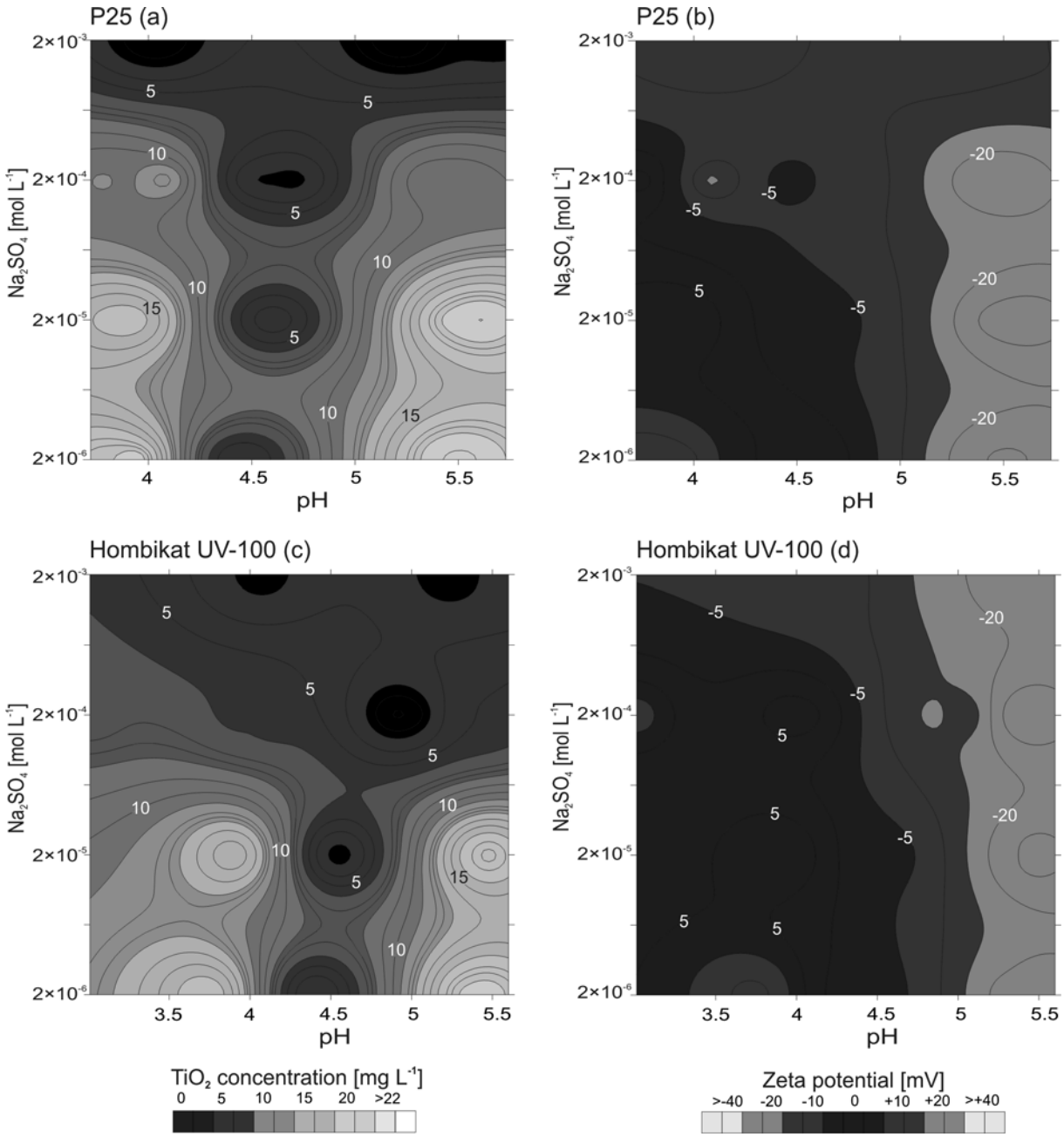

Figure 19. TiO_2 concentration (a, c) and z-potential (b, d) of P25 and Hombikat UV-100 in the presence of Na_2SO_4 at different pH values.

In contrast to phosphate and carbonate the sulfate ion retains its divalent character throughout the tested pH range, which also enables a direct comparison between divalent and monovalent anions (i.e. between Na_2SO_4 and NaCl). Considering the slightly different pH-ranges plotted for P25 and Hombikat UV-100 in Figure 19, the similarities in particle concentration and ζ-potential demonstrate that both materials again behave comparably regardless of their different BET specific surface area. More clearly visible than in the other sets is the clustering of the 60 data points

around certain electrolyte concentrations. Based on the findings of Fernandez-Nieves and de las Nieves (1999), sulfate would be expected to effectively destabilize the dispersions, at least at pH values below the IEP (*118*). In our set sulfate is destabilizing at concentrations >0.2 mmol L^{-1} for Hombikat UV-100, and about 2 mmol L^{-1} for P25 at all pH levels tested. Below these threshold concentrations both materials aggregate only in the vicinity of their IEPs which remain unchanged. From the ζ-potential plots it is evident that sulfate interacts with the surface of the particles at pH > IEP, leading to more negative ζ-potentials below -20 mV as compared to the NaCl additions. At pH < IEP this interaction prohibits the development of ζ-potentials above ~ -5 mV which is clearly different from the results for Na^+ and Ca^{2+}. A similar behavior was also observed for Na_2SO_4 additions to P25 by Fernandez-Nieves and de las Nieves (1999). Despite the fact that for pH < 4.5 the ζ-potential is between 0 and 5 mV for all conditions tested, elevated particle concentrations are found for sulfate concentrations below 0.2 mmol L^{-1} which also correspond to small measured particle sizes. This can be taken as another indication that, especially with multivalent ions, the correlation between low ζ-potential magnitude and low dispersion stability does not always exist.

2.5 Conclusions

As a compromise between traditional concepts for ENP fate testing an experimental assessment procedure is presented which is more universal than the synthetic/natural water approach and less restricted in the number of conditions that can be explored than mechanistic investigations. By using only one variable (a single aquatic species, NOM) versus pH at a time we tested the behavior of the ENPs, still in a setting of reduced complexity. The results demonstrate the advantages and strength of the general concept of the test layout. The results are to a large extent in accordance with previous findings (*89; 96*) and reveal comparable behavior between similar materials, which has not always been found, e.g. for bare TiO_2 nanoparticles which react differently with, for example, serum albumin (*119*). The results also reveal reactions that have not been previously recognized, such as, e.g., stabilization at elevated Ca^{2+} concentrations. Also visible is the dominant influence of NOM on the stabilization. We believe that that the presented approach is a suitable methodology to assess the behavior of ENPs in a wide range of water chemistries and that it

enables the direct comparison of different materials and surface modifications. Such a direct comparison could resolve variations in the ENP behavior induced by tailored modification of core or surface chemistry, and could further support a “safety by design” process, as well as supporting testing strategies for ENPs on a more general basis (*120*). The presented approach only considers homo-aggregation, but in situations where the concentration of natural particles and flocs is much larger that the ENP concentration a hetero-aggregation process is more likely. Determination of aggregation rate constants in such heterogeneous systems is challenging (*121*) and development of analytical methods is needed (*100*). The presented experimental concept is, in principle, also able to determine the dispersion stability in hetero-aggregation experiments. However, the turbidity analysis would no longer be sufficiently specific and would need to be replaced, either by methods probing the ENP directly or via its chemical composition (e.g. elemental analysis). There would also be a need to adapt the method to the applied ENPs and the chosen natural particles. Consequently, there will be a need to develop standard models for a typical assemblage of natural particles to be used in testing ENP behavior.

2.6 Acknowledgment

We acknowledge the provision of the P25 Aeroxide from Evonik Degussa GmbH and Hombikat UV-100 from Sachtleben Chemie AG.

3 The Behavior of Titanium Dioxide in Natural Water

Stability tests on titanium dioxide in natural and synthetic waters.

F. v.d. Kammer, S. Ottofuelling, T. Hofmann

To be submitted to Environmental Science & Technology 2010

3.1 Abstract

Engineered nanoparticles (ENP) from industrial applications and consumer products are already released into the environment. The distribution within the environment is among other factors largely determined by the dispersion state of the nanoparticles which in turn affects the exposure of organisms. The stability is regulated by the water chemistry, surface properties of the particles and their influence on ENP size. In this context, this paper shows results from static stability tests of titanium dioxide (TiO_2) nanoparticles in well controlled synthetic waters covering a wide range of pH and water chemical conditions, standard synthetic (EPA) waters and natural waters. Results demonstrate in detail the dependency of TiO_2 aggregation on ionic strength, the presence of relevant mono- and divalent ions, presence and co-presence of natural organic matter (NOM), and of course the pH. Results from the matrix testing in well controlled batch systems allow predictions on the behavior in the wider natural environment. Our study provides the basis for a testing scheme and data treatment technique to extrapolate and finally predict nanoparticle behavior in a wide variety of natural waters

3.2 Introduction

Engineered nanomaterials and nanoparticles (ENP) are already released and can e found in the environment (*36-37*). The growing production and application of ENP will inevitably lead to a further increasing discharge into the environment. The most prominent distribution pathway of ENP to the environment is thought to be via wastewater treatment plants (WWTP) to aquatic or soil systems (*36; 41; 122*). The continuous release of ENP into the environment raises concerns about adverse effects on organisms or whole ecosystems (*55*) and co-transport of contaminants (*42*)

in surface and ground waters (*7*). It has been shown that some ENP pose adverse effects to organisms of the aquatic environment (*77; 83; 90*). It is generally accepted that a detailed understanding of ENP behavior in the aquatic environment is crucial to be able to fully assess related risks (*33*). Therefore, dispersion studies need to be an essential part of the requested characterization of ENPs in order to predict their transport and fate in natural systems and correctly evaluate and compare results from toxicological test (*33*). As a result potential effects of nanoparticles related to their environmental behavior can be identified and minimized before they can cause risk to humans and biota.

Recent studies have attempted to find analytical methods and standardized tests to comprehend and describe the ENP behavior in synthetic growth media (*123*), natural waters (*90*), waste water (*92*) and well controlled synthetic waters (*124*). The stability and transport of nanoparticles in aqueous systems is controlled by their surface properties as well as the chemistry of the aqueous system (*52; 59; 83; 110*). Factors such as ionic strength, valence of counter ions, pH, or the presence of organic matter will either cause aggregation or stabilization of ENP (*110*). For example, the presence of Ca^{2+} could out rule or diminish the stabilizing effects of natural organic matter (*19*). Through specific interaction water constituents such as NOM or polyvalent ions can enhance, decrease, neutralize or even reverse the surface charge of certain nanoparticles (*52*). Expanding/compressing the electrostatic double layer by decreasing/increasing the ionic strength (IS) will change stability (*125*). Also, preferential adsorption of ions (e.g. Ca^{2+}, Mg^{2+}) may induce nanoparticle aggregation (*118*); divalent ions also screen the charge of the surface more efficiently (*114*). The surface charge of oxide nanoparticles is governed by protonation or deprotonation of surface hydroxyl groups and specific adsorption of e.g. carbonate, cations or NOM. The surface charge of e.g. TiO_2 varies with pH and is negative at a pH above the point of zero net proton charge (pznpc) and positive below the pznpc (*126*). At the pznpc aggregation of particles is promoted (*89*).

To understand the behavior and the characteristics of ENP in aquatic systems researchers conduct experiments in complex natural (*90; 92*) or synthetic waters (*95-96*). Results from natural waters might be more realistic, but often do not give information on processes. Results from synthetic waters are not necessarily

representative for natural systems (*56*), but provide more information on basic principles. Additional mechanistical descriptions can be deduced from dynamic studies (*97-98*), which determine aggregation, coagulation and particle growth rate constants as well as evolution of particle size or sedimentation rate (*89; 92*). Also, in natural systems hydraulic and hydrochemical variations should be taken into account. Thus, testing a wide range of water constituents concentrations might help to understand ENP behavior in aquatic systems.

The present paper investigates the stability of TiO_2 nanoparticles in the presence of mono and divalent ions and NOM in a wide but realistic range of concentrations and pH values. TiO_2 has been chosen since it is commonly used ENP in consumer products (*78*) and can be found in the environment already (*37*). Additionally, P25-TiO_2 (Evonik, Germany) has been selected as a representative of manufactured nanomaterials by the Organization for Economic Cooperation and Development (OECD) to be tested under the sponsorship program.

The first objective of this study was to investigate the effects of multiple competing ions on the stability of TiO_2 nanoparticles under conditions that cover a range of hydrochemical conditions typically encountered in natural aquatic systems. We hypothesized that the combination of several electrolytes at concentrations found in natural freshwaters will reveal regions of TiO_2 nanoparticle stability and instability further, enabling the estimation of TiO_2 stability in arbitrary surface waters with known hydrochemical composition.

3.3 Material and methods

Electrolytes composition and pH were varied by a semi-automated titration and sampling procedure. Samples were taken from the supernatant at defined depth (2 cm) and after a defined aggregation and sedimentation period (15 hours) comparable to other stability tests (*124*). Particles in the supernatant were characterized by measuring their concentration, hydrodynamic diameter and electrophoretic mobility. Subsequently, the stability of TiO_2 was further studied in well-characterized natural and synthetic test water.

3.3.1 Nanoparticles

TiO_2 P25 (Evonik, Germany) was obtained from a batch produced for the OECD testing program. A detailed description of the TiO_2 material is given in the Supporting Information (Table 2).

Table 2. Characteristics of TiO_2 P25

		Titanium dioxide
	unit	**Aeroxide P25 (1)**
CAS-Nr.		13463-67-7
EG-Nr.		236-675-5
TiO_2 content	%	99.9
HCl content	%	0.14
Anatase content	%	88
Rutile content	%	12
Average primary particle size (TEM)	nm	19.8
Particle size (d50) according to ISO 13320	nm	52.2
Specific surface area (BET)	$m\ g^{-2}$	57
Density	$g\ cm^{-3}$	3.8
pH value (40 g L^{-1})		3.6
Ignition loss	w%	1.1
Loss on drying	w%	1.3

The TiO_2 stock dispersions for the matrix testing were prepared by suspending TiO_2 particles (50 mg L^{-1}) in Milli-Q water, followed by 30 min. ultrasonication (2×60 W indicated power, Sonorex RK 106, Bandelin, Germany). Water (MQ-water) was from a Millipore Advantage A10 system (Millipore, Billerica, US) equipped with a Bio-Pak™ ultrafilter (5000 Dalton molecular weight cut-off) for final clean-up. Suwannee River natural organic matter purchased from the International Humic Substances

Society (*127*) was used as a NOM surrogate. NOM has been calculated to DOC concentration (factor 0.41) and is therefore used as synonym, if not stated otherwise. 10 mM HCl and $NaHCO_3$ stock solutions were prepared for titration. All reagents were of analytical grade purchased from Fisher Scientific, Austria. The final TiO_2 concentration in the test vessels prior to the aggregation/settling period was 25 mg L^{-1}.

3.3.2 Natural and synthetic water samples

Water samples (HOE, LUNZ, TAB, TAN, FRA, WWI and WWO) were taken from various sources: groundwater (Hoersching, Austria), lake water (Lunz, Austria), tap water (household tap, Vienna, Austria), peat bog (Tanner Moor, Austria), waste water inflow and outflow from a waste water treatment plant (WWTP, Vienna, Austria) and sea water (Normandy, France). Synthetic test water was prepared following the Environmental Protection Agency protocol (EPA-821-R-02-013) and is subsequently referred to as EPA water. All waters were 0.2 µm cellulose acetate membrane filtered (Whatman, Austria) and stored at 4°C in the dark.

Preparation of EPA synthetic test water according to the protocol (EPA-821-R-02-013)

1. Place 4 L MQ-water in plastic carboy
2. Add respective amount of $MgSO_4$, $NaHCO_3$ and KCl (seeTable 3)
3. Aerate over night
4. Add respective amount of $CaSO_4$ (see Table 3) to 1 L MQ-water in a separate flask, stir on magnetic stirrer until calcium sulphate is dissolved, add this to the 4 L
5. Aerate the combined solution vigorously for an additional 24 h to stabilize the medium

Table 3. Reagents used for the preparation of EPA very soft (VS), moderately hard (MH) and very hard (VH) water

Water type	Reagent added (mg L^{-1})				Approx. water quality		
	$NaHCO_3$	$CaSO_4$ $2H_2O$	$MgSO_4$ $7H_2O$	KCl	pH	Alkalinity (mg L^{-1})	conductivity (µS cm^{-1})
very soft	12	7.5	15.35	0.5	6.4-6.8	10.0-13	35
moderately hard	96	60	122.86	4	7.4-7.8	57-64	310
very hard	384	240	491.44	16	8.0-8.4	225-245	1046

3.3.3 Water chemistry

Dissolved organic carbon (DOC) was measured using a GE Power & Water DOC analyzer (Sievers 900, USA). The pH and conductivity (EC) were measured using a portable pH/conductivity meter (SenTix 61 and TetraCon 325 probes, respectively, WTW, Germany). Inductively coupled plasma optical emission spectroscopy (ICP-OES) (Optima 5300 DV, Perkin-Elmer, Austria) was used to analyze major cations, i.e. Na^+, K^+, Ca^{2+}, Mg^{2+}, Si^{2+}, Mn^{2+} and Al^{3+}. Cl^-, NO_3^- and SO_4^{2-} were analyzed by ion chromatography (ICS-1000, Dionex, Austria). In the natural water hydrogen carbonate was determined by titration to pH 4.3, the HCO_3^- concentration in the EPA water was known from the protocol (*128*).

3.3.4 Nanoparticle analysis

For the test matrix we suspended TiO_2 in MQ-water, added NaCl, $CaCl_2$, Na_2SO_4 or NOM through one of the dosing units and titrated with HCl/$NaHCO_3$ to the chosen pH values. HCO_3^- was used to counter pH shifts due to CO_2 equilibration while at the same time being the dominant buffer in most natural aqueous systems. We followed the titration and sampling protocol described earlier in v.d. Kammer et al. (*124*). In short, the auto-titration system (Metrohm Titrando 836) was equipped with four individual dosing units (Metrohm Dosino 807) and 20 or 50 mL burettes (Metrohm Dosino 800) and was used together with a robotic sample processor (Robotic sample Processor XL 815) and a fast reaction pH electrode (Metrohm Aquatrode Plus), all devices were purchased from Metrohm, Switzerland. We placed 25 mL of the TiO_2 stock suspension (T_{stock}) in the polyethylene test vessels and then added the electrolyte or NOM stock solution (E/N_{stock}) in respective amount. Preliminary tests revealed the amount of $NaHCO_3$ or HCl needed ($A/B_{estimate}$) to achieve the target pH. To consistently reach a total volume of 50 mL (V_{tot}) in each sample the system calculates the amount of MQ-water (MQ_{final}) needed by the following equation:

$$\mathbf{V_{tot} - T_{stock} - E/N_{stock} - A/B_{estimate} = MQ_{final}} \qquad \textbf{Equation 5}$$

Electrode calibration (buffers used were pH 4, 7and 10, Fisher Scientific, Austria) was performed before, after one experimental set, the drift was below ±0.1 pH units. After 15 hours sedimentation 10 mL were sampled with a stainless steel needle in

exactly 2 cm depth through a hole in the lid. We analyzed the sample on its particle size distribution, concentration and zeta potential. The pH and electric conductivity was measured in the remaining suspension.

For tests with the natural and EPA water a stock suspension of 1250 mg L^{-1} TiO_2 was ultrasonicated for 30 minutes. One mL of this suspension was added to 49 mL of natural or EPA water to reach a TiO_2 concentration of 25 mg L^{-1}. As in v.d. Kammer et al. (29) the nanoparticle stability was operationally defined as the fraction of particles in the supernatant after a 15 hour sedimentation time. After 15 hours sedimentation we sampled 10 mL from the supernatant and determined the pH in the remaining 40 mL. The supernatant was analyzed for nanoparticle concentration, hydrodynamic diameter and electrophoretic mobility and we followed the measurement protocol as described in v.d. Kammer et al. (*124*). In brief, hydrodynamic diameter and electrophoretic mobility were determined by photon correlation spectroscopy (PCS) with a Zetasizer ZS (Malvern Instruments, UK). The method of cumulants was applied to determine the intensity-weighted diffusion coefficient (z-average, 1^{st} cumulant), while the CONTIN mode was used to derive the particle size distribution and each result consists of ten stacked individual measurements of 10 s each. The electrophoretic mobility was measured using laser Doppler anemometry and the zeta potential as a proxy for the ENP surface charge was calculated from the electrophoretic mobility applying the Smoluchowski approximation. By running the experiments over a defined pH range the isoelectric point (IEP) was defined. Excluding specific adsorption and if H^+/OH^- are the only potential determining ions, the isoelectric point equals the point of zero net proton charge and the point of zero charge. The concentration of TiO_2 in the supernatant was determined by measuring the nephelometric turbidity (Hach 2100N IS Turbiditymeter, LED light source λ = 870) as described in (*83*). Detection is at 90° angle in a 25 mL glass cell, the correlation of TiO_2 concentration versus turbidity is shown below.

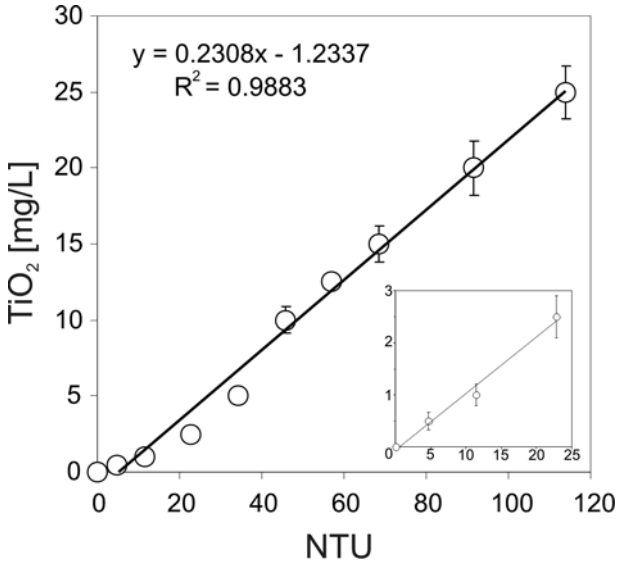

Figure 20. Concentration of TiO_2 versus turbidity measurement.

The experiments were done in triplicates (n = 3), results presented are averaged values and the standard deviation (±1SD). Results of the sedimentation tests were plotted in interpolated surface contour plots processed by the software Surfer 7.0 (Golden Software, Inc.) with the inverse distance weighting algorithm. Results of the sedimentation tests (concentration, particle size and zeta potential) were plotted in interpolated surface contour plots processed by the software Surfer 7.0 (Golden Software, Inc.) with the inverse distance weighting algorithm. The interpolated surface is a distance weighted average of the observed parameters, i.e. with increasing distance between data points their relative contribution to the interpolation declines with distance from the grid node according to equation below:

$$Z_j = \frac{\sum_{i=1}^{n} \frac{Z_i}{h_{ij}^{\beta}}}{\sum_{i=1}^{n} \frac{1}{h_{ij}^{\beta}}} \quad \text{with} \quad h_{ij} = \sqrt{d_{ij}^2 + \delta^2} \qquad \text{Equation 6}$$

where h_{ij} is the effective separation distance between grid node j and the neighboring point i. Z_j is the interpolated value for grid node j; Z_i are the neighboring points; d_{ij} is the distance between the grid node j and the neighboring point i; β is the weighting power and δ is the smoothing parameter determined with 0.2.

3.4 Results and discussion

3.4.1 Behavior and characteristics of TiO_2 in the testing matrix

In the present study we stabilized the pH by adding carbonate (as $NaHCO_3$) to establish a water chemistry being typical for most buffered systems in nature. The influence of solely HCO_3^- on the stability of TiO_2 nanoparticles has been tested (Figure 21).

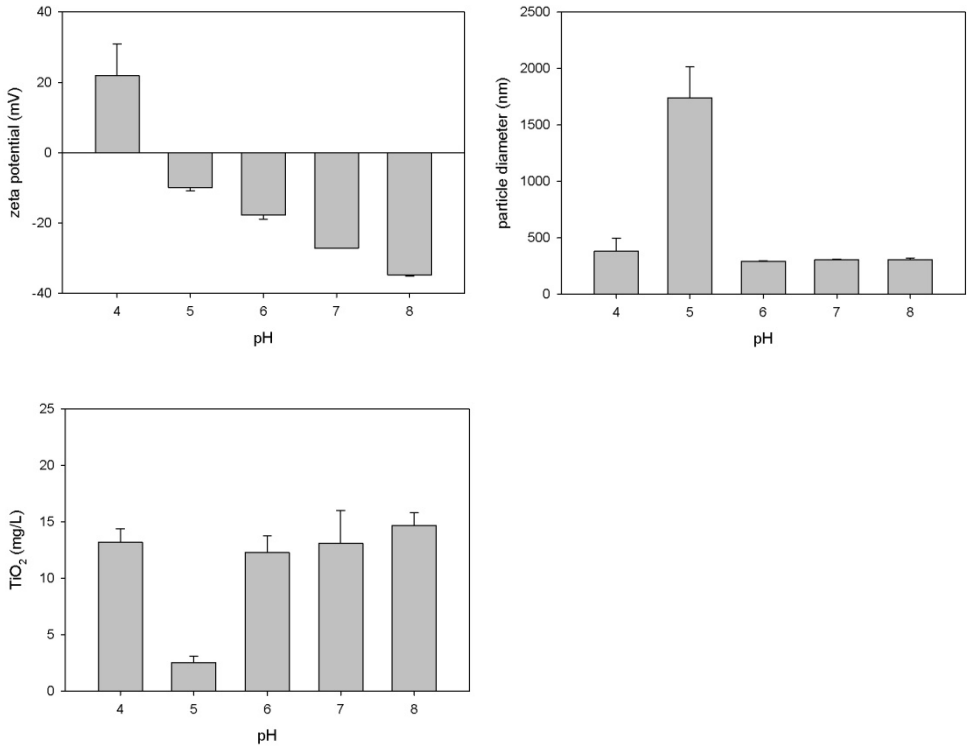

Figure 21. The zeta potential, particle diameter and concentration of TiO_2 nanoparticles in MQ-water titrated to various pH values with 10 mM HCO_3^- and 10 mM HCl for pH 4, respectively.

At pH above and below the IEP TiO_2 particles (residual concentration 13 mg L^{-1} or 52% of the initial concentration which was 25 mg L^{-1} in all experiments) had a diameter of ~300 nm. At the IEP (pH 5.0) the particles remained in the supernatant (20%) were large aggregates of > 2.5 µm in diameter (Figure 22).

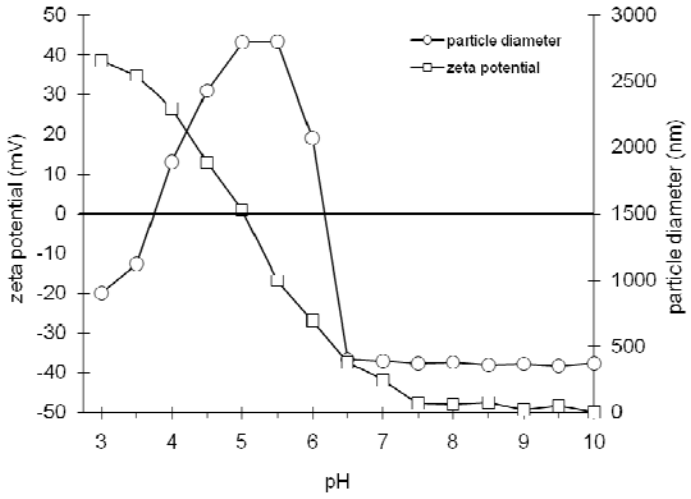

Figure 22. The isoelectric point (IEP) for TiO_2 (25 mg L^{-1}) and respective particle diameter has been determined in MQ-water from pH 3 to 10 (HCO_3^- titration).

The stability of TiO_2 in the presence of sodium chloride is dominated by the NaCl concentration and the pH (Figure 23). Below 5 mM NaCl the system is relatively stable with TiO_2 concentrations > 6 mgL^{-1} (24% of initial) above and below the IEP and is predominantly regulated by the pH. Above ~5 mM NaCl particles are aggregated to entities larger than 1.5 µm and the concentration in the supernatant is reduced (< 6 mg L^{-1}). This is congruent with finding from French et al. who investigated the stability of TiO_2 in a dynamic, time resolved set-up and found strong aggregation in the beginning of the experiment at pH values above 5.8 (*89*). The IEP is shifted from pH 5 to pH 6.5 with increasing NaCl (from 0.1 to 500 mmol L^{-1}) indicating a weak interaction of the Na^+ with the surface of the TiO_2 at higher concentrations. We conclude that at elevated NaCl concentrations and higher pH values aggregation of TiO_2 is promoted due to interactions of sodium with the TiO_2 surface.

The effects on TiO_2 stability of a positively charged divalent ion and a monovalent anion were investigated by using calcium chloride (Figure 23). In the test matrix we used $CaCl_2$ in concentrations ranging from 0.01 to 10 mmol L^{-1}. Typical environmental concentrations of calcium range from 1.0 mg L^{-1} in rainwater, 40 mg L^{-1} in surface water to 430 mg L^{-1} in seawater (Table 4). Increasing calcium chloride concentration resulted in a charge reversal at pH values above 6.5 and an IEP shifting from acidic to basic pH. TiO_2 particles are generally aggregated in the

presence of Ca^{2+} (> 1000 nm) but two regions of stability can be identified. One region is at pH 4 to 5 (Ca^{2+} > 0.05 mmol L^{-1}) resulting in TiO_2 concentrations > 8 mg L^{-1} and particle diameters < 900 nm. However, above 5 mM the particles aggregated (> 900 nm) accompanied by a decrease of TiO_2 in the supernatant (< 7 mg L^{-1}). The second region of stability is at pH > 6 and Ca^{2+} concentrations < 0.05 mM (> 6 mg L^{-1} and < 900 nm). These findings are in agreement with von der Kammer et al. (*124*) and Domingos et al. (*95*).

Table 4. Composition of natural water types

	Rain water [2]	**Lake water** [3]	**River water** [3]	**Seawater** [4]
	mg L^{-1}	mg L^{-1}	mg L^{-1}	mg L^{-1}
Na^+	1.1	0.0	3.1	11145
K^+	0.3	0.0	0.9	414
Mg^{2+}	0.4	6.0	8.7	1339
Ca^{2+}	1.0	45.6	43.0	429
Cl^-	1.1.	2.5	2.8	20065
HCO_3^-	1.2	12.6	9.4	1787
SO_4^{2-}	4.2	15.0	53.0	230

We used sulfate as sodium sulfate for a typically occurring divalent anion in concentrations ranging from 0.01 to 10 mmol L^{-1} (Figure 23). Compared to the monovalent Na^+ and the divalent Ca^{2+} the presence of the divalent anion SO_4^{2-} strongly promotes aggregation under all tested conditions. In general 80% of the initial TiO_2 was removed from the supernatant due to aggregation and sedimentation. The IEP is outside the parameter window (< 4) due to interaction of the SO_4^{2-} ion with the surface of the TiO_2 and increase of the negative zeta potential. The zeta potential of TiO_2 in SO_4^{2-} suspension is nearly independent of the Na_2SO_4 concentration and mainly controlled by the pH. The shift of negative zeta potential (-30 mV) towards a minimum (-5 mV) from high to low pH is congruent with the increase of particle diameter from 1000 to 1600 nm. The comparison with the NaCl matrix (Figure 23) shows the differences between the influence of the chloride and the sulfate anion on TiO_2 stability. At certain concentrations a charge neutralization may be induced as reported for anatase particles in SO_4^{2-} suspension (*129*).

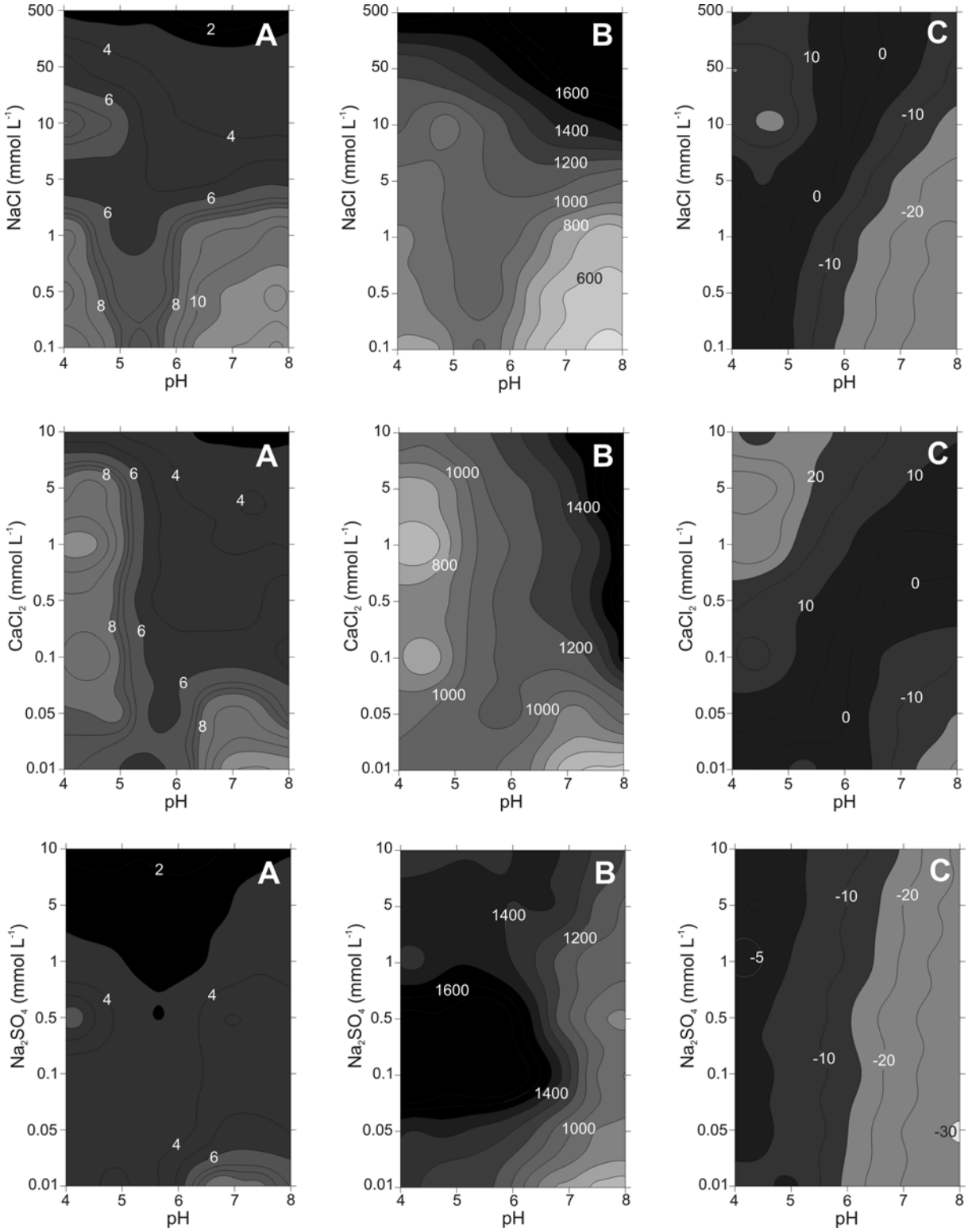

Figure 23. Regions of TiO_2 nanoparticle stability expressed as the concentration (A), particle diameter (B) and zeta potential (C) in the presence of NaCl, $CaCl_2$ and Na_2SO_4.

The combined effects of a divalent positive Ca^{2+} and a negative SO_4^{2-} charged ion on the TiO_2 stability is represented in Figure 24. In this set the concentration of $CaSO_4$ is ranging from 0.01 to 5 mmol L^{-1}. Only at pH < 5 and $CaSO_4$ concentrations below 0.1

mM TiO_2 particles are less aggregated with diameters of < 1000 nm and concentrations > 6 mg L^{-1}. Above both thresholds TiO_2 is aggregated with average particle diameters of up to 1600 nm and concentrations less than 20% of the initial concentration. The zeta potential is increasing from -20 mV at pH 8 to zero at pH < 5. With increasing $CaSO_4$ (1 mM) the IEP shift towards pH 6. However, the impact of Ca^{2+} adsorption to TiO_2 at pH 4 is still visible by a slightly positive zeta potential at intermediate $CaSO_4$ concentrations. Figure 24 shows the effect of two interacting divalent but counter charged ions with the TiO_2 surface. While SO_4^{2-} 'alone' with the nearly indifferent sodium as counter ion shifted the zeta potentials at all concentrations and all tested pH negative and the calcium 'alone' with the nearly non interacting chloride as counter ion shifted the zeta potential positive at elevated concentrations and low pH here a balancing of both effects is visible. Calcium and sulfate both result in a low zeta potential magnitude and corresponding colloidal instability of TiO_2 particles.

NOM adsorbs to the surface of metal oxides and may reduce or neutralize an existing positive surface charge as well as (at sufficient concentrations) induce a reversal from positive to negative surface charge. The effects of NOM were tested by choosing concentrations ranging from 0.2 to 41.1 mg L^{-1} DOC (Figure 24). Above 0.4 mg L^{-1} DOC the organic matter throughout stabilizes the TiO_2 nanoparticles in suspension which is congruent with finding by other studies (*93*). Zhang et al. (2009) tested the stability of TiO_2 at various DOC concentrations and observed stability over 2 hours with 0.4 mg L^{-1} DOC. Below 0.2 mg L^{-1} DOC and with pH < IEP the particles are aggregated (~1000 nm) and the zeta potential is least negative (-10 mV). Above this DOC concentration and pH > IEP TiO_2 particles are screened with organic matter with a zeta potential >-20 and particle diameters of 200 nm. Having shown the effects of weakly and strongly interacting, surface potential determining inorganic ions and the stabilizing effect of even small amounts of NOM we aimed to demonstrate the effect of a combination of both. As Ca^{2+} interacts with NOM and TiO_2 and acts as a strong coagulant we chose $CaCl_2$ as the additional reagent in a multicomponent testing (*95-96*). We set the NOM concentration to 1 mg L^{-1} DOC as background and tested a range of $CaCl_2$ concentrations from 0.01 to 10 mmol L^{-1} over the pH range from 4 to 8 (Figure 24).

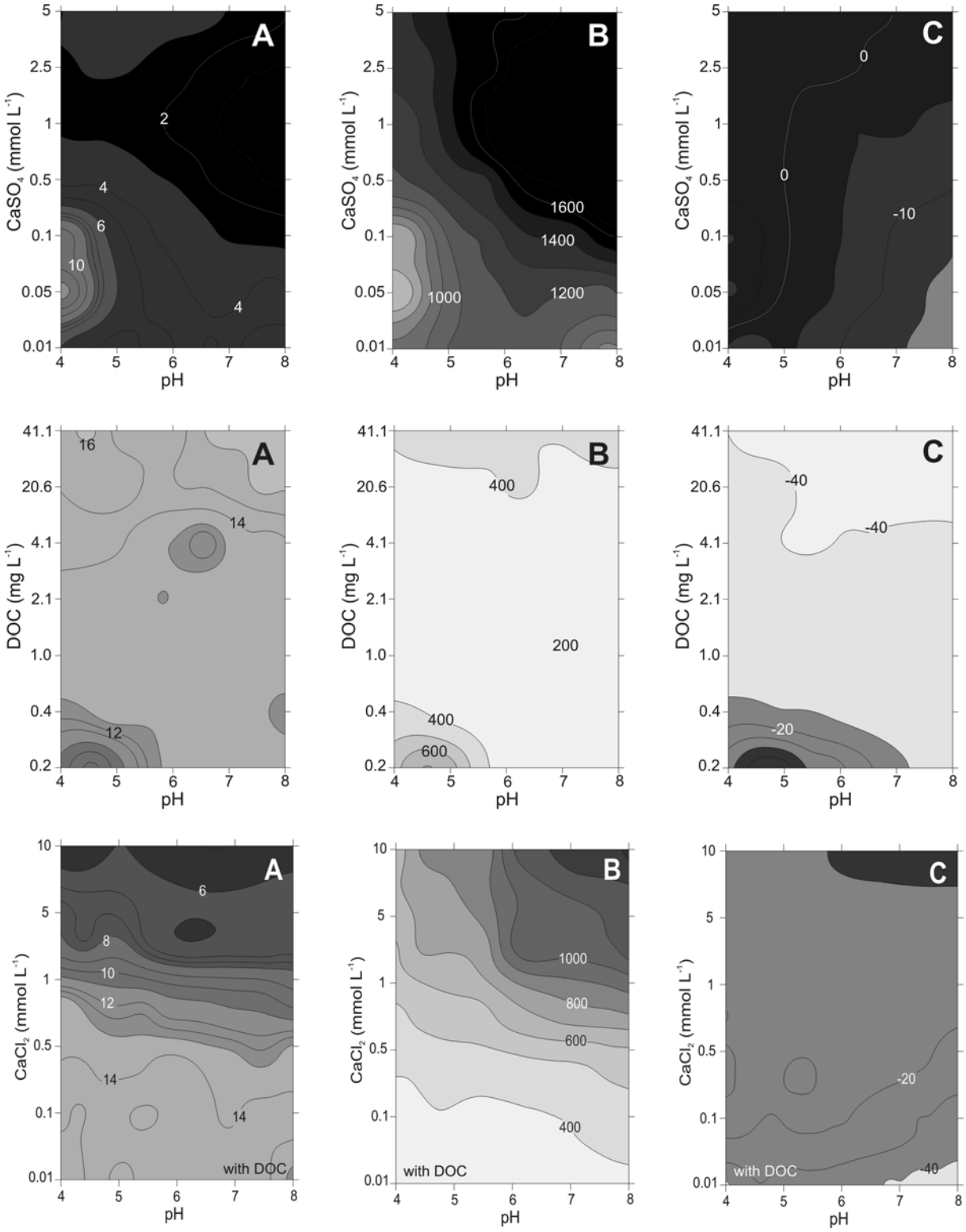

Figure 24. Regions of TiO_2 nanoparticle stability expressed as the concentration (A), particle diameter (B) and zeta potential (C) in the presence of $CaSO_4$, DOC and $CaCl_2$ with a DOC background of 1 mg L^{-1}.

In this system the relatively low NOM concentration of 1 mg L^{-1} DOC completely changes the behavior of the TiO_2. At $CaCl_2$ concentrations below 1 mmol L^{-1} elevated colloidally stable concentrations of TiO_2 are observed (≥ 50% of the initial concentrations). This equals exactly the concentrations found in the NOM matrix at 1 mg L^{-1} DOC and are higher than those of any pure inorganic matrix in this test. Apart from this remarkable effect of NOM blow 1 mM $CaCl_2$ the $CaCl_2$ concentration rather than the pH further controls the stability of TiO_2 in this test. With increasing $CaCl_2$ concentration the magnitude of the negative zeta potential is reduced at all pH. The according reduced colloidal stability can be related to the reduction in electrostatic stabilization. It is not possible to distinguish between effects of compression of double layer thickness and reduction of NOM charge density by complexation of Ca^{2+} by the NOM carboxyl groups. No indications for a steric stabilization by the NOM are observed. Above 1 mM $CaCl_2$ a slight increase of zeta potential with increasing pH and an even more expressed increase in aggregate size is observed. This is remarkable, since at low pH protonation of the NOM accompanied by reduction of the negative surface potential of the surface adsorbed NOM was expected. The observed behavior may be caused by the complexation of Ca^{2+} by carboxyl functional groups in the NOM structure (*130*) or by a combined effect of reduction of NOM adsorption to the TiO_2 followed by adsorption of Ca^{2+} to negatively charged surface functional group. Although the nanoparticles are coated with NOM the aggregation is enhanced in the presence of $CaCl_2$ and 24% to 56% of the initial TiO_2 concentration remained stable. The difference to the pure DOC plot is that the effect of HCO_3^- is overruled by the Ca^{2+}. Above 0.5 mM $CaCl_2$ we observed an increase of particle diameter from 260 to 900 nm at pH < 6, and strong aggregation occurred at pH > 6 with particle diameters of 1.7 µm concomitant with a lower negative zeta potential.

3.4.2 Behavior and characteristics of TiO_2 in natural and EPA waters

A range of waters including marine, fresh and waste waters have been selected in order to cover a range of different naturally occurring types of waters. The chemical characteristics of are summarized in Table 5. The pH does not differ much between sources (except the low buffered peat bog water from a granite source rock, pH 5.2). The ionic strength (IS: 0.5 to 146 meq L^{-1}) and the DOC content (< 0.5 to 68 mg L^{-1}), however, varies significantly. Additionally, three synthetic waters proposed by the

EPA (*128*) were chosen to cover different pH ranges (pH 6 to 8) and hardness (soft to hard water). The IS of the EPA waters is ranging from 0.3 meq L^{-1} to 9.4 meq L^{-1}.

Table 5. Water chemical parameters of natural and EPA synthetic water

		Ground water	Lake water	Tab water	Peat bog water	Sea water	Waste water inflow	Waste water outflow	EPA very soft	EPA moderately hard	EPA very hard
	unit	**HOE**	**LUNZ**	**TAB**	**TAN**	**FRA**	**WWI**	**WWO**	**VS**	**MH**	**VH**
EC	µS cm^{-1}	363	246	295	41	56500	1209	1012	35	310	1046
DOC	mg L^{-1}	1.57	2.12	1.03	37.2	<0.5	67.5	10.1	<0.5	<0.5	<0.5
pH		7.8	7.9	8.0	5.2	8.0	8.1	8.2	6.4	7.4	8.4
IS	meq L^{-1}	3.5	1.6	1.8	0.5	146.5	2.9	2.5	0.3	2.5	9.6
HCO_3^-	mg L^{-1}	290.3	145.2	160.9	10.1	1491.0	170.0	120.0	8.0	63.6	254.5
Na^+	mg L^{-1}	12.4	n.d	0.1	1.2	8500.0	37.3	35.7	4.0	32.4	129.5
K^+	mg L^{-1}	3.2	n.d	n.d	0.6	340.0	17.8	9.3	0.3	2.1	8.4
Ca^{2+}	mg L^{-1}	92.9	46.2	50.8	3.6	430.0	47.7	43.9	2.1	17.2	68.6
Mg^{2+}	mg L^{-1}	20.2	6.6	10.3	0.4	1300.0	12.5	12.1	1.7	13.9	55.7
Mn^{2+}	mg L^{-1}	n.d	n.d	n.d	0.2	n.d	n.d	n.d	n.d	n.d	n.d
Cl^-	mg L^{-1}	18.2	0.8	1.6	7.0	22523.1	60.7	55.9	0.2	1.9	7.6
NO_3^-	mg L^{-1}	23.4	3.6	4.8	3.0	n.d	n.d	6.9	n.d	n.d	n.d
SO_4^{2-}	mg L^{-1}	28.5	2.2	16.4	12.0	2925.5	44.5	57.5	8.0	41.4	298.0
Si^{2+}	mg L^{-1}	3.6	0.7	0.8	5.26	n.d	1.7	1.9	n.d	n.d	n.d
Al^{3+}	mg L^{-1}	n.d	n.d	n.d	0.12	n.d	n.d	n.d	n.d	n.d	n.d
Fe^{3+}	mg L^{-1}	n.d	n.d	n.d	3.50	n.d	0.1	n.d	n.d	n.d	n.d

n.d. = not detectable; all water 0.2 µm filtered

3.4.3 Stability of TiO_2 in natural, waste and synthetic EPA waters

The stability of TiO_2 in natural water is strongly influenced by the presence of DOC and the concentration of mono- and divalent ions (Table 6). The concentration of TiO_2 in the supernatant in the natural water samples is decreasing with decreasing DOC content. The organic matter in the low mineralized peat bog water (TAN) stabilized the TiO_2 nanoparticles most effectively (24 mg L^{-1} TiO_2 in the supernatant). Congruent to the TiO_2 concentration we found small particle sizes (TAN: 219 nm) and negative surface charges (TAN: -26) which has been shown in other studies for carbon nanotubes (*111*), iron bearing oxides (*131*) and metal oxide nanoparticles (*93*).

Table 6. Aggregation state of TiO_2 nanoparticles in natural and synthetic EPA water. The particle diameter (z-average), zeta potential and concentration as averages of 3 replicates (n = 3) and ±1SD were analyzed in the supernatant after 15 hours sedimentation.

		Ground water	Lake water	Tab water	Peat bog water	Sea water	Waste water inflow	Waste water outflow	EPA very soft	EPA mod. hard	EPA very hard
	unit	**HOE**	**LUNZ**	**TAB**	**TAN**	**FRA**	**WWI**	**WWO**	**VS**	**MH**	**VH**
particle diameter	nm	1159 (±154)	1184 (±54)	1173 (±118)	219 (±10)	1344 (±92.4)	750 (±55.1)	1208 (±91.5)	1194 (±165)	1477 (±90)	1524 (±96)
zeta potential	mV	-0.5 (±0.6)	-14.6 (±0.6)	-8.7 (±0.3)	-26.1 (±0.2)	+1.7 (±2.2)	-17.0 (±1.18)	-13.5 (±0.8)	-19.5 (±1.6)	-15.6 (±0.6)	-9.7 (±0.2)
Colloidal stable fraction	mg L^{-1}	2.2 (±0.6)	2.3 (±0.1)	2.2 (±0.2)	23.8 (±1.2)	1.0 (±0.1)	14.6 (±2.2)	8.9 (±1.5)	7.5 (±0.7)	2.4 (±0.1)	1.1 (±0.4)

all water 0.2 µm filtered

Compared to the TAN sample the 0.2 µm filtrated WWTP inflow has higher DOC content (68 mg L^{-1}) but the TiO_2 stability was decreased. The remaining 15 mg L^{-1} TiO_2 particles had a diameter of 750 nm and a zeta potential of -17 mV. The IS and specifically the presence of divalent ions (WWI: Ca^{2+} 48 mg L^{-1} and SO_4^{2-} 45 mg L^{-1}) is promoting aggregation as has been shown in the matrix tests visible in Figure 23. Some studies propose destabilizing effects due to bridging effects or charge neutralization in the presence of NOM and Ca^{2+} (*19; 97*). This is in accordance with Zhang et al. (*93*), who found a threshold of 4 meq L^{-1} Ca^{2+} inducing aggregation of NOM coated TiO_2 nanoparticles due to the reduction of the energy barrier. In our study we found increased aggregation for samples with Ca^{2+} exceeding 2 meq L^{-1} (Figure 23 and Table 6). For those samples the zeta potential was close to the IEP (HOE: -0.5, TAB: -8.7, FRA: +1.7, VH: -9.7 mV) resulting in aggregation and sedimentation of nearly 90% (Table 6).

Additionally to the natural waters we tested the stability of TiO_2 in a near natural test water of reduced complexity as well. We used the EPA proposed very soft (VS), moderately hard (MH), and very hard (VH) types (*128*). These waters are in equilibrium with CO_2, pH is stable at 6.4 (VS), 7.4 (MH) and 8.4 (VH), with increasing IS from 0.3 to 9.6 meq L^{-1} and an electrical conductivity from 35 to 1046 µS cm^{-1} for VS, MH, VH EPA water, respectively. In the EPA waters the TiO_2 stability is

decreasing with increasing pH and IS. The zeta potential is -20 mV (VS), -16 mV (MH) to -10 mV (VH). The particle diameter of the remaining 30% (VS) and 10% (MH) and 5% (VH) TiO_2 in the supernatant is increasing from 1190 nm (VS), 1480 nm (MH) to 1520 nm (VH). This finding is supported by other studies which found a decrease of negative surface charge with increasing IS (*92*). Our results show that the behavior of TiO_2 nanoparticles in natural water is governed by the presence of organic matter and the concentration of electrolytes. Further, we demonstrate that although the water chemistry varies significant there are similarities in the behavior of TiO_2 in the chosen water types (e.g. groundwater and lake water).

3.4.4 Predictive potential of the test matrix

Having demonstrated the usefulness of the matrix testing to elucidate general behavior of TiO_2 under simplified but typical hydrochemical conditions the comparison with TiO_2 stability in natural and near natural waters can demonstrate how the synthetic matrix test results can be used to predict the behavior in natural waters and test media. There is a clearly expressed need for appropriate and standardized test methods for the characterization and measurement of nanoparticles (*33*). One of the critical knowledge gaps is related to the uncertainties about ENP behavior (e.g. dispersion or aggregation) in the aquatic environment. The state of dispersion will alter the toxicity of nanoparticles (*45; 55; 120*) and change the transport behavior (*132-134*).

The most important step to relate the matrix testing to real natural waters is to identify which matrix represents the natural water best. The natural waters as well as the synthetic EPA waters were therefore classified by identifying the water chemistry through a STIFF diagram plotting procedure (developed by H.A. Stiff 1951).

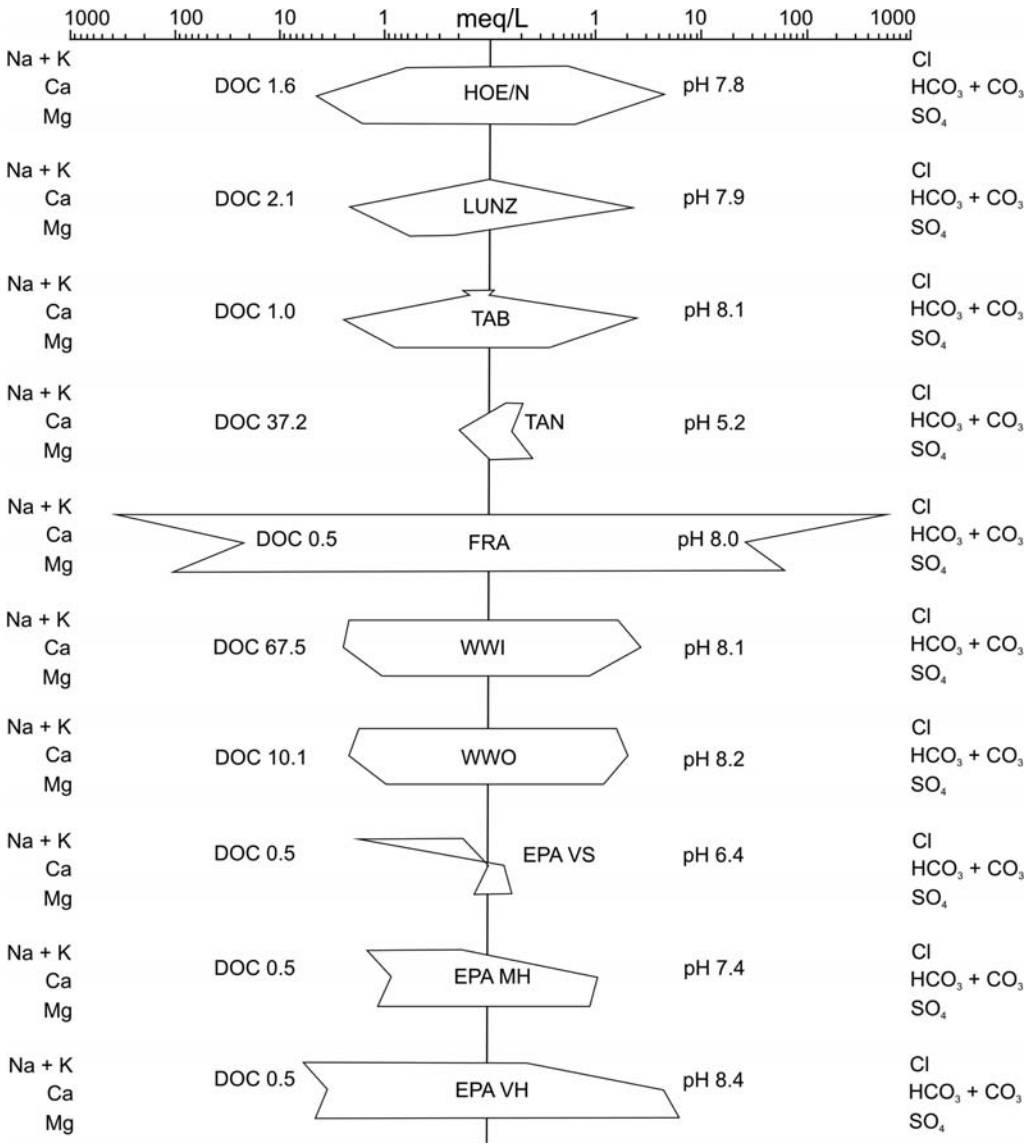

Figure 25. Stiff diagram for a classification of water types on the basis of the water chemistry. The concentration of ions and DOC is in mg L^{-1}.

This enables the correct choice of the related matrix testing plot (FIGURE AND FIGURE). Ground water (HOE) is classified as a Ca^{2+} type and lake water (LUNZ), tab water (TAB), and EPA waters (VS, MH, VH) as Ca^{2+}/SO_4^{2-} types. The organic rich waters such as peat bog (TAN) and the waste water inflow (WWI) and outflow (WWO) were rated as Ca^{2+}/DOC types. The seawater (FRA) was excluded from further studies due to ion concentrations exceeding the test matrix by a factor greater than 10. The interpolated values for the TiO_2 concentration, particle diameter and zeta potential from the test matrix were extracted. The value from the natural and EPA water was plotted versus the corresponding value in the test matrix (Figure 26).

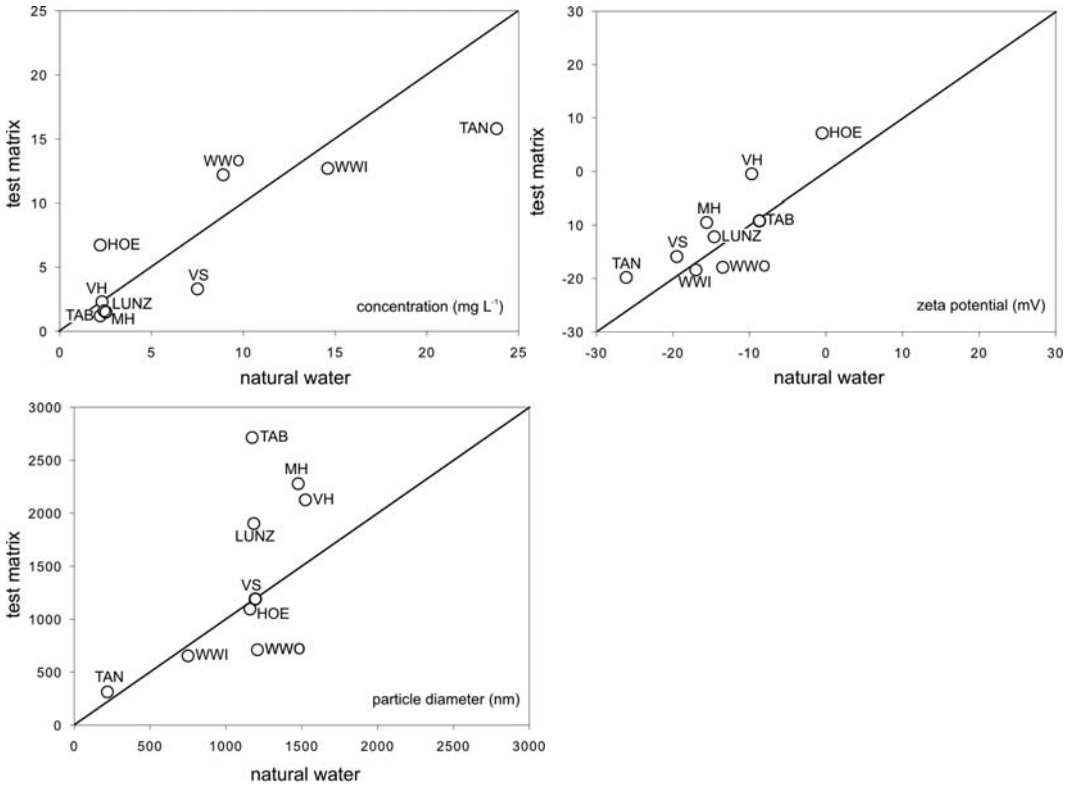

Figure 26. Correlating TiO_2 concentration, zeta potential and particle diameter in natural/synthetic water with results from the respective test matrix.

The results from the test matrix characterize the natural and EPA waters well, however, in some cases the test matrix underestimates (TAN) or overestimates (HOE, WWO) the measured value in those waters (Figure 26). There is a considerable amount of mono- and divalent anions (NO_3^- and SO_4^{2-}) present in the natural water samples, which promote aggregation (Table 6). The results from WWTP inflow (WWI) are well represented in the test matrix. Due to the high organic content TiO_2 nanoparticles are stabilized. Limbach et al. found stabilizing effects of waste water on cerium oxide nanoparticles which is attributable to the peptides (component of digested proteins) in the waste water (*39*). The NOM surrogate is stabilizing the TiO_2 particles less efficiently than the natural organic rich water (TAN) and consequently the test matrix underestimates the concentration of TiO_2 in the supernatant. The adsorption and hence stabilizing capacity of NOM is correlating with their carbon functionality (*59*). Moreover the TAN NOM is peat bog derived while the SRNOM used in the test matrix is surface water derived. The TAN sample might have more functional groups available and adsorption to TiO_2 might be stronger. We see evidence for a NOM-type related difference in TiO_2 stabilization but to verify this

observation has been outside the scope of this study. Also the presence of Ca^{2+} in the test matrix will promote aggregation. However, if the results from the TAN sample plotted in the DOC-matrix (Figure 24), the test matrix would overestimate the zeta potential by a factor of 1.6. Surprisingly, the very soft EPA water (VS) with the lowest IS was not well represented by the test matrix (Figure 26). The TiO_2 concentration in the EPA water is reduced by a factor of 2.3 compared to the value received from the corresponding test matrix (Ca^{2+}/SO_4^{2-}-matrix). The correlation for zeta potential measurements fits very well. However, the matrix systematically underestimates the zeta potential of several samples (TAN, VS, MH, VH, HOE). This is due to the low concentration of DOC in all the natural samples which is not represented in the pure inorganic matrix tests used to predict the behavior in these waters. With increasing NOM adsorption to the TiO_2 surface zeta potentials are more negative (e.g. *93*) and the correlation of natural samples (WWI, WWO) fits well to the matrix (Ca^{2+}/DOC).

The particle size analysis in the EPA water and in the matrix does not match well for aggregated systems, i.e. LUNZ, TAB, MH and VH. The algorithm for the calculation of the hydrodynamic diameter is based on the assumption that particles in suspension are spherical, which is not the case for aggregated TiO_2 structures. The applicability of dynamic light scatter techniques for aggregated and heterogeneous dispersions is therefore limited (*117; 135*). Also, the very low concentration of particles in the supernatant of those four samples (< 3 mg L^{-1}) did not allow a representative analysis of the particle diameter by PCS. Therefore, particles with a diameter > 1.5 µm and polydispersity index PDI > 0.7 were excluded from the graphical presentation in Figure 26.

3.4.5 Environmental implications

The stability of TiO_2 nanoparticles is regulated, among others, by the water chemistry in the aquatic environment. The state of aggregation determines the fate and transport in the aqueous environment and may alter ENP exposure to microorganisms. In addition, also local and/or seasonal variation of the chemistry of natural waters makes a prediction and generalization of the ENP behavior difficult. Here we presented a testing scheme for the stability and aggregation of ENP, exemplarily for TiO_2, and validated this through experiments in natural waters. From

results in synthetic water with a wide variation of composition, ion concentration and pH we identified regions of TiO_2 nanoparticle stability and aggregation. Combining this information with results from tests in natural water we show that it is possible to predict the general behavior of TiO_2 nanoparticles. This approach is expected to succeed also for other types of nanoparticles. It allows for a standardized and comparable testing procedure and directs to a first prediction of the ENP behavior in the aquatic environment. Future work should address the effects of various types of NOM and include other engineered nanoparticles.

4 The Transport and Toxicity of Titanium Dioxide

Nanostructured TiO_2: Transport behavior and effects on aquatic microbial communities under environmental conditions

T. J. Battin, F. v.d. Kammer, A. Welhartner, S. Ottofuelling, T. Hofmann

4.1 Abstract

Industry has already commenced the large-scale production of some nanomaterials. Evidence for toxic effects of engineered nanoparticles (ENP) on model organisms is increasing. However, in order to assess the consequences of environmental hazards, a better understanding is required of the behavior of ENP in aquatic ecosystems and their impact on complex communities. In this research, through experimenting with different TiO_2 nanoparticles in stream microcosms, we have shown that microbial membranes were significantly compromised, even under ambient ultraviolet radiationandnano-TiO_2 concentrations predicted for surface waters. Our results suggest adverse effects are not necessarily only attributable to individual particles smaller than 100 nm but also to low concentrations of larger, naturallyagglomeratingTiO_2 nanoparticles. Cell membrane damage was more pronounced in free-living cells than in biofilm cells, indicating the protective role of cell encapsulation against TiO_2 nanoparticles. The generation of intracellular reactive oxygen species (ROS) further suggests nano-TiO_2-induced effects inside the microbial cells. Our findings indicate a high sensitivity of microbial communities to levels of ENP concentration that are to be expected in the environment, with as yet unknown implications for the functioning and health of ecosystems.

4.2 Introduction

The exposure of humans and the environment to engineered nanoparticles (ENP) has generated substantial research during recent years (*8; 42; 55*) and triggered discussion on regulation of the nanotechnology sector (*48*). While the potential risks of ENP are still being debated, large-scale production of commercially important ENP is either already taking place or will soon be implemented. Titanium dioxides (TiO_2)

figure among these ENP. Nano-TiO_2 was identified and recommended by the Organization for Economic Co-Operation and Development (OECD) “Working Party of Manufactured Nanomaterials” for extensive testing because of its commercial relevance and potentially adverse effects. Despite this development, the environmental concentrations of most ENP remain unknown. Exposure modeling (*78*) recently estimated emissions of carbon nanotubes (3 kg y^{-1}), nano-Ag (620 kg y^{-1}), and nano-TiO_2 (47300 kg y^{-1}) into surface waters in Switzerland; the resulting concentrations in surface waters were within the nano-and microgram range. It has been estimated that up to 10% of the ENP pass through a wastewater treatment plant and are discharged into surface waters (*39*). On the basis of the known behavior of other persistent pollutants, a 1000 to 10000-fold enrichment of ENP in river sediments seems realistic. Koelmans et al. calculated sediment enrichment factors for carbonaceous ENP to reach a maximum of 4000000 (*86*). ENP agglomeration, settling, and accumulation in sediments will largely determine the degree of exposure of planktonic and attached microorganisms. Microorganisms form the basis of the food web and serve most ecosystem functions and services within aquatic ecosystems. In streams and rivers, for instance, biofilms (surface-attached and matrix-enclosed microbial communities) contribute greatly to carbon fluxes at ecosystem and global levels (*136*). Biofilms may also interact directly with ENP. For instance, the physicochemical characteristics of the biofilm matrix (extracellular polymeric substances) determine to a certain extent the scavenging of ENP (*137*), which because of their small size are not subject to significant settling. Consequently, biofilms may be exposed to dramatically higher ENP concentrations than planktonic communities. It is therefore essential to clarify the behavior of ENP in natural aquatic ecosystems and their potential impact on complex microbial communities. Our current knowledge of nano-TiO_2 toxicity is largely based on distinct model organisms such as bacterial and algal monocultures, daphnids, and human cell lines (*81; 132; 138*). These studies applied nano-TiO_2 concentrations several orders of magnitude higher than the predicted environmental concentrations (PEC, 0.016 mg L^{-1}) in surface waters (*78*) and levels of UV radiation typically used for water sterilization (*139*) (Table 7).

Table 7. Representative publications studying the toxicity effect of high-concentration nano-TiO_2 on various organisms.

nano-TiO_2 concentration (mg L^{-1})	**Organism**	**Reference**
100 - 2000	E. coli	Cho et al. (*140*)
1000	E. coli, MS-2 phage	Cho et al. (*141*)
1000	E. coli	Gogniat and Dukan (*142*)
12.5 - 50	Daphnia magna, Desmodesmus subspucatus	Hund-Rinke & Simon (*143*)
100	Enterobacter cloacae, gram(-) bacteria	Ibanez et al. (*144*)
250 - 1250	Salmonalle, Vibrio, Listeria	Kim et al. (*145*)
1 - 1000	Norovirus	Lee et al. (*146*)
100	E.-coli, EPS-bacteria	Liu et al. (*137*)
50 – 500	Daphnia magna	Lovern and Klaper (*70*)
100 – 1000	E. coli	Maness et al. (*147*)
3 - 3000	Human cell lines	Sayes et al. (*81*)
1000	E. coli	Rincón et al. (*148*)
1000	E. coli	Rincón and Pulgarin (*149*)
250 - 1500	E. coli	Rincón and Pulgarin (*150*)

While such studies help in understanding the toxicity mechanisms, their extrapolation to the natural environment remains problematical. In this research, by experimenting with two different TiO_2 nanoparticles in stream microcosms, we have shown the effect of benthic biofilms on the transportation behavior of ENP and in turn the impact of nano-TiO_2 on microorganisms under natural conditions. We used low concentrations of agglomerated, aggregated, and polydisperse nano-TiO_2 (rather than monodisperse primary particles) under ambient levels of UV radiation to simulate ENP release into a recipient stream. Upon their entry into the stream microcosms, suspended nano-TiO_2 significantly damaged the cell walls of planktonic microorganisms. ENP deposited and accumulated in the benthic biofilms, where they compromised cells to a lesser extent than in the water column. To further clarify possible mechanisms underlying the nano-TiO_2 toxicity, we applied a cell permeant detector for reactive oxygen species (ROS) on free-living cells and found the intercellular action of ROS to parallel cell wall damage. Our results contribute to a small but growing body of information on ENP microbial cytotoxicity in natural aquatic ecosystems that correlates poorly with results from studies on monocultures (*80*).

4.3 Material and methods

4.3.1 Nano-TiO_2 preparation and characterization

We used Evonik Degussa Aeroxide P25 and Sachtleben Hombikat UV-100 as supplied by the manufacturers for TiO_2 nanoparticles. They are widely used as photocatalysts or UV filters and have been well-investigated (Table 8). P25 is an 80:20 anatase:rutile mixture with a primary particle size of about 20 nm and 50 $m^2\ g^{-1}$ specific surface area. Hombikat UV-100 is comprised of pure anatase particles, with a primary particle size of about 10 nm and a specific surface area greater than 250 $m^2\ g^{-1}$.

Table 8. Nanoparticle characteristics

Characteristics of TiO_2 Hombikat UV100 and TiO_2 P25

	TiO_2 P25, Evonik (Degussa)	**TiO_2 Hombikat UV-100, Sachtleben**	
Characteristic			**Reference**
Behaviour towards water	hydrophilic	hydrophilic	Ettlinger (*101*), Sachtleben (*102*)
Production method	flame hydrolysis of $TiCl_4$	sulfate process, precipitation	Ettlinger (*101*), Sachtleben (*102*)
Composition	80% anatase, 20% rutile; 72.6% anatase, 18.4% rutile, 9% amorphous	100% anatase; 67.2% anatase, 32.8% amorphous	Ettlinger (*101*), Jensen (*151*), Sachtleben (*102*)
Primary particle diameter [nm]	~ 21	< 10	Ettlinger (*101*), Sachtleben (*102*)
Aggregate size [nm]	1283 ± 87	1085 ± 26	this study
Zeta potential [mV]	-18.9 ± 1.7	-20.2 ± 1.3	this study
SSA BET [$m^2\ g^{-1}$]	50 ± 15	> 250	Ettlinger (*101*), Sachtleben (*102*)
Isoelectric point	6.9; 7.7	6.2; 6.1	Dutta et al. (*152*), this study
Density [$g\ mL^{-1}$] [1)]	3.7	3.9	Ettlinger (*101*), Sachtleben (*102*)
Tapped density [$g\ L^{-1}$]	~ 130	-	Ettlinger (*101*)
Drying loss, 2h at 105°C [wt%]	< 1.5	-	Ettlinger (*101*)
Purity [%]	99.5	-	Ettlinger (*101*)
Pore volume [$mL\ g^{-1}$]	0.15	0.34	Colón (*103*)
Pore size distribution	little porosity, peak at 31.5 nm	heterogeneous, peak at 3.5 nm; mesopores ~5.6 nm	Colón (*103*)
Light absorption peak [nm]	peak at 250	peak at 310	Colón (*103*)
1) determined with a pyknometer			

Although often addressed as nanoparticles, these materials are highly aggregated and are therefore better described as nanostructured materials (*153*). In aqueous dispersion, both materials exist as large and weak agglomerates built from aggregated primary particles (*47; 154-155*). We suspended particles in filtered (0.45

*μ*m cellulose acetate membrane, Schleicher & Schuell, Germany) surface water (Lunzer Untersee, Austria) and probe sonicated them (30 s) (Branson Sonifier W-250D, 25 W at 10% energy input) to break apart larger agglomerates (>1 *μ*m) and homogenize the dispersion Figure 27 (*47*). We did not aim at a full breakdown to the primary particle size because this was not feasible (*155*) but also, and more importantly, because it would not provide a realistic representation of natural conditions (*89*).

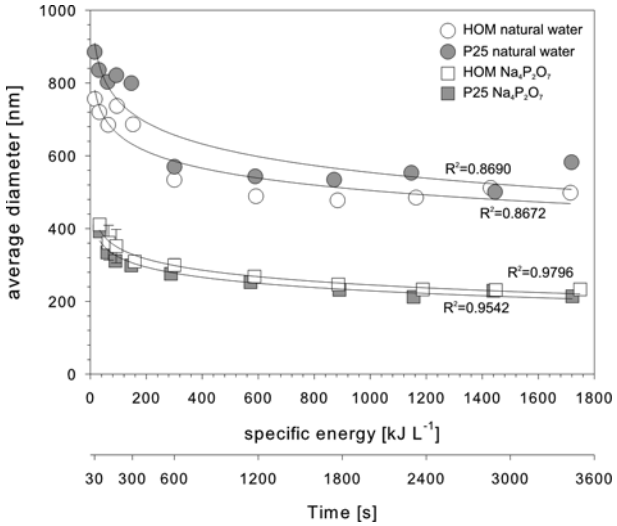

Figure 27. Average particle diameter (n=3, ±1SD) as a function of the specific US induced energy (kJ L^{-1}) for TiO_2 P25 and Hombikat UV-100 agglomerate break up in 5 mM $Na_4P_2O_7$ suspensions and natural lake water (0.45 μm CA membrane filtered, Lunzer Untersee, Austria).

Particle size distribution was measured by dynamic light scattering (DLS) at a 173° angle using a Zetasizer Nano ZS (Malvern Instruments, U.K.). We used the method of cumulants for derivation of the average particle diameter (*z*-average) and polydispersity index (PDI); CONTIN analysis was used for size distributions. Measurements were performed in triplicate, each replicate consisting of 10 individual runs of 10 s each. The electrophoretic mobility of the particles was measured with the same instrument, and the Smoluchowski approximation was used to calculate *ζ* potentials. We calculated average values for *ζ* potential and standard deviation from triplicates.

4.3.2 Experimental setups

Experiments on planktonic and biofilm communities were performed using natural surface water (Lunzer Untersee, Austria).The chemical characteristics of the water were Ca^{2+} 40.6; Mg^{2+} 6.0; Na^{+} 0.5; K^{+} 0.4; NO^{3-} 2.2; Cl^{-} 0.4; $(SO_4)^{2-}$ 2.9; and HCO_3^{-} 134.6 mg L^{-1}. Fe and Mn were below the LOD (<0.01 mg L^{-1}) as were NO_2^{-} and PO_4^{3-} (<0.02 mg L^{-1}); the ionic strength was 3.47 mmol L^{-1}. For batch experiments we amended unfiltered surface water with nutrients and glucose. At a cell abundance of 1.2 × 108 cells mL^{-1}, aliquots (40 mL) were transferred into sterile Schott bottles (100 mL) and diluted with 0.2 *μ*m-filtered water (cellulose acetate membrane, Schleicher & Schuell, Germany) to achieve an initial batch cell abundance of 9.6 × 107 cells mL^{-1}, as determined by flow cytometry (Beckman Coulter, Cell Lab Quanta, Krefeld, Germany). Triplicate batches were set up for the nano-TiO_2 treatments (5.3 mg, TiO_2 L^{-1}) and the control (without nano-TiO_2). Triplicate samples were collected initially and again after 24 h. Batches (rotary shaker 120 rpm, 24 h) were operated under simulated natural light using Phillips TL-D 58/33-640 halogen lamps (maximum emission, 500 and 600 nm; mean photon flux density, 52 *μ* mol m^{-2} s^{-1} between 380 and 780 nm). To test for a possible nonphotocatalytic impact of nano-TiO_2, we ran parallel sets (P25, Hombikat UV-100, control) under dark conditions. For biofilm growth, we adapted previously described microcosms (*156*) (Figure 28).

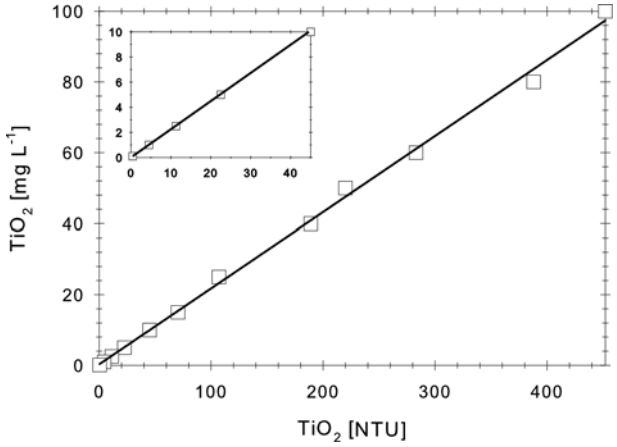

Figure 28. Technical drawing (scale: m) of the flume setup (lateral view) during re-circulation and details of the baffle construction at the flume inlet (bf: baffle, gs: glass slides, vv: valve, fl: flume, pp: pump) after Singer et al. (2006).

Glass slides served as a substratum for biofilms developing from the natural inoculum in the raw surface water under transitional flow (Reynolds number for open channel flow, 1040). Triplicate microcosms were operated for P25 and for Hombikat

UV-100 and duplicate microcosms for controls without nano-TiO_2. After 24 days of biofilm growth, each flume was switched individually to a closed recirculation system with a water depth of 15 mm. The system included a sink (glass beaker of 2000 mL, Schott Duran, Germany) and PVC tubing (2.8 m long, 7 mm I.D.); the recirculation volume was 1400 mL. P25 and Hombikat UV-100 nanoparticles (final concentration, 5.3 mg, TiO_2 L^{-1}) were injected into the respective flumes and recirculated (48 h) under the afore mentioned UV irradiation conditions. Biofilms were exposed over their entire growth to this irradiation source prior to the nanoparticle additions to exclude light-induced stress. Triplicate slides were collected (4, 24, and 48 h after the nano-TiO_2 addition) from each microcosm for further analyses.

4.3.3 Nano-TiO_2 transportation behavior

We monitored TiO_2 concentrations and particle sizes in the water column during the entire recirculation period. TiO_2 concentration was derived from nephelometric online turbidity measurements (Turbiditymeter 2100N IS, Hach, Germany) following ISO 7027 standards and applying a mass concentration calibration curve (Figure 29).

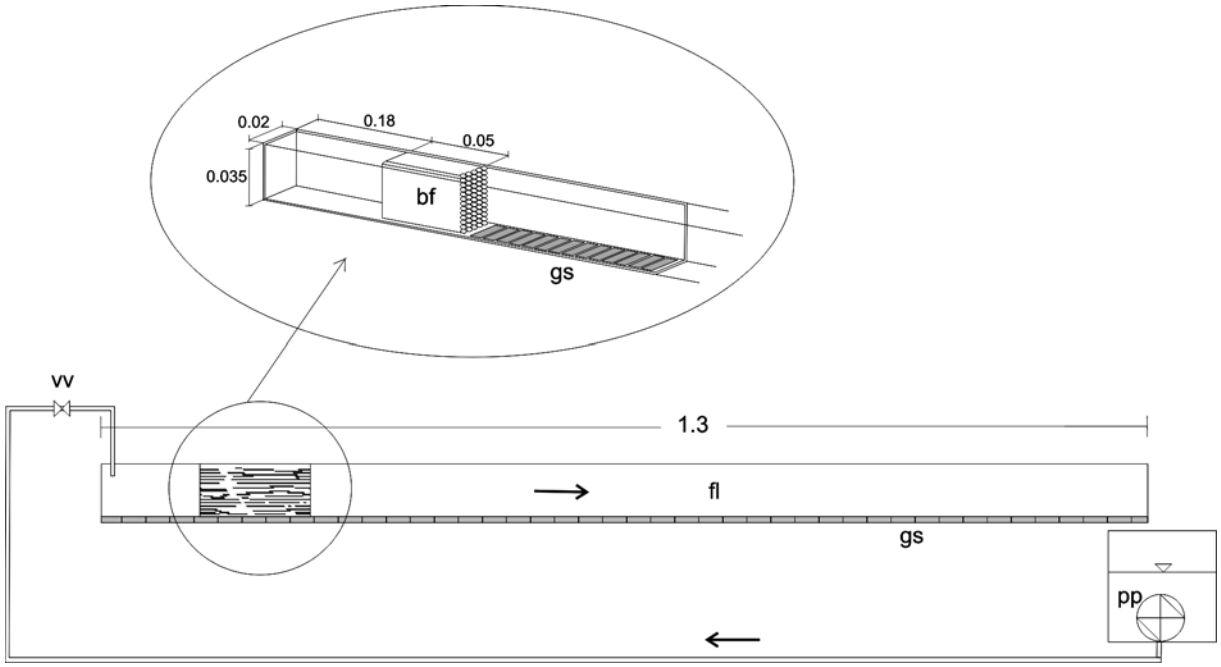

Figure 29. Plot of TiO_2 concentration (mg L^{-1}) versus turbidity (NTU).

The use of an IR-LED source at 860 nm reduces the problems usually encountered with nephelometric measurements (*106*). Nanoparticle settling velocity and travel

distance were computed from the exponential decay curve of TiO_2 concentration over time (Figure 34). Particle size was measured frequently over the recirculation period.

The filtration coefficient λ is an empirical descriptor of nano-TiO_2 deposition and is the deposition rate constant (s^{-1}) for the removal of TiO_2 from the recirculating water. The concentration of TiO_2 in the recirculating flume decays exponentially over time. In this case, the concentration of TiO_2 in the flume over time can be described by a first order deposition model:

$$\boldsymbol{C = C_0\, e^{(-\lambda t)}} \qquad \textbf{Equation 7}$$

where C is the concentration of nano-TiO_2 at time t (s) and C_0 is the initial concentration of dispersed nanoparticles.

The settling velocity (v_s) in m s^{-1} was determined for successive time intervals of 1 hour by

$$\boldsymbol{v_s = \lambda h} \qquad \textbf{Equation 8}$$

with h (m) the effective water depth in the recirculating flume.

With v_s from (eq. 4) and (eq. 5) the flux Φ (mg s^{-1} m^{-2}) of TiO_2 to the biofilm can be calculated:

$$\boldsymbol{\phi = v_s C} \qquad \textbf{Equation 9}$$

While v_s is calculated from the deposition rate, the concentration of TiO_2 particles C is measured in the experiments and known for each time interval or can be accessed through the exponential decay function (eq. 4).

The recirculating flume is a closed system. The decrease of total mass M_{tot} (mg) of TiO_2 particles can be calculated by combining equations (eq. 4), (eq. 5) and (eq. 6) into

$$\boldsymbol{M_{tot} = \int \phi A_F\, dt} \qquad \textbf{Equation 10}$$

with A_F the total flume area (0.026 m^2).

Based on the assumption of first-order deposition kinetics, the particle travel distance is evaluated by calculating the travel length R_T (m) by

$$\boldsymbol{R_T = -\frac{h}{\overline{v_s}}\, ln\left(\frac{C}{C_0}\right)\Theta_s} \qquad \textbf{Equation 11}$$

with $\overline{v_s}$ the average settling velocity, $\frac{C}{C_0}$ = 0.001 (i.e. 99.9% particle deposition) and Θ_s the flow rate in m s^{-1}.

4.3.4 Polarization microscopy and raman spectroscopy

Polarization microscopy (1000×) and Raman spectroscopy (Renishaw RW 1000) served to identify and locate anatase (excitation wavelength, 632.8 nm; He-Ne laser) in selected biofilm samples (Figure 30 and Figure 31).

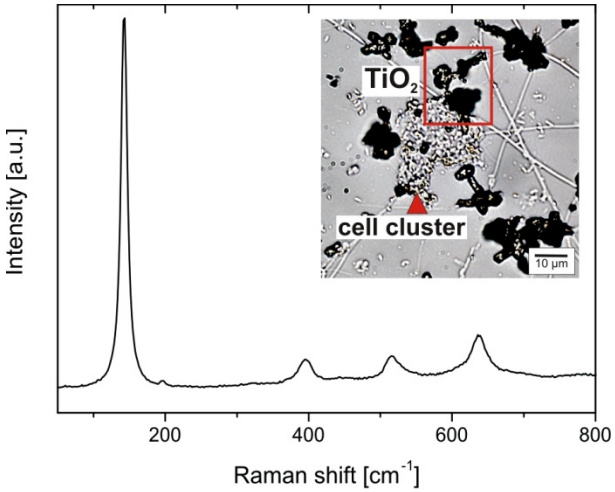

Figure 30. Raman spectroscopy confirmed the presence of TiO_2 nanoparticles and their aggregates (as anatase) in close proximity of the cells in the biofilm.

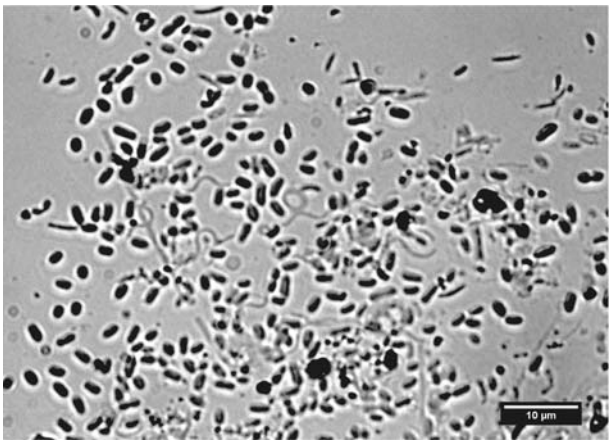

Figure 31. Control image of biofilm without being exposed to TiO_2 nanoparticles.

4.3.5 Cell membrane integrity

We used dual nucleic acid stains to assess the membrane integrity of microbial cell (*157-158*). SYTO13 (Molecular Probes, Inc., Eugene, OR) stains and dead and living gram-positive and gram-negative cells. Ethidium homodimer-2 (EthD-2) (Molecular Probes, Inc.) was used as an indicator of the membrane integrity (*157-158*). Dual stained cells (2.5 *µ*M SYTO13, 2.5 *µ*M EthD-2, 20 °C, 15 min, for planktonic and biofilm cells) were counted on 0.2 *µ*m membrane filters (GTBP; Millipore Corp., Bedford, MA) using epifluorescence microscopy (Zeiss Imager.M1, Jena, Germany). In total, 30 randomly selected fields (125 *µ*m × 125 *µ*m) were screened to account for 300-400 cells; the same protocol was used for planktonic and biofilm cells. Prior to microscopic analysis, biofilms (preserved in formaldehyde 2.5%) were removed from the slides using sterile blades and sonication (Branson Sonifier W-250D, 15 W at 10% energy input).

4.3.6 ROS detection

We used carboxy-H2DCFDA (2′,7′-dichlorofluorescein diacetate) (Molecular Probes, Inc.), a nonpolar cell permeant ROS indicator that is nonfluorescent until it is hydrolyzed by intracellular esterases to the profluorescent polar derivative, DCFH, which accumulates within the cell. In the presence of ROS, DCFH is further oxidized to the highly fluorescent DCF within the cell. Carboxy-H2DCFDA is characterized by enhanced intracellular retention of the fluorescein cleavage product and worked well for TiO_2-photosensitized ROS in human skin fibroblasts (*159*). Sample aliquots (2.7

mL) of the batches were transferred into 0.3 mL 10×PBSbuffer and immediately incubated with 3 μL carboxy-H2DCFDA(10 μM). The incubation (20 min) took place under light conditions to prevent abortion of ROS formation. Previous experiments revealed no effect of irradiation (without cell activity) on ROS generation. ROS generation was determined with a Hitachi F-7000 spectrofluorometer (EX490, EM525). Triplicate samples for ROS detection in the batch cultures were collected after periods of 1, 4, and 24 h.

4.4 Results and discussion

Measurements and estimates of nano-TiO_2 concentrations in surface waters are rare. For wastewater treatment plants (WWTP) Kiser et al. (*37*) determined peak TiO_2 concentrations, including aggregates up to approximately 5 mg L^{-1} (mean 1.4 mg L^{-1}) in headworks waters and up to 0.11 mg L^{-1} (mean 0.06 mg L^{-1}) in the tertiary effluent. Mueller and Nowack (*78*) calculated environmental TiO_2 concentrations in Swiss surface waters for a high emission scenario to be 0.016 mg L^{-1}. However, in their calculation, 10% of the sewage water received by a treatment plant will bypass the system untreated. This untreated overflow totals almost 50% of the total mass flow and will lead to far higher concentrations in the receiving river during such overflow events. Hence, the concentrations used in our study may represent a realistic scenario for untreated discharge or overflow events of a wastewater treatment plant. Transmission electron microscopy (TEM) confirmed the presence of aggregates formed of primary particles for P25 and Hombikat-100 nanoparticles (Figure 32).

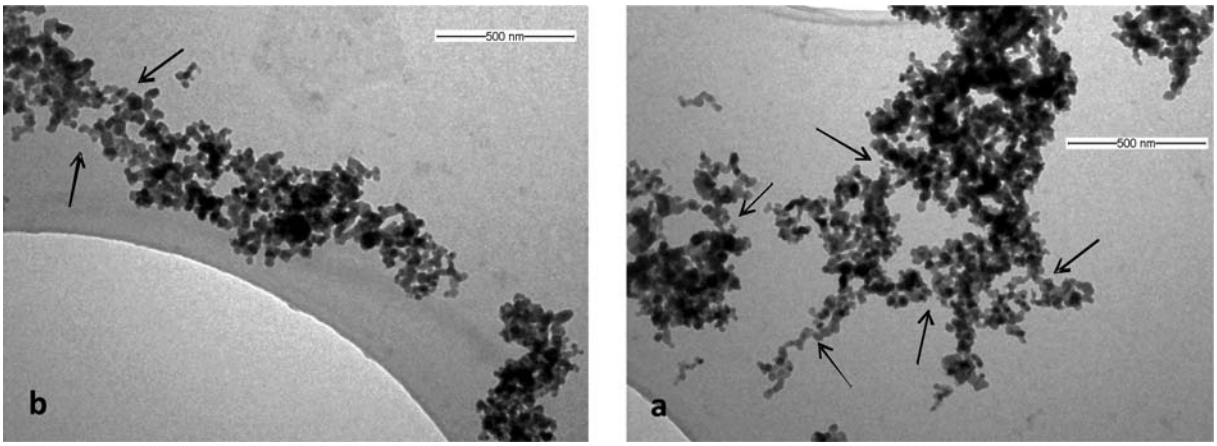

Figure 32. TEM images of TiO_2 P25 and TiO_2 Hombikat. Arrows show weak conjunctions in the aggregate structure prone to break up. Scale bar represents 500 nm.

Because their point-of-zero charge occurs at around neutral pH, TiO_2 nanoparticles in surface waters are expected to occur as agglomerates rather than as individual and well-dispersed primary ENP (*47*). We therefore broke apart by sonication the size fraction larger than 1 μm to ensure that P25 and Hombikat-100 were only present as small agglomerated aggregates in all experiments. Nevertheless, DLS intensity-weighted particle size distribution revealed that larger agglomerates (~1 μm) were also initially abundant in the recirculating water.

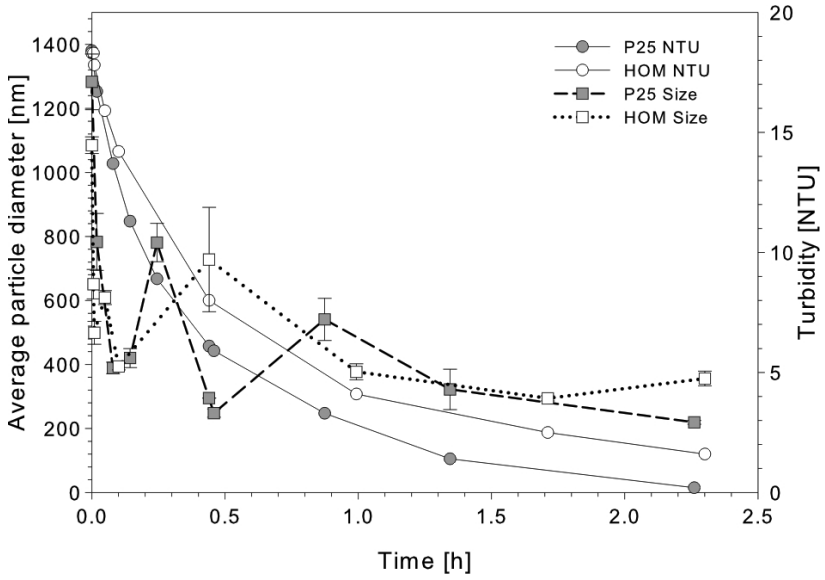

Figure 33. Decrease of TiO_2 average particle diameter (in nm; n = 3, ±1 SD) and turbidity (in NTU) as a function of time in flumes with biofilm.

After the initial phase, particle sizes remained relatively stable and only showed a trend toward decreasing particle size for P25 during the remainder of the experiment (Figure 33). In general the removal of particles from the water phase is due to attachment of the particles to surfaces of the experimental system. By measuring the concentration decay in the bare system, clean flumes, and biofilm-covered flumes, we are able to distinguish between processes related to the flume bed surface and the system (Figure 34).

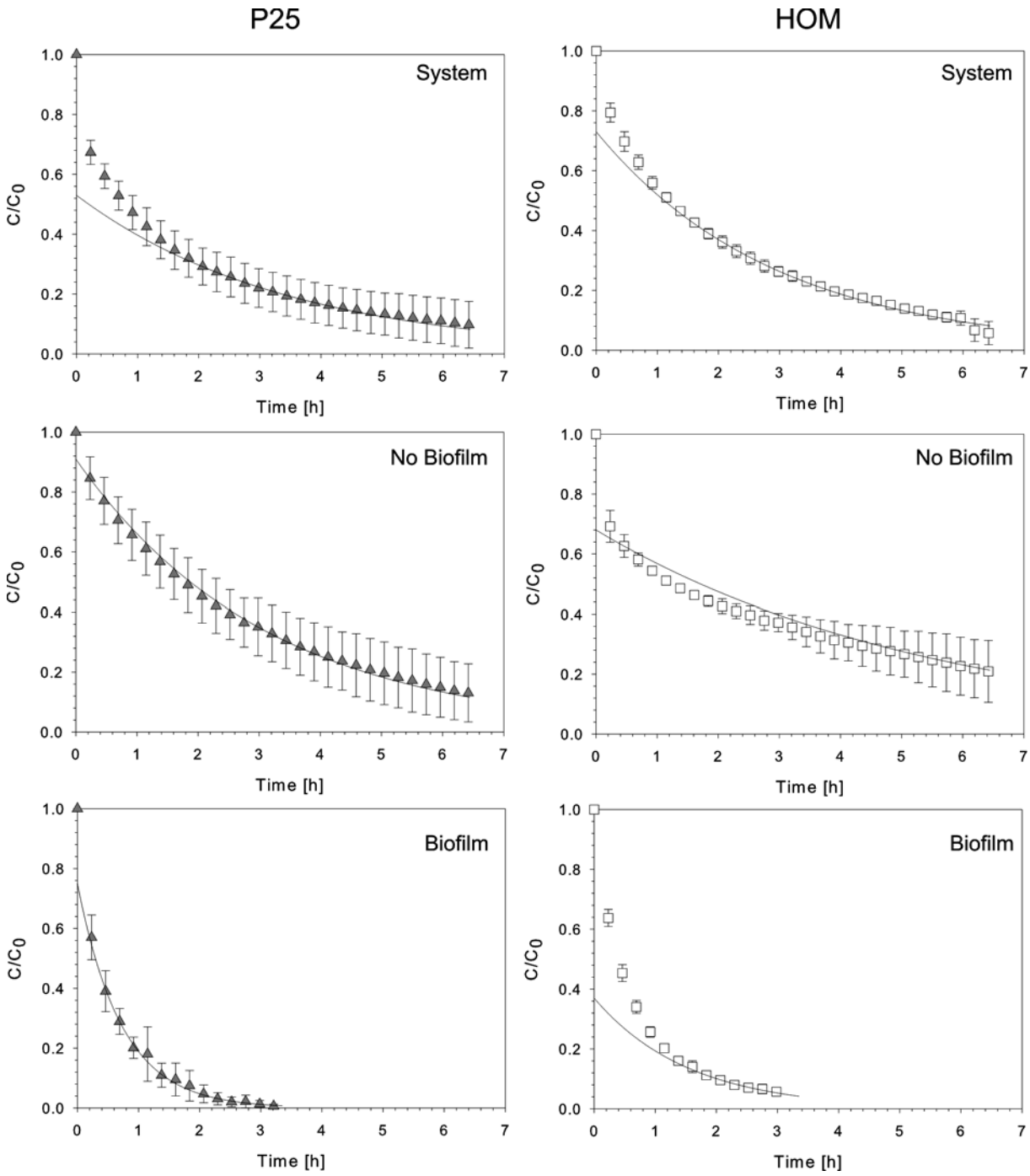

Figure 34. Deposition of TiO_2 P25 and Hombikat UV-100 (HOM) in the system without flume (system), in the flume without biofilm (no biofilm), and in flume with biofilm (biofilm). Background-corrected and normalized data based on turbidity measurements. Points denote 25% of the whole data set as mean values and ±1SD (number of experiments, *n* = 3; *n* = 2 for blank).

The elimination of the particles from the water phase is taking place in a two-step process. First, the particles must be transported to the surface, and second, they must stick to the surface and not be remobilized. The ratio of collisions resulting in an attachment to the surface over total number of collisions is the attachment efficiency.

While the characteristics of the surface will influence the attachment efficiency, on average the transport of the particles to the surface will not change if particles have the same size, shape, and density, and the flow regime is constant. The transport to the surface is a complex process composed (mainly) of particles gravitational settling, advective transport in turbulent flow, and Brownian motion of the particles. Regarding the initial phase of the transport experiments, the removal rate here exceeds the exponential decay (first-order deposition kinetics), which however fitted the data correctly for the majority of the experiment (Figure 34). Acknowledging the proven abundance of larger particles in this phase, we attribute this behavior to the contribution by gravitational settling of larger agglomerates. Biofilms had a remarkable effect on the travel distance of Hombikat UV-100 and P25 nanoparticles (Figure 35).

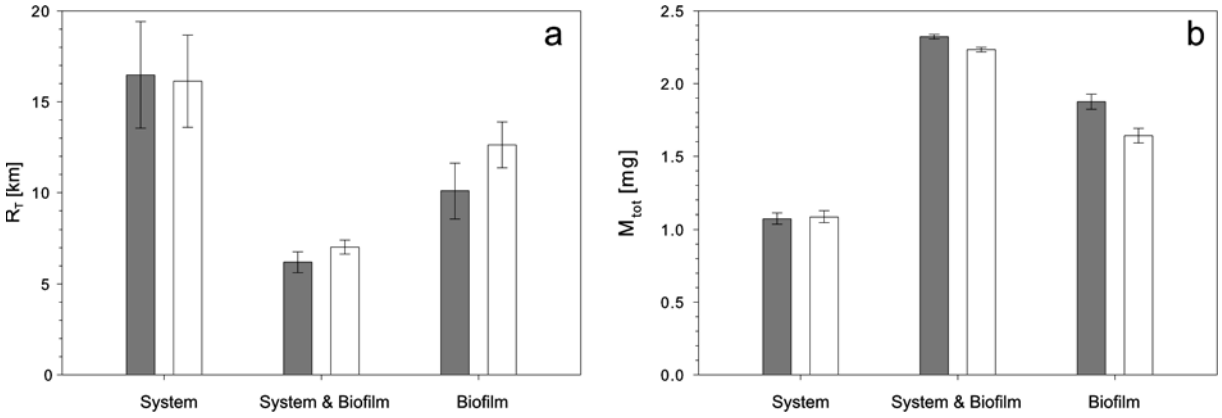

Figure 35. Travel distance of P25 (gray) and Hombikat UV-100 (white) nanoparticles in the flume until 99.9% removal from the water phase (a) and total mass of nanoparticles deposited in the flume after 3 h experimental time (b). The notation “biofilm” refers to the data attributable to the biofilm only (after subtracting flume and system components).

In the control flume without biofilm, P25 and Hombikat UV-100 nanoparticles traveled on average 10 km and 12 km downstream, respectively, before 99.9% of their initial mass concentration was removed from the water (Figure 35a). Biofilms reduced the travel length on average 2.3 times for Hombikat UV-100 and 2.7 times for P25. This agrees with observed effects of biofilms on the transportation of natural particles within the micrometer-sized range (*136*). The deposition of TiO_2 nanoparticles induced substantial accumulation in the biofilms (Figure 35b). Raman spectroscopy confirmed the presence of anatase nano-TiO_2 in close proximity to biofilm cells (Figure 30). Figure 31 shows a control image of cell clusters that were not exposed to TiO_2 nanoparticles. If ENP released from, for example, a sewage treatment plant,

undergo size fractionation during longitudinal transport, then mass concentration alone may not be a suitable parameter to describe an exposure to nanoparticles. Organisms in the receiving surface waters may be exposed to ENP of the same substance but of different particle sizes, depending on the distance from the emission source. We recognize, however, the model nature of our experimental system: in natural streams, streambed roughness and hydrodynamic exchange, including pumping (*160*), for instance, would further reduce the travel distance of ENP, while the different ratio of flow velocity to stream bed depth may contribute to longer travel distances. Our results complement the recent findings by Boncagni et al. (2009) highlighting the effects of benthic biofilms on EPN exchange between the water and streambed. To investigate the effect of nano-TiO_2 on planktonic microorganisms downstream of a hazard, we exposed free living cells to P25 and Hombikat UV-100 under dark and light conditions. Nucleic acid stains and epifluorescence microscopy showed that after 24 h of exposure nano-TiO_2 (initial concentration 5.3 mg L^{-1}) had significantly damaged cell membranes (two-way ANOVA, $F_{2,12}$ = 106.7, P < 0.001); the interaction with light was also significant ($F_{2,12}$ = 39.4, P < 0.001).

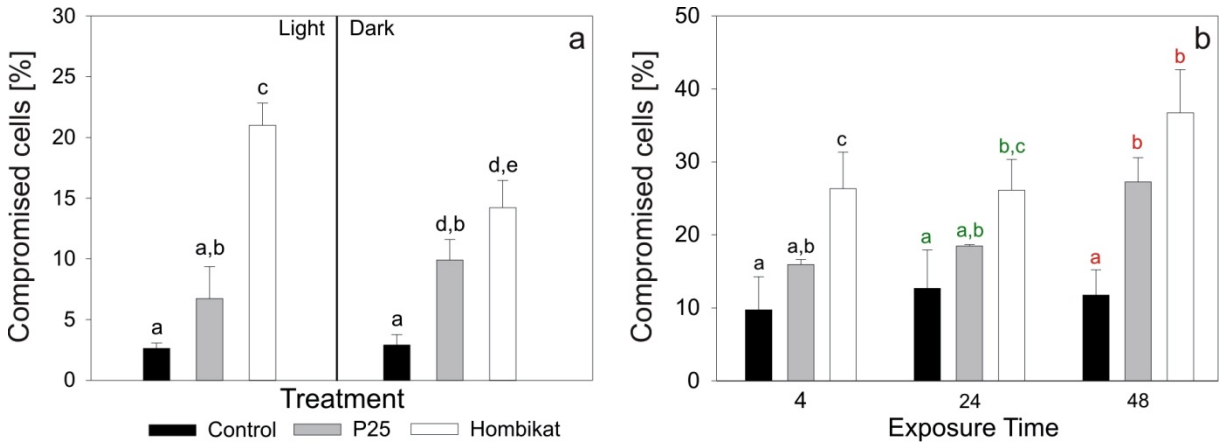

Figure 36. Percentage of compromised cells (EthD-2 counts as a % age of total SYTO13 counts) in free-living communities under light and dark conditions (a) and in biofilm (b). Error bars denote ±1SD (n = 3). Bars with the same letter within a given time or treatment (light, dark) are not significantly different (p > 0.05).

The proportion of damaged cells was on average 155% and 700% higher in the P25 and Hombikat UV-100 light treatments, respectively, compared to that of the controls (Figure 36a). We found similar patterns of microbial cell membrane damage in the biofilms (Figure 36b). Repeated measures ANOVA (repeated measures, time;

treatment, nano-TiO_2) identified significant treatment effects of nano-TiO_2 ($F_{2,18}$ = 65.7, P < 0.001) and a significant effect of time ($F_{2,18}$ = 13.1, P < 0.001) on cell membrane damage in biofilms; the interaction of effects was not significant. After 48 h of exposure, the proportion of cells with damaged membranes was on average 136% and 222% higher in the treatments with P25 and Hombikat UV-100, respectively, compared to that of the controls (no nano-TiO_2). Despite the nano-TiO_2 concentration effect of biofilms, cell damage was less in biofilms than in the planktonic cells, which we attribute to the protective nature of the biofilm matrix (*161*). In fact, radicals have an extremely short lifetime and must be produced in close proximity to the cell membrane if they are to oxidize some of its components (*162*). This is unlikely in biofilms, where cells are encapsulated in the extracellular matrix. However, possible differences in community structure between planktonic and biofilm communities as previously observed in similar systems (*163*) may also contribute to the observed differences of the ENP impacts on free-living and attached cells. More work is required to unveil the relationship between ENP and possible community shifts. The typical toxicity route of the photocatalytic nano-TiO_2 reaction occurs via the extracellular generation of reactive oxygen species (ROS) and subsequent damage of the lipid membrane (e.g., perioxidation of the polyunsaturated phospholipids) and disordering of the cellmembrane architecture (*147*). This agrees with our results from dual staining indicative of increased permeability of the outer and cytoplasmic membranes (*164*).

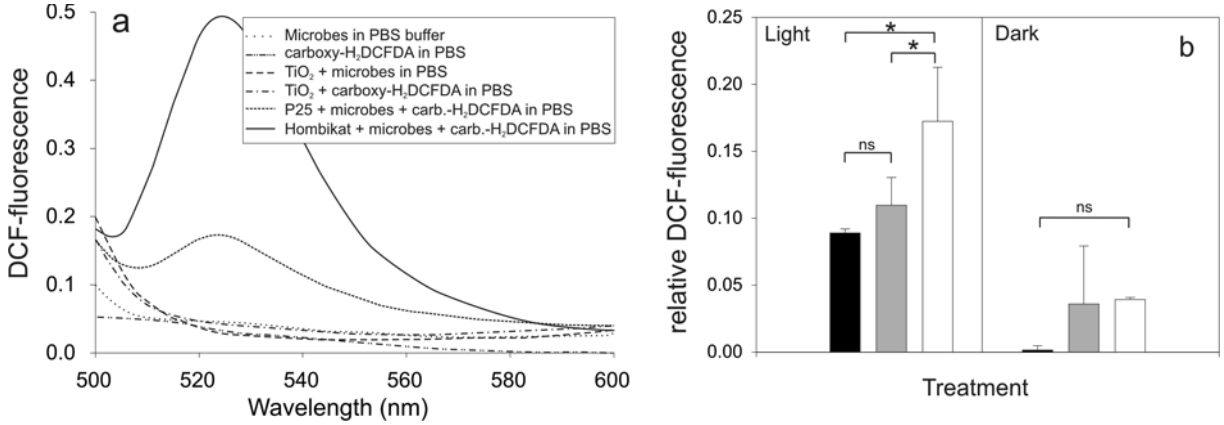

Figure 37. Fluorescence spectrum showing higher dichlorofluorescein (DCF) fluorescence induced by Hombikat UV 100 than by P25 nanoparticles in the presence of microorganisms (a). Relative DCF fluorescence induced by Hombikat UV 100 and P25 nanoparticles (and controls) under light and dark conditions (b). Error bars ±1SD (n = 3). Asterisk indicates significant differences (p < 0.05); ns indicates non significant effects (p > 0.05).

To identify and monitor intracellular oxidative stress as a possible additional cause of cell damage, we used carboxy-H2DCFDA (*159*) as a ROS detector in the planktonic community. Control experiments showed that carboxy-H2DCFDA reacted only in the presence of both nanoparticles and microorganisms; it did not react with nanoparticles or microorganisms alone (Figure 37a). After 4 h of exposure to nano-TiO_2, DCF fluorescence was 8.6 times higher in the light treatment than in the dark treatment for Hombikat UV-100 and 3 times higher for P25 (Figure 37b). Under dark conditions, nanoparticle treatments did not differ significantly from the control. Collectively, these results suggest various toxicity effects of TiO_2 nanoparticles on microorganisms, in agreement with earlier reports (*165*), but the underlying mechanisms remain elusive. For instance, extracellular activity of nano-TiO_2 and membrane permeabilisation may enhance subsequent penetration of nanoparticles or extracellular generated ROS into the cell as has been shown for ZnO nanoparticles (*165*), although this certainly requires close spatial proximity between the cell and site of ROS production (*162*). While our results suggest a relationship between intracellular ROS production and percentage of compromised cells (r^2 = 0.67, $p < 0.05$), we have not been able to determine a clear causal relationship between ROS and membrane damage. This would corroborate findings failing to establish a clear link between the antibacterial activity of fullerenes and ROS mediated damage (*166*). EthD-2 is a particularly large (MW = 1292.7) molecule and is widely used as a fluorochrome that provides a conservative indication of massive cell membrane damage (*167*). Intact bacterial cell membranes have pores with an effective hole size typically ranging from 2 to 3 nm (*168*) and are thus not permeable to primary particles (approximately 10 nm). However, primary particles might pass through substantially damaged membranes. Once within the cell, ENP can lead to additional ROS production or directly damage the DNA (*169*). Alternatively, extracellular action of nanoparticles such as their adsorption to the cell membrane (*170*) may induce intracellular ROS. Such non photocatalytic and extracellular effects would be supported by our observed increase in cell damage under dark conditions (Figure 36a). Our findings agree with results from human cell lines showing TiO_2-induced ROS generation and cell damage in the absence of light (*81*). Further work is required to establish the underlying mechanisms. The higher toxicological impact of Hombikat UV-100 nanoparticles (Figure 36a, b) may be attributable to their composition because the pure anatase phases of Hombikat UV-100 may generate

more ROS than the mixed anatase rutile phases of P25 (*81; 171-172*). However, the mechanisms underlying the different nanotoxicity impacts of anatase versus rutile-based TiO_2 nanoparticles remain a matter of debate. Primary particle and aggregate sizes, surface areas, the availability of active sites, and their binding affinity to organic molecules as well as matrix effects may all affect their nanotoxicity (*82; 172-173*). This study provides the first evidence that nano-TiO_2 impacts significantly on natural microbial communities under natural levels of UV radiation and TiO_2 concentrations expected (*78; 174*) in surface waters. We have shown that the transportation behavior of nano-TiO_2 particles is influenced by biofilms in a similar way to natural microscaled particles. They attach to and accumulate in biofilms, which enhances their removal from the water as they propagate downstream from an emission source (e.g. wastewater treatment plant). There, nano-TiO_2 can significantly compromise free-living and attached microbial cells. While this study has revealed the toxicity impact of ENP on microbial communities under natural conditions, interdisciplinary research is now required to reveal the full picture of the toxicity mechanisms and consequences on the functioning and health of ecosystem.

5 The Toxicity of Titanium Dioxide and the Bioavailability of Cadmium

Algal testing of titanium dioxide nanoparticles - Testing considerations, inhibitory effects and modification of cadmium bioavailability

N.B. Hartmann, F. v.d. Kammer, T. Hofmann, M. Baalousha, S. Ottofuelling, A. Baun

5.1 Abstract

The ecotoxicity of three different sizes of titanium dioxide (TiO_2) particles (primary particles sizes: 10, 30, and 300 nm) to the freshwater green alga *Pseudokirchneriella subcapitata* was investigated in this study. Algal growth inhibition was found for all three particle types, but the physiological mode of action is not yet clear. It was possible to establish a concentration/dose–response relationship for the three particle sizes. Reproducibility, however, was affected by concentration-dependent aggregation of the nanoparticles, subsequent sedimentation, and possible attachment to vessel surfaces. It is also believed that heteroaggregation, driven by algal exopolymeric exudates, is occurring and could influence the concentration–response relationship. The ecotoxicity of cadmium to algae was investigated both in the presence and absence of 2 mg L^{-1} TiO_2. The presence of TiO_2 in algal tests reduced the observed toxicity due to decreased bioavailability of cadmium resulting from sorption/complexation of Cd^{2+} ions to the TiO_2 surface. However, for the 30 nm TiO_2 nanoparticles, the observed growth inhibition was greater than what could be explained by the concentration of dissolved Cd(II) species, indicating a possible carrier effect, or combined toxic effect of TiO_2 nanoparticles and cadmium. These results emphasize the importance of systematic studies of nanoecotoxicological effects of different sizes of nanoparticles and underline the fact that, in addition to particle toxicity, potential interactions with existing environmental contaminants are also of crucial importance in assessing the potential environmental risks of nanoparticles.

5.2 Introduction

While many of the anticipated applications of nanomaterials remain to be seen, titanium dioxide (TiO_2) nanoparticles (NPs) are examples of manufactured nanosized materials that are already widely used. Many applications are based on the ability of the particles to absorb UV-light and their photocatalytic activity, which has been found to increase with decreased particle size (*175*). Consequently, TiO_2 NPs will inevitably reach the aquatic environment, where they have so far been traced from urban applications into receiving waters of urban runoff (*36*). Here the effects on the aquatic biota are largely unknown. TiO_2 is generally considered to be an inert material. However, for nanosized particles, the surface area per mass increases exponentially and so does the reactivity. This increased reactivity is expected to change their interactions with living organisms, and possibly lead to changes in their toxicity. In addition, these NPs may have the ability to reach sites inaccessible by larger particles, where they may accumulate or where toxic effect may take place. Toxic effects of TiO_2 NPs have been demonstrated by several studies and have been suggested to be a result of the formation of reactive oxygen species (ROS) upon UV irradiation, leading to damage on cellular and subcellular structures(*176-178*). The photocatalytic activity of TiO2 NPs has been found to depend on concentration, crystal structure (rutile/anatase/amorphous) and UVA (λ < 385 nm) light intensity (*151; 171; 179*). However, it has also been suggested that TiO_2 particles may cause physical disruptions of cell membranes as a result of the structure and surface properties of the NPs (*179*). Indications of size-dependant toxicity make it interesting to study the potential environmental effects of TiO_2 NPs in comparison to larger particles. Furthermore it emphasizes the importance of including TiO_2 with different particle sizes in toxicity testing. TiO_2 is insoluble in water and suspensions are formedwhenTiO_2 particles are added to aqueous media. The testing of such suspensions represents challenge for ecotoxicological tests, developed for testing dissolved chemicals. In the ecotoxicological studies carried out so far, the short-term toxicity of TiO_2 NPs to algae, daphnids, juvenile and adult zebrafish has been reported to be low (*180*). For freshwater green algae (*181*) found an EC50 value of 9.73 mg L^{-1} for particles with sizes from 25 to 70 nm. While cellular uptake of TiO_2 particles has been demonstrated in human alveolar epithelial cells (*182*), the interactions between the algal cells and the particles may be different due to the

presence of a semi-permeable cell wall surrounding the algal cells. For this reason, the active biological uptake processes for NPs described for eukaryotic cells (such as phagocytosis and endocytosis (*183-185*) is impeded as it requires interaction and crossing of the cell wall. If the cell wall is penetrated, passage through the plasmamembrane by endocytosis may be possible (*40*). This may directly lead to cell damage due to the effect of TiO_2, but could also facilitate the transport of other environmental pollutants through cell membranes. Hence, independent of direct toxic effects, the presence of TiO_2 NPs may cause indirect effects, for example by influencing toxicity and bioaccumulation of other pollutants present in the aquatic environment. If cell membrane damage is caused by the particles, uptake, bioaccumulation and toxicity of other xenobiotic compounds in the aquatic environment might be influenced. Indirect effects can also be a result of environmental pollutants adsorbing onto the particles, as it has been observed for other types of NPs (*76; 186*). For example, the enhanced accumulation of cadmium (Cd) and arsenic (As) found in carp (Cyprinus carpio) in the presence of TiO_2 NPs by Zhang et al. (*187*) and Sun et al. (*75*) was attributed to facilitated transport into different organs. Hence it was found by Zhang et al. (2007) that BCF for Cd in the presence of TiO_2 NPs increased more than 10 times compared to experiments without TiO_2 and that the measured accumulation of TiO_2 corresponded well with the accumulation of Cd. As only a few studies describe TiO_2 NP toxicity to algae (*40*) and as the role of nanoparticles as carriers for other contaminants is largely unknown, this study has two aims: The first is to investigate the applicability of standardized algal growth inhibition test methods for testing of TiO_2 particles with different primary particle sizes (10, 30, and 300 nm), as well as to study the inhibitory effect of these particles. The second is to study the potential carrier effect of TiO_2 for other pollutants through a series of experiments, designed to reveal the influence of TiO_2 particles on the algal toxicity of cadmium.

5.3 Materials and methods

5.3.1 Chemicals

Three different types of TiO_2 (CAS no. 13463-67-7) nanoparticles were used in this study, namely (i) Degussa P25 TiO_2 NPs (purchased from Frederiksen, Ølgod, Denmark), (ii) UV100 TiO_2 NPs and (iii) LW-S TiO_2 NPs (both provided by Sachtleben Chemie GmbH). Selected properties of the NPs are listed inTable 9. Analytical grade potassium dichromate ($K_2Cr_2O_7$, CAS no. 7778-50-9) was purchased from Fluka Chemika and cadmium ('STD Cadmium 1000 ppm' in 2% HNO_3, CAS no. 7440-43-9) was purchased from PerkinElmer.

Table 9. Properties of the three types of TiO_2 particles. The particles have been characterised by use of a number of different techniques both as dry powder (BET) and suspended in algal test media (Zeta potential, hydrodynamic diameter). Values for primary particle size and crystalline structure are from particle suppliers or other studies. a Sachtleben (*188*); b Jensen et al. (*151*); c Sachtleben (*102*).

	Particle type		
	Hombikat UV100	**Degussa P25**	**Hombitan LW-S**
Primary particle diameter (nm)	<10 [(a)]	~30 [(b)]	~300 [(a)]
Zeta potential (mV)	-23	-21	-25
Surface area (m^2/g (BET multiplepoint)	288	47	11.5
z-average hydrodynamic diameter in algal test media (nm) ±1SD of duplicates C_{TiO2} : 2 mg/L)	1261±0.00	416±78.0	492±46.4
Polydispersity index	1.00±0.00	0.64±0.05	0.70±0.06
Amorphous and crystalline (anatase/rutile) phase	67.2% anatase 32.8% amorphous [(b)]	72.6% anatase 18.4% rutile 9% amorpous [(b)]	anatase, content of amorphous TiO_2 not specified [(a)]

5.3.2 Preparation of media, stock solutions and suspensions of TiO_2

Algal test medium was prepared according to ISO 8692 (International Organization for Standardization 2000). The medium contains nutrient salts as well as a chelator (Na_2EDTA) to keep iron available for algal growth. The resulting medium had ameasured alkalinity of 0.6 meq L^{-1} and an ionic strength of 1.5 mM, as calculated by use of PHREEQC speciation modelling software for Windows, Version 2.3.08 (*189*). TiO_2 stock solutions were prepared by suspending TiO_2 particles in algal test medium in a concentration of 250 mg L^{-1} followed by 10 min sonication in a water bath (Elgasonic, 50W). These suspensions were kept at 5 C° in the dark and sonicated again 10 min prior to preparation of test suspensions.

5.3.3 Algal growth rate inhibition tests

A modified version of the ISO 8692 (International Organization for Standardization, 2002) algal growth inhibition tests were carried out with green algae species *Pseudokirchneriella subcapitata* (Korshikov) Hindak (formerly known as *Selenastrum capricornutum* Printz) as test species. The ISO algal medium was used to prepare a range of concentrations of the test substance, which were then inoculated with exponentially growing algae to a density of 104 cells mL^{-1}. For TiO_2 inhibition tests, 16 concentrations (0.6 - 250 mg L^{-1}) were tested using single replicates. In tests of the effect of cadmium in the absence or presence of TiO_2 (2 mg L^{-1}) 6 concentrations (10 - 320 g L^{-1} Cd) were tested in triplicate. Six controls, containing only ISO test medium and algae, were included in each test run. A mini-scale test with 4 mL test solutions in 30 mL polystyrene containers (Nunc) was applied in this study (*190*). The containers were placed on a shaker (200 rpm) at 20 ± 1 ◦C to allow for mixing and CO_2 diffusion and continuously illuminated at 80–105 µE $m^{-2}s^{-1}$ (measured under the test vessel). The light source in the tests was a cold light fluorescent tube emitting light in the visible spectrum. Light intensity in the test setup was measured using a LI-COR light meter (model LI-189) with an attached quantum sensor, measuring light within the wavelength range 400 - 700 nm. The tests were conducted at a pH of 7.4 - 7.8 with typical control growth rates of 1.4 - 1.6 d^{-1} during the 72 h incubation. Samples of 0.4 mL were taken at times 0, 48 and 72 h and the algal growth rates were calculated on the basis of total algal biomass in each sample quantified by acetone extractions of chlorophyll, as described by Mayer et al. (*191*). The fluorescence of the samples were subsequently measured on a fluorescence spectrophotometer (Hitachi F-2000) using an excitation wavelength of 430 nm and emission wavelength of 671 ± 20 nm. In order to minimize interference, samples containing TiO_2 particles were allowed to settle for 48 - 72 h prior to fluorescence measurements. Frequent fluorescence measurements of the control samples during this period showed no influence on the chlorophyll content of the samples from this longer storage period. Growth rates and concentration-response curves were estimated by use of a nonlinear-regression program with control variance weighting (*192*) assuming lognormal distribution. By use of logistic curve fitting and inverse estimation EC-values were determined with corresponding 95% confidence limits.

5.3.4 Influence of light intensity on TiO_2 toxicity towards algae

In order to investigate the influence of light intensity on the measured effects of TiO_2, algae were exposed to 10 mg L^{-1} TiO_2 under three different light conditions. Three replicates were made for each particle type (LW-S, UV-100, P25) at each light intensity level. Light intensities were chosen within the range specified in the standard test procedure (International Organization for Standardization, 2002): low (~60 µE $m^{-2}s^{-1}$), medium (~90 µE $m^{-2}s^{-1}$), and high (~120 µE $m^{-2}s^{-1}$). Furthermore, three control replicates were made for each light intensity level. Fluorescence of algal pigments was used as the biomass measure and determined at test start and again after 48 and 72 h. Furthermore a shading test was made similar to the tests described by Hund-Rinke and Simon (*143*) and Aruoja et al. (*181*). The test setup consisted of two stacked 12-well polystyrene tissue culture test plates, with the bottom one containing different concentrations of TiO_2 NPs (0 - 100 mg L^{-1}) and the upper plate containing exponentially growing algae. The plates were illuminated from below with a light intensity of 90 µE $m^{-2}s^{-1}$.

5.3.5 Sorption of cadmium to TiO_2 in suspension

After a number of initial tests, showing sorption of cadmium to TiO_2 NP to reach a maximum level within 30 min, a series of sorption studies were carried out with a fixed sorption time of two hours using total nominal concentrations in the range 10 - 320 µg L^{-1} Cd and 2 mg L^{-1} TiO_2 NPs. A total of four tests were carried out in parallel with cadmium alone (control experiment), cadmium & P25, cadmium & UV100 and cadmium & LW-S, respectively. Test solutions were prepared in algal test medium (International Organization for Standardization, 2002) in polystyrene test tubes. An amount of 6mL test solution was added to each test tube, and three replicates were made for each Cd concentration in each test. After 2 h the test tubes were centrifuged for 20 min at 1370 g (Hettich Rotanta 460 R, Tuttlingen, Germany) after which 3 mL of the supernatant was removed for analysis of water phase cadmium concentration. Freundlich sorption isotherms ($\log Cs = n \times \log Cw + \log KF$) were determined by linear regression. An additional test with increased centrifugation time (1 h) and higher g-force (4437×g) did not show a decrease in water phase concentrations (data not shown).

5.3.6 Chemical analysis and particle/aggregate characterizations

Cadmium analysis was performed using a PerkinElmer graphite furnace AAS AAnalyst 800. Prior to analysis samples were added a small amount of 65% HNO3 (10 µL per 10 mL sample) lowering pH to ≤ 2. Particle surface area measurements were made using the Brunner-Emmett-Teller (BET) method. Transmission electron microscopy (TEM) was performed using an EM 208 (Philips) equipped with MegaView III & Item 5 at 100 kV. Samples were prepared in milliQ water. Scanning electron microscopy (SEM) was performed using a FEI apparatus (model Quanta 200) in combination with energy dispersive X-ray spectroscopy (EDX) (model EDAX). Samples were made in algal test medium and prepared for SEM by placing a drop of the sample onto a cellulose filter. Inductively coupled plasma-optical emission spectroscopy (ICP-OES) of the different TiO_2 particle types was carried out using an Optima 5300DV (Perkin Elmer) with ICP multi-element standard (CertiPUR, Merck). Particle sizes were measured in intervals (initially and after 2, 6, 48 and 72 h) by dynamic light scattering (DLS) using a Zetasizer NanoZS (model ZEN3600, Malvern Instruments, UK). The method of cumulants was used to determine the z-average hydrodynamic diameter and CONTIN to derive the 1st mode of the size distribution. DLS determines the diffusion coefficient of particles or molecules by measuring the short-term scattered light intensity fluctuations, which are caused by the Brownian motion of the particles. DLS provides in first place intensity weighted size averages and distributions. The z-average, i.e. the first cumulant fitting the autocorrelation curve, is not unambiguous for polydisperse samples. Also size distributions calculated from the autocorrelation curve by mathematical models like CONTIN do not have a single solution, but choose the simplest from a set of solutions. The physical principles, mathematical treatment and limitations of the DLS for particle sizing in complex environmental media are described in detail elsewhere (*105; 117*). To check the suspensions for the presence of aggregates above the maximum particle size quantifiable by the DLS method (~3 µm at the density of TiO_2) a particle sizer (Galai CIS-1, LOT Germany) was used, where the determination of particle size and number density distributions is based on the obscuration of a focused, circularly rotating laser beam using the time-of-transition principle. Due to the optical recognition of particles the lower size limit is 0.5 µm in diameter and particles smaller than this are not detected. The fact, that the system counts single particles, makes it

comparably sensitive and concentrations in the µg L^{-1} range can be analyzed if counting times are long enough and the sample is stable.

5.4 Results and discussion

5.4.1 Characteristics of TiO_2 particles

Characteristics of the different TiO_2 NPs tested in this study are summarized in Table 10. Data clearly show the increase in particle surface area with the decrease in primary particle size. It is also clear that the particles in stock solutions, as well as in test media, form aggregates of different sizes. TiO_2 particles were characterized under the same experimental conditions as in the effect testing but without algae (algal test media, 72 h, 200 rpm on a horizontal shaker).

Table 10. TiO_2 nanoparticle characterisation by DLS (ZetaSizer) (n = 2, ± 1SD).

Particle Type	Experimental Time (h)	Polydispersity Index (PDI)	z-average (nm)	1st Mode (nm)
LW-S	0	0.70 ± 0.06	492 ± 46.4	213 ± 21.9
LW-S	2	0.66 ± 0.02	529 ± 26.7	201 ± 2.82
LW-S	6	0.49 ± 0.03	477 ± 20.6	227 ± 12.0
LW-S	48	0.52 ± 0.04	441 ± 136	254 ± 73.5
LW-S	72	0.88 ± 0.17	1206 ± 511	180 ± 15.5
P25	0	0.64 ± 0.05	416 ± 78.0	234 ± 12.7
P25	2	0.75 ± 0.28	575 ± 268	188 ± 24.0
P25	6	0.37 ± 0.02	343 ± 56.1	235 ± 4.24
P25	48	0.42 ± 0.05	274 ± 44.4	217 ± 22.6
P25	72	0.46 ± 0.03	449 ± 33.3	185 ± 28.9
UV100	0	1.00 ± 0.00	1261 ± 72.0	243 ± 7.07
UV100	2	0.98 ± 0.03	1158 ± 123	211 ± 12.7
UV100	6	0.73 ± 0.12	858 ± 194	267 ± 37.4
UV100	48	0.65 ± 0.14	474 ± 5.65	403 ± 57.2
UV100	72	1.00 ± 0.00	2107 ± 397	96 ± 6.50

As shown in Table 10, the 1st mode for all three materials remained constant over the experimental time. The z-average hydrodynamic diameter generally decreased (until 48 h of experimental time). The inspection of the autocorrelation function and the cumulant and distribution fit of the Malvern DLS software showed that parts of the data, predominantly for later times of sampling, were no longer fitted correctly. This clearly indicates the presence of entities which were outside of the applicability window of the DLS system.

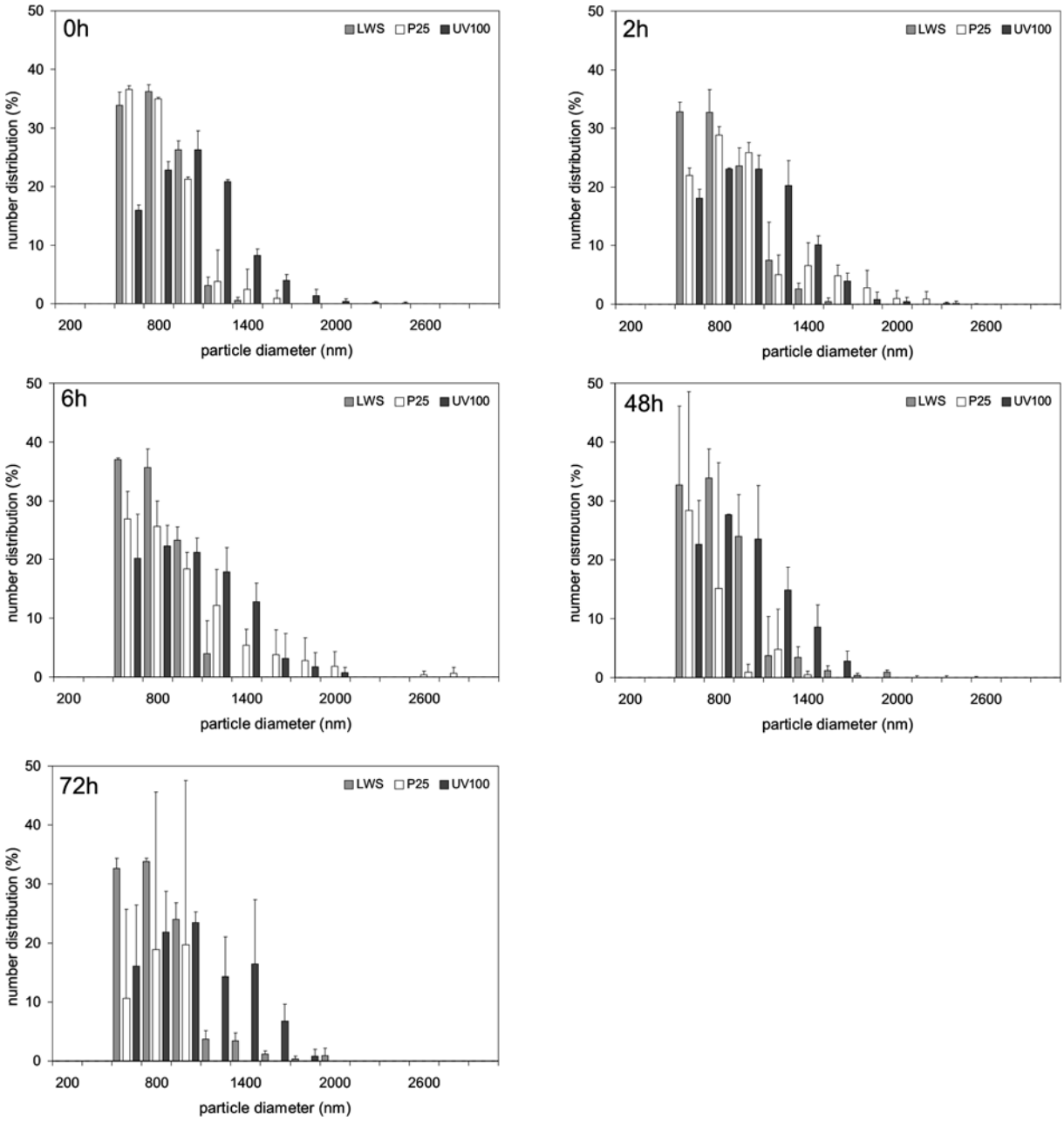

Figure 38. Particle diameter of TiO_2 (2 mg L^{-1}) given as number density distributions over the experimental time (72 hours) in algal test media for Hombitan LW-S, P25 and Hombikat UV100, analysed by GALAI CIS-1, each sample was measured in duplicate and ± 1SD is given as error bars.

By measuring the samples using the particle counter (CIS-1) no aggregates above 3 µm could be detected. For Hombikat UV100 a shift was observed to larger sized aggregates (Figure 38) over the 72 h period, which is also confirmed by DLS analysis expressed by the z-average (Figure 39).

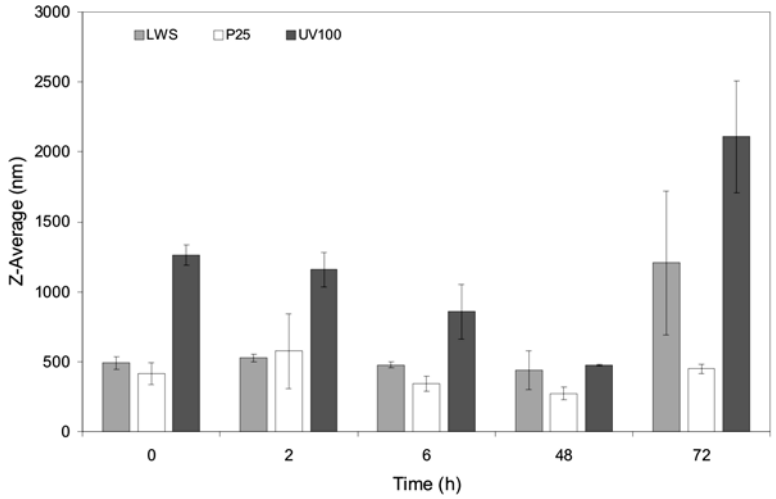

Figure 39. Z-Average hydrodynamic diameter of TiO_2 nanoparticles (2 mg L^{-1}) in algal test media over experimental time (72 h) analysed by PCS in duplicates and ± 1SD.

A slight increase of aggregate size was observed for P25 and Hombitan LW-S. The increase of size was accompanied by an increase in deviation within the replicates (n=2, ±1 SD). However, the PDI of Hombikat UV100 samples was always higher, which indicates a broader size distribution (Figure 40).

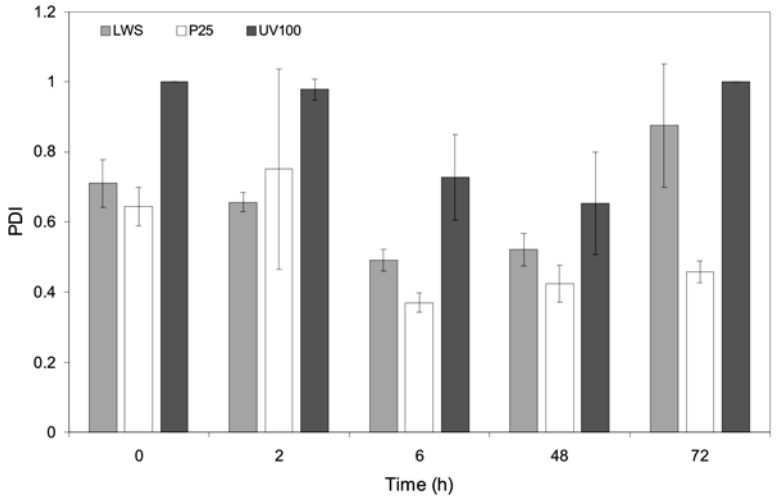

Figure 40. Polydispersity index (PDI) for TiO_2 nanoparticles (2 mg L^{-1}) in algal test media over experimental time (72 h) analysed by PCS in duplicates and ± 1SD.

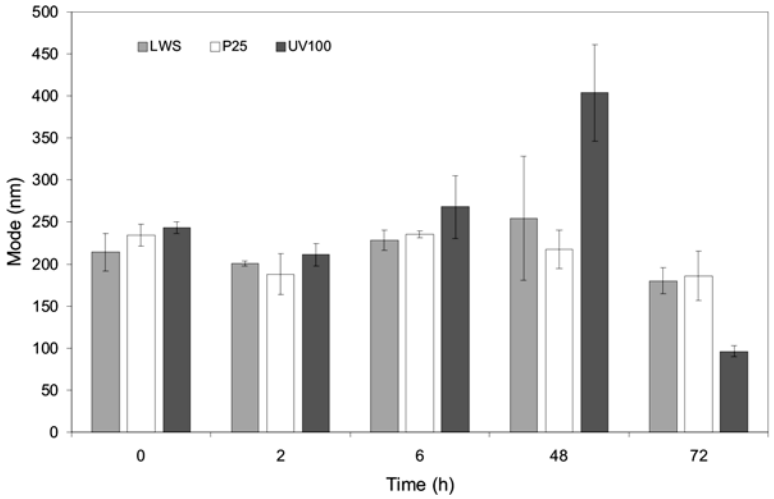

Figure 41. Mode (1st peak) for TiO_2 nanoparticles (2 mg L^{-1}) in algal test media over experimental time (72 h) analysed by PCS in duplicates and ± 1SD.

The 1st mode of all samples remained constant, but decreased after 72 h which is attributable to the shift to larger sized aggregates (Figure 41). At the ionic strength of the algal medium (1.5 mM) it could be expected that the influence of the medium constituents is less pronounced in suspensions with high particle concentrations. Accordingly, additional tests (data not shown) showed that aggregates in the stock suspension (250 mg L^{-1}) were smaller than in the 2 mg L^{-1} dilution although both suspensions were prepared in the same media. This can be explained by the increased cation/particle ratio with dilution, leading to changes in electrostatic repulsion, and hereby, changes in stability (*193*) or by the fact that disequilibrium with surrounding water chemical conditions produce charge heterogeneity (see the low negative z-potential), which also supports aggregation. Although the reported sizes suggest the formation of large aggregates in the test media, they do not imply the absence of smaller aggregates or individual NPs due to the intensity weighted character of the DLS determinations. The time series with five consecutive DLS and CIS-1 measurements showed the tendency of the materials to aggregate and sediment and also revealed the presence of smaller aggregates. The sedimentation of aggregates can induce further aggregation by differential settling effect. In this experimental setup P25 shows a pronounced aggregation and settling resulting in larger particle diameters and higher PDI.

5.4.2 Algal toxicity of different TiO_2 particle types and sizes

As can be seen from Table 11 and Figure 42, the three particles yielded different concentration-response profiles. The lower slope of the fitted concentration-response curve for UV100 (Figure 42) reflects a relatively constant inhibition over the middle part of the test concentration range.

Table 11. Effect concentrations for inhibition of algal growth rates (*Pseudokirchneriella subcapitata*) for the three different types of TiO_2 particles tested in a concentration range of 0.2 - 250 mg L^{-1} and inhibition (in %) found in experiments with 2 mg L^{-1}. The incubation time was 72 h and the growth rate of the controls was 1.5 d^{-1}. The pH of the control samples was 7.8 (start) and 7.2 (end). The pH of the highest concentrations were 7.5 (start) and 7.4 (end) (UV100), 7.7 (start) and 7.4 (end) (P25), 7.6 (start) and 7.6 (end) (LW-S).

	Hombikat UV100	**Degussa P25**	**Hombitan LW-S**
EC_{10} (mg/L)	3.3 $[0.5;20.6]_{95\%}$	15.5 $[10.9;22.1]_{95\%}$	18.0 $[11.5;28.4]_{95\%}$
EC_{20} (mg/L)	14.5 $[4.4;48.5]_{95\%}$	26.2 $[20.1;34.1]_{95\%}$	36.9 $[26.7;51]_{95\%}$
EC_{50} (mg/L)	241 $[95.6;609]_{95\%}$	71.1 $[59.4;85.1]_{95\%}$	145 $[112;118]_{95\%}$
Growth rate inhibition of 2 mg/L TiO_2 (growth rate as % of control)	79% SD: 4.4%	101% SD:3.6%	105% SD:2.3%

The EC_{10} values for the three particle types have overlapping confidence intervals; nonetheless, there is a tendency of the smallest particle type (UV100) to induce higher inhibition at lower concentrations. However, comparison of EC50 values suggests that the P25 particles are more toxic than UV100 and LW-S (Figure 42 and Table 11) in good agreement with the findings by Hund-Rinke and Simon (*143*). An extra data analysis was carried out using a three parameter log logistic curve fitting with a hormesis parameter added as described by Brain and Cousens (*194*) and with a lack of fit model as described by Cedergreen et al. (*195*). This analysis revealed statistically significant stimulation of the algae at the lower concentrations for P25 ($p = 0.0355$) and LWS ($p = 0.0128$), whereas no stimulation is seen for UV100. It should be mentioned that it proved difficult to obtain reproducible concentration-response relationships for UV100, as also indicated by the deviation of data shown in Figure 42.

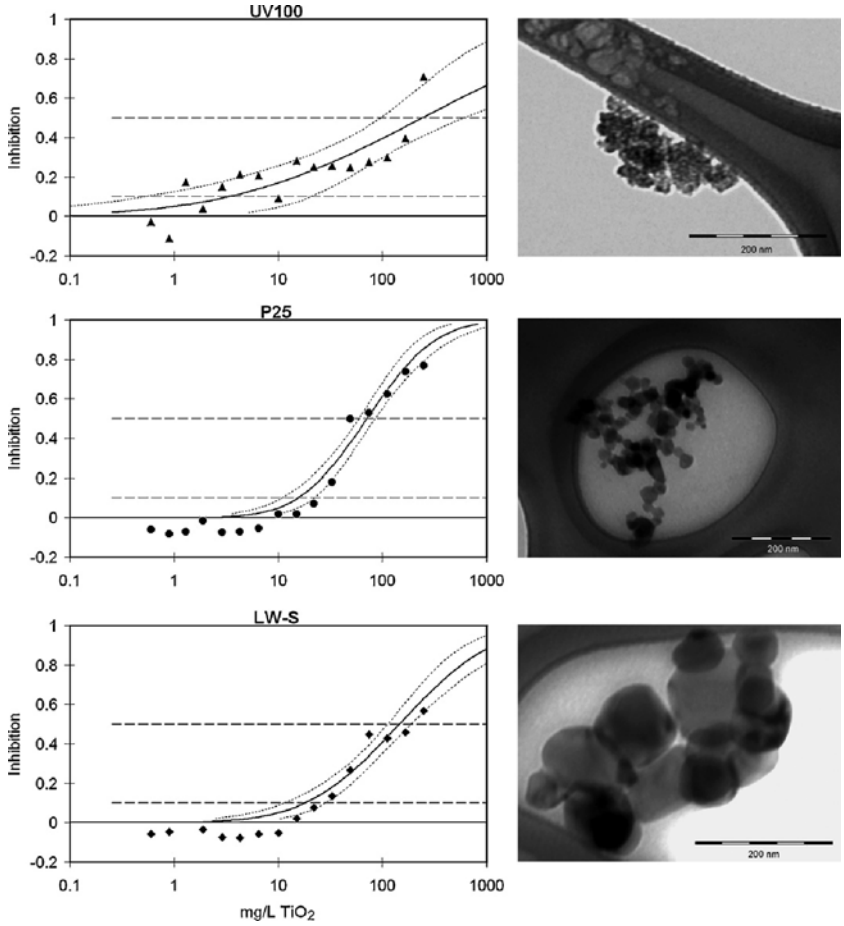

Figure 42. Growth rate inhibition of *Pseudokirchneriella subcapitata* exposed for 72 h to three different types of TiO_2 particles together with TEM pictures of TiO_2 suspensions. Experimental data is shown together with estimated concentration–response curves obtained by fitting with a log-logsitic model. Particle types: UV100 – primary particle size <10 nm, P25 – primary particle size 30 nm, LW-S – primary particle size 300 nm.

In the present study, it has not been possible to elucidate the reason for the problems with testing UV100. However, this is presumably due to the extensive aggregation of NPs in the test media due to the high salt concentration and possibly also affected by excretion of exopolymeric substances to mitigate the stress induced by the exposure to NPs as described for macroalgae by Nielsen et al. (*196*). Such influence from aggregation might be more pronounced for the UV100 particle type compared to the two larger particle types. Other possible factors include a non-linear concentration-aggregation relationship (*53*). Nevertheless it was consistently found that concentrations of UV100 in the range of 1-10 mg L^{-1} gave rise to significant inhibition. In a series of additional tests (Table 11), it was found that at concentrations of 2 mg L^{-1}, only UV100 reduced the algal growth rate (a 21% reduction was observed)

whereas slight stimulation of algal growth again was seen for P25 and LWS. The differences in effects of the three particle types might be attributed mainly to differences in particle size, but also other parameters such as the crystalline composition, are expected to influence the toxicity of TiO_2. The UV100 and LWS particle types are both anatase, whereas P25 also contains rutile. Also content of amorphous TiO_2 differs between the three particle types (see Table 9). The anatase form of TiO_2 has been found to be superior photocatalyst compared to the rutile crystal structure (*81; 197*). However, other studies have found that the rutile form has a higher bactericidal activity than photoactive anatase and mixed phase TiO_2 (P25), which is believed to be partly due to particle preparation and morphology (*178*). The photocatalytic activity has been found to decrease with increased amorphous content, whereas the activity increases with an increased amount of surface OH groups. UV100 has higher fraction (47%) of surface OH groups compared with P25 (29%); although, UV100 has a higher content of amorphous TiO_2 (*151*).

In conclusion, it is possible that these differences in crystalline structure may contribute to explain the differences in the observed toxicity in this study. However, a correlation between crystalline structure and toxicity is not straight forward. Hence, a large number of factors may play a role in the ecotoxicological effects of the particles. In the interpretation of toxicity test results of TiO_2 particles, factors such as aggregation behavior and impurities have to be considered, as they could all potentially influence toxicity. In this study no (inorganic) impurities were detected by SEM-EDX or by ICP-OES (data not shown).

The changes observed in aggregate sizes when solutions are diluted (Table 10) may greatly influence the growth rate inhibition found in standard algal tests. It is also possible that the tested solutions (here the surface functional groups of the particles) were in disequilibrium since the dose-response experiments were initiated shortly after dilutions were carried out. If the aggregate size varies as a function of concentration and/or chemical equilibrium state of functional groups, the standard approach to concentration–response testing do in fact include interdependent variables (e.g. concentration and aggregation state). As a result, inhibition found in the standard test cannot be claimed, with confidence, to be only dependent on TiO_2 concentration, and further experimental studies are needed to separate different

influencing parameters (size, aggregation, aggregate structure, shape, crystallinity, etc.). In addition, accurate characterization of the NPs not only at the time of dosing and start of exposure but also during and after exposure will improve our understanding of the dose–response relationship. This again highlights the necessity of in-situ characterization techniques, which are unavailable at present. Decreased growth rates in algal tests may also be caused by adhesion of TiO_2 to the cell surfaces. In a recent study by Aruoja et al. (*181*) nanosized particles were observed to cover the algal surfaces to a larger extent than the bulk particles, for which more particle-free algal cells were seen. Tests of shading (with separate particle and algae phases) and light intensity effects showed that algal growth was not affected by either of these parameters (this study, data not shown; Aruoja et al., 2009; Hund-Rinke and Simon, 2006). However, a 'direct' shading effect caused by the encapsulation of the cells by particles cannot be excluded. Particle adhesion may also lead to physical effects (such as disruption of cell membrane) or reducing cellular uptake of nutrients. Interruption of energy transductions (related to ATP synthesis) has also been suggested as a possible effect mechanism (*178*), as well as reduction reactions of adsorbed particles on the cell membrane leading to oxidative stress (*170*).

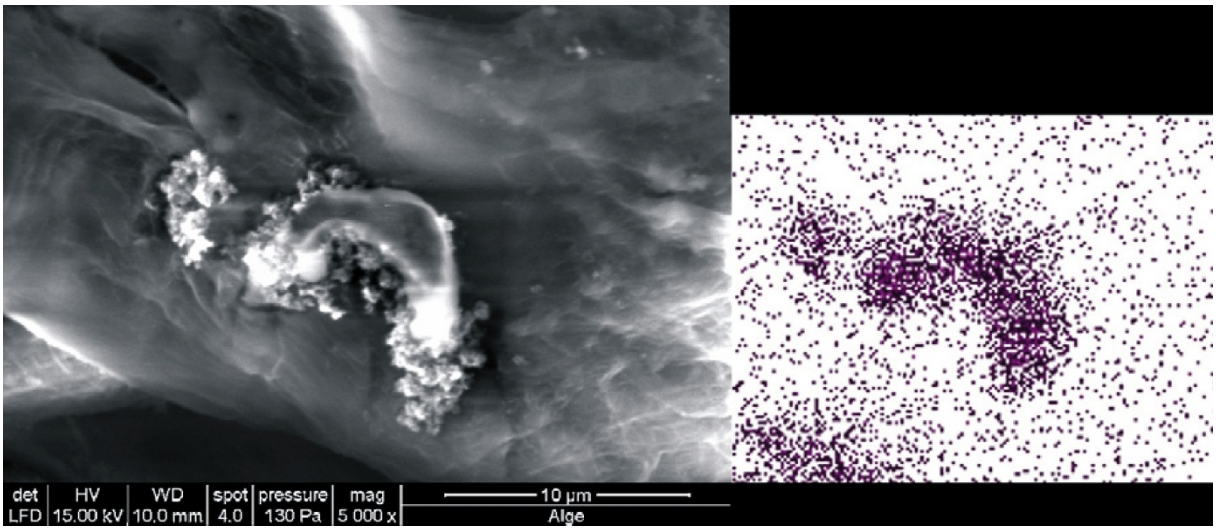

Figure 43. SEM image of an alga after exposure (50 mg L^{-1} TiO_2 in ISO algal test media, 48 h) and an EDX dot map showing the distribution of Ti. It can be seen that the TiO_2 is attached to the surface of the algae.

As can be seen from Figure 43, the aggregates are found to attach to the surface of the algal cells, which makes these effect mechanisms plausible. Generation of photocatalytical ROS is another frequently mentioned reason for cytotoxicity of TiO_2 NPs and the photocatalytic effects of rutile and anatase type TiO_2 will be induced by an excitation wavelength below 413 nm and 388 nm, respectively (*198*). In a standard algal growth test setup, the photocatalytic activity of TiO_2 NPs is therefore expected to be limited since white fluorescent light is used as light source (International Organization for Standardization, 2002) and the polystyrene test vessels were found to reduce transmission of light, in the wavelengths relevant for photocatalysis of TiO_2 (Figure 44).

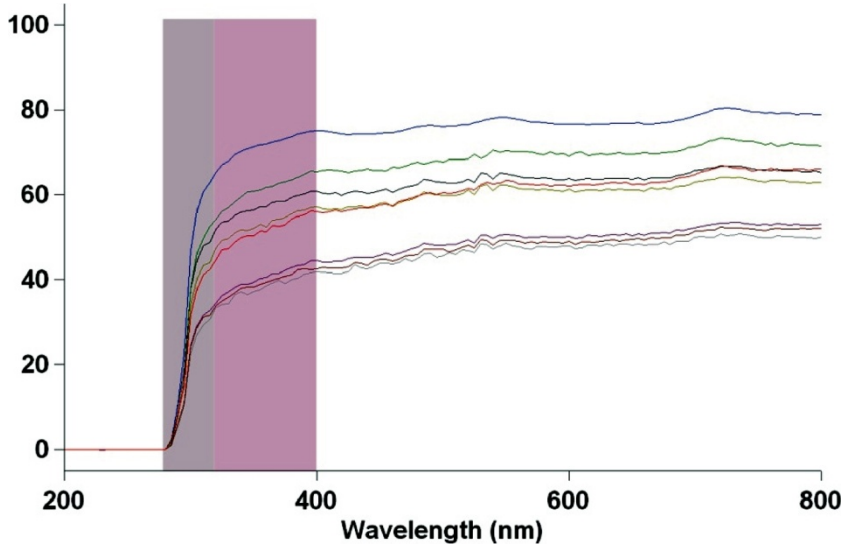

Figure 44. Transmission of light (λ=200-800nm) through the bottom of the polystyrene test vessel. The UVA and UVB areas are indicated. The 8 different curves are all measurements from the same polystyrene test vessel, rotated and placed in 8 different positions. This was done do to inscription and differences in the bottom of the test vessel, resulting in areas with different light transmission.

It should be mentioned, however, that for P25 the photocatalytic activity has been found to be extended into the visible light wavelengths due to the mixed crystalline phases (*32*). In our experiments, the toxicity of TiO_2 was not affected by changes in light intensity. TiO_2 induced photocatalytical generation of reactive oxygen species cannot be excluded but is not believed to play a major role in the toxicity of TiO_2 in algal tests. This is in correspondence with other studies (*199*) showing that antibacterial activity of TiO_2 was observed under both dark and light conditions, indicating effects due to mechanisms other than photocatalytical ROS.

5.4.3 Sorption of cadmium to TiO_2 in suspension

Sorption of cadmium onto TiO_2 particles was found to be a fast process, reaching a steady state within 30 - 60 min (data not shown). This is in correspondence with results reported by Zhang et al. (*187*). Figure 45A shows the Freundlich sorption isotherms for cadmium sorption onto the three different types of TiO_2 particles, which have been determined based on experimental values as described in Section 2.5. The isotherm equations were found to be: log Cs = 0.54×log Cw + log (19.63) (LW-S), log Cs = 0.49×log Cw + log (68.71) (P25) and log Cs = 0.52×log Cw + log (153.46) (UV100). When comparing these results to particle characteristics in Table 1 it is seen that sorption capacity increases with decreasing primary particle size and increasing surface area. When sorption is normalized to the surface area, the sorption isotherms for larger particles (LW-S) and the 25 nm NPs (P25) are very similar (Figure 45B).

The sorption capacity of the smallest particle type (UV100) is significantly lower. Similar results have been seen for the sorption of Pb to TiO_2 particles, where sorption capacity and affinity was lower for smaller particles, than for larger particles, when normalized to surface area (*200*). Similarly, it has been described by Gao et al. (*201*) that sorption affinity of Cd^{2+} onto 8 nmTiO_2 NPs was found to be smaller than that of other TiO_2 particles with primary particle sizes of 21–145 nm. Differences in adsorption energy were thought to be due to intraparticle electrostatic effects or Ti-site disorder (disorder of the TiO_2 lattice and the structure of Ti atom sites) for particles less than 20 nm (*201*). Furthermore, as a dry powder, UV100 TiO_2 NPs have been found to form very compact aggregates, whereas P25 forms rougher aggregates with amore porous surface (*103*). In the present study the three particle types were suspended in milliQ water and investigated by use of TEM. As can be seen from Figure 42, the formation of more compact aggregates for UV100 TiO_2 NPs seems also to be the case in aqueous media, and could therefore influence sorption capacities. Hence, not only the surface of the primary particle, but also the aggregate surface characteristics, might influence sorption of Cd onto the particles. Finally, the more amorphous structure of UV100 TiO_2, compared to P25 and LW-S, as well as the fact that the BET surface area is measured in vacuum, and not in dispersion, should be taken into account.

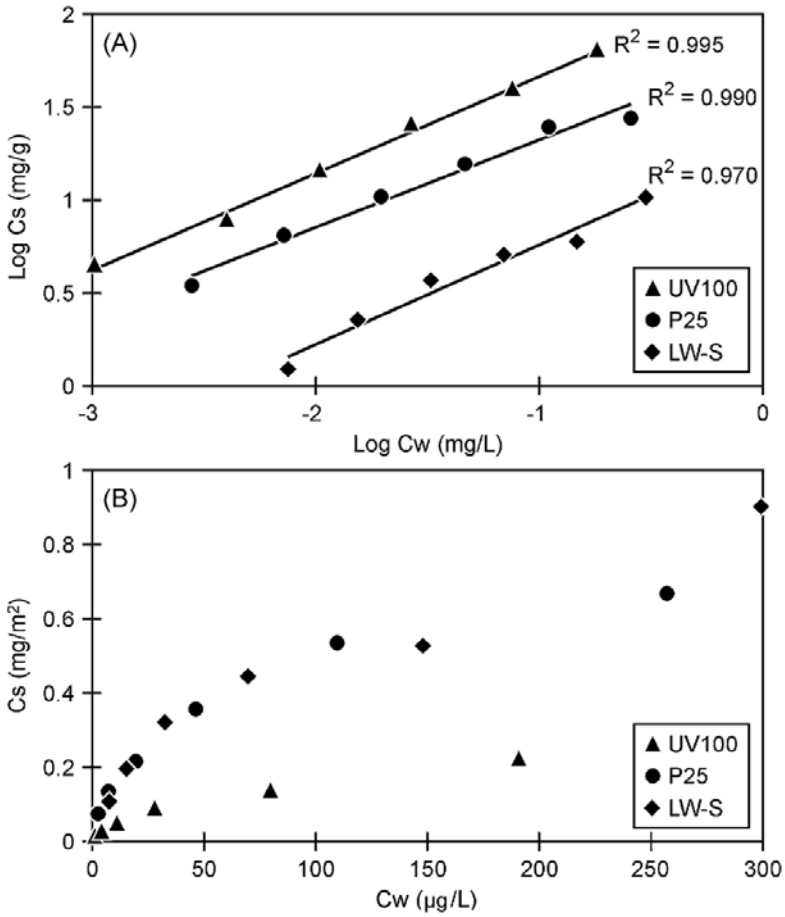

Figure 45 (A): Concentrations of cadmium sorbed to titanium dioxide (Cs) as a function of water phase concentrations (Cw) of cadmium and estimated Freundlich sorption isotherms with the following coefficients: KF = 154, n = 0.52 (UV100), KF = 69, n = 0.49 (P25), KF = 20, n = 0.54 (LW-S). Titanium dioxide was kept constant at a concentration of 2 mg L^{-1} TiO_2. **(B):** Sorption of cadmium onto 2 mg L^{-1} TiO_2.Water phase concentrations (Cw) of total cadmium are plotted against the solid total cadmium concentration (Cs) expressed as cadmium mass m^{-2} TiO_2.

5.4.4 TiO_2 as a modifying factor on cadmium toxicity

A series of algal growth inhibition tests were carried out in order to determine whether the presence of TiO_2 particles affected the toxicity of cadmium towards algae. Tests were made to determine the concentration–response relation for cadmium alone (concentration range: 10 - 320 µg L^{-1}) and for cadmium in the presence of 2 mg L^{-1} TiO_2 particles. Due to the toxicity of UV100 in low concentrations, only P25 and LW-S particle types were used in these tests. The results can be seen in Table 12. Cadmium toxicity can be affected by factors such as illumination, temperature and pH (*202*). Even though these factors were kept constant, toxicity tests of cadmium in

the presence of TiO_2 were always combined with a test of cadmium alone, so that comparisons could be made without errors due to unidentified changes in test conditions. Based on the results from the sorption tests the cadmium concentrations were expressed as water phase concentrations, i.e. concentrations of solute species, which are mainly Cd^{2+}, $CdCl^{+}$ and $Cd(Edta)^{-2}$ as estimated by geochemical modeling in PHREEQC (*189*) using ISO media composition as input. This was done since effects of cadmium are expected to change as a result of reduced bioavailability due to sorption. However, by expressing the cadmium concentration as concentration of dissolved Cd(II) species this sorption is taken into account, making it possible to quantify the influence of TiO_2 particles on cadmium toxicity. The effect concentrations obtained in algal tests of cadmium, with and without addition of TiO_2 suspensions, are therefore shown in Table 12 in terms of both total concentrations and water phase concentrations of cadmium. When comparing effect concentrations for cadmium alone with effect concentrations of cadmium in the presence of TiO_2 particles (water phase concentrations) changes in cadmium toxicity were observed.

Table 12. Effect concentrations and 95% confidence intervals for cadmium in the presence and absence of TiO_2 particles in the ISO algal test (International Organization for Standardization, 2002). Test organism: *Pseudokirchneriella Subcapitata*, incubation time: 72 h. The tests were repeated several times as indicated by the numbers I–IV. Comparisons of test results in the presence and absence of TiO_2 should primarily be within the same test run (i.e. results from assay I for 'Only Cd' should be compared with results from assay I 'with P25'). Cadmium concentrations are expressed as total Cd(II) concentrations as well as concentration of dissolved Cd(II) species in the water phase (Cd_w).

	EC_{10} (µg Cd_{total}/L)		EC_{20} (µg Cd_{total}/L)		EC_{50} (µg Cd_{total}/L)		Test run no.
Only Cd	**35.9** [32.3;39.8]		**44.4** [41.0;48.0]		**66.5** [63.6;69.5]		I
	27.3 [24.6;30.4]		**33.6** [31.0;36.5]		**50.0** [47.6;52.5]		II
	20.0 [18.3;21.9]		**26.3** [24.5;28.2]		**44.3** [42.5;46.2]		III
	18.5 [16.6;20.6]		**25.1** [23.1;27.3]		**45.2** [43.0;47.5]		IV
	EC_{10}		EC_{20}		EC_{50}		
	(µg Cd_{total}/L)	(µg Cd_w/L)	(µg Cd_{total}/L)	(µg Cd_w/L)	(µg Cd_{total}/L)	(µg Cd_w/L)	Test run no.
Cd and TiO_2 P25	**45.1** [32.3;39.8]	**22.9** [20.5;35.6]	**51.8** [48.3;55.5]	**27.2** [24.9;29.6]	**67.6** [65.2;70.0]	**37.8** [36.2;39.5]	I
	36.6 [33.2;40.2]	**17.6** [15.6;19.8]	**46.9** [43.7;50.4]	**24.0** [22.0;26.2]	**75.6** [72.1;79.3]	**43.4** [41.0;46.0]	I
	36.6 [32.9;40.9]	**17.7** [15.5;20.3]	**44.5** [41.0;48.4]	**22.6** [20.3;25.0]	**64.7** [61.4;68.1]	**35.8** [33.6;38.2]	II
Cd and TiO_2 LW-S	**50.8** [20.9;124.0]	**46.4** [21.8;98.7]	**63.6** [33.1;122.0]	**57.8** [33.3;100.0]	**97.4** [78.1;121.0]	**87.9** [73.0;106.0]	III
	31.1 [28.9;33.5]	**24.8** [22.9;26.9]	**38.8** [36.7;41.1]	**31.6** [29.7;33.6]	**59.1** [57.1;61.3]	**50.1** [48.2;52.1]	IV

As shown in Table 12 a decrease in cadmium toxicity was observed in the presence of LW-S (test run no. III & IV), which is believed to be due to sorption of cadmium without internalization of the particles. On the other hand the presence of P25 TiO_2 nanoparticles resulted in significantly decreased EC-values for cadmium (test run no. I&II). This could be a result of combined toxicity (e.g. increased cadmium uptake due to cell membrane damage caused by TiO_2 or a consequence of the sorption of cadmium to the TiO_2 NPs, where the adsorbed cadmium is still bioavailable to the algae (either due to particle sorption to algal surface or internalization of the NPs). However, these hypotheses need further investigation before any conclusions on effect mechanisms can be made.

5.5 Conclusion

This study shows that, while it is in principle possible to use standardized test for evaluation of the algal toxicity of TiO_2 nanoparticles, it is difficult to reproduce the obtained test results. Concentration- and time-dependent aggregation, Heteroaggregation and particle crystallinity will influence the test results. These issues represent a large challenge to standardized tests and further investigations are needed to clarify the mechanisms occurring. In this study, however, it was consistently found that, out of three types of commercially available TiO_2 particles, the smallest TiO_2 particle type (primary particle size <10 nm) resulted in higher inhibition at lower concentrations than the two other particle types (30 and 300 nm). The effects mechanisms for all three types are believed to comprise others than generation of reactive oxygen species and possible mechanisms include adhesion of TiO_2 to algal cells and physical disruption of the cell membranes. However, it is not possible to make a general conclusion on the factors determining the algal toxicity of TiO_2 at the current state of knowledge. By adding TiO_2 NPs to algal tests of cadmium changes in toxicity were observed. For the 30 nm particle the toxicity was greater than what could be explained by the concentration of dissolved Cd(II) species. This indicates either a combined effect of cadmium and TiO_2 or that TiO_2 increases the bioavailability of cadmium for the algae. These results underlines that the potential interactions of engineered nanoparticles with existing environmental contaminants must be taken into account in environmental risk assessments of nanoparticles.

5.6 Acknowledgements

The authors acknowledge the kind gift of titanium dioxide (Hombitan LW-S and Hombikat UV100) from Sacthleben (Duisburg, Germany). The authors would like to thank Sihn Nguyen (DTU Environment) for performing BET measurements, Susanne Kruse (DTU Environment) for carrying out chemical analysis, Signe Qualmann (DTU Environment) for assisting with ecotoxicological tests and Associate Professor Nina Cedergreen (Copenhagen University) for assistance with data analysis.

6 Conclusions and Outlook

This study addressed the first objectives by identifying the regions of stability and aggregation of TiO_2 nanoparticles in various aqueous milieus. We hypothesized that it is possible to generalize and extrapolate the information gained from static sedimentation tests in synthetic water to the prediction of nanoparticle behavior in complex aqueous matrices. We therefore validated the data from synthetic water by introducing the chosen model nanoparticle (TiO_2) in natural water of higher chemical complexity. It was possible to receive good correlation of values identifying the state of TiO_2 stability or aggregation.

Particle size, zeta potential and remaining concentration in the supernatant were determined with photon correlation spectroscopy (PCS) and turbidity measurement. The limitations of the analytical methods became obvious in the course of this study. PCS is not the adequate technique for environmental/natural samples and polydisperse systems. The contamination of the sample through other colloids or dust confines the application of PCS. Further, aggregation of nanoparticles causes directed movement (sedimentation) within the measurement cell which is against the principal theory of dynamic light scattering techniques. High polydispersity index produce incorrect data in both PCS analysis and turbidity measurements.

The chosen semi-automated titration approach enables large data-sets and a highly repetitive output. The graphical presentation of this large data set as interpolated contour plots is enabling good interpretation and prediction across the measured data by extrapolation. However, the choice of the underlying mathematical interpolation (IDW) is questionable in its applicability for this data-set since it represents spatial distribution. Until now, we did not find a better technique.

A second objective of this study was to determine the parameters controlling the distribution and transport of TiO_2 nanoparticles in the aquatic environment. Therefore we monitored the transport of nano-TiO_2 in microcosm flume experiments. Results show that the distribution of nanoparticles is determined by the hydrodynamic and hydrochemical behavior as well as the presence of biofilm. The results from the first two studies explain the aggregation and hence sedimentation behavior of TiO_2

nanoparticles in aqueous systems and are basic information for the flume experiments. The flume experiments also enable to investigate the toxicological effects of various TiO_2 nanoparticles on microorganisms embedded in the biofilm.

The choice of the model compound is reasonable since TiO_2 is commercially available, already introduced in various consumer products and due to its photoreactivity implemented in many representative studies. Additionally, the compound is registered in the nanoparticle testing program of the OECD which makes TiO_2 of interest for researchers. However, TiO_2 is not very suitable for many analytical methods (e.g. PCS) and is difficult to quantify by means of e.g. inductively coupled plasma spectrometry because of its insolubility (except hydrochloric acid). Further, due to its hydrophobic character the chosen TiO_2 is very difficult to handle in the laboratory and causes long lasting contamination of any material coming in contact with TiO_2.

The presented studies suggest that TiO_2 nanoparticles interact with other contaminants and the biota within the aquatic environment causing adverse effects. The behavior of nanoparticles is governed by the particle size, shape, surface charge and presence of other materials (e.g. natural organic matter) or contaminants in the environment. We demonstrated that TiO_2 nanoparticles aggregate in certain water types, depending on the chemistry, presence of ions and organic matter. The dispersion state alters the toxicity of nanoparticles and therefore a throughout characterization is necessary for toxicological tests. In order to compare scientific results, preliminary testing routines are crucial.

To summarize, in order to assess the environmental behavior and the potential risks of engineered nanoparticles a characterization in the aquatic system is necessary. The existing testing techniques need to be adapted to the difficulties encountered by the special behavior of engineered nanoparticles. Because there are no testing routines for both characterization and toxicological tests only little comparable results exist until now. Therefore, proposed risks related to engineered nanoparticles in the environment needs to be validated and evaluated with care. Additionally, the concentrations of engineered nanoparticles in the environment are very low and therefore the fear of toxicity is more due to lack of information and education of the

society. Although, advanced scientific methods are able to detect nanoparticles in environmental samples it is very difficult to differentiate between natural nanoparticles and engineered nanoparticles.

The rapid development and implementation of nanoparticles in consumer products needs to be accompanied by research. Therefore, basic and applied sciences about nanoparticles and research on nanoparticles in the environment are crucial for any further scientific and social progress.

7 Literature

(1) Maynard, A. D.; Aitken, R. J.; Butz, T.; Colvin, V.; Donaldson, K.; Oberdorster, G.; Philbert, M. A.; Ryan, J.; Seaton, A.; Stone, V.; Tinkle, S. S.; Tran, L.; Walker, N. J.; Warheit, D. B. Safe handling of nanotechnology. *Nature* **2006**, 444, 267-269.

(2) Taniguchi, N. **1974**. On the basic concept of Nanotechnology. Proc. Inl. Conf. Prod. Eng. Japan Society of Precision Engineering, Tokyo.

(3) Society, R. Nanoscience and nanotechnologies: opportunities and uncertainties. Royal Society and Royal Academy of Engineering. **2004**. 113.

(4) Hochella, M. H. There's plenty of Room at the Bottom: Nanoscience in geochemistry. *Geochimica et Cosmochimica Acta* **2002** 66, 735-743.

(5) Eigler, D. M.; Schweizer, E. K. Positioning single atoms with a scanning tunnelling microscope. *Nature* **1990**, 344, 524-526.

(6) Society, R.; Engineering, R. A. o. Nanoscience and nanotechnologies: opportunities and uncertainties. The Royal Society. **2004**.

(7) Lead, J. R.; Wilkinson, K. J. Aquatic colloids and nanoparticles: Current knowledge and future trends. *Enviornmental Chemistry* **2006**, 3, 159-171.

(8) Christian, P.; von der Kammer, F.; Baalousha, M.; Hofmann, T. Nanoparticles: structure, properties, preparation and behaviour in environmental media. *Ecotoxicology* **2008**, 17, 326-343.

(9) Lead, J. R.; Wilkinson, K. J. (Eds.). **2006**. Aquatic colloids and particles: behaviour, structure and characterisation. John Wiley and Sons, Chichester.

(10) Wigginton, N. S.; Haus, K. L.; Hochella, M. F. J. Aquatic environmental nanoparticles. *Journal of Environmental Monitoring* **2007**, 9, 1306-1316.

(11) Nowack, B.; Bucheli, T. D. Occurrence, behavior and effects of nanoparticles in the environment. *Environmental Pollution* **2007**, in Press.

(12) Kroto, H. W.; Heath, J. R.; O'Brien, S. C.; Curl, R. F.; Smalley, R. E. C60: Buckminsterfullerene. *Nature* **1985**, 318, 162-163.

(13) Iijima, S. Helical microtubules of graphitic carbon. *Nature* **1991**, 354, 56-58.

(14) Cao, G. **2004**. Nanostructures and Nanomaterials: Synthesis, Properties and Applications. Imperial College Press, London.

(15) Ju-Nam, Y.; Lead, J. R. Manufactured nanoparticles: An overview of their chemistry, interactions and potential environmental implications. *Science of The Total Environment* **2008**, 400, 396-414.

(16) Brant, J.; Lecoanet, H.; Hotze, M.; Wiesner, M. Comparison of electrokinetic properties of colloidal fullerenes (n-C60) formed using two procedures. *Environmental Science & Technology* **2005**, 39, 6343-6351.

(17) Deguchi, S.; Alargova, R. G.; Tsujii, K. Stable Dispersions of Fullerenes, C60 and C70, in Water. Preparation and Characterization. *Langmuir* **2001**, 17, 6013-6017.

(18) Deguchi, S.; Mukai, S.; Tsudome, M.; Horikoshi, K. Facile Generation of Fullerene Nanoparticles by Hand-Grinding. *Advanced Materials* **2006**, 18, 729-732.

(19) Chen, K. L.; Mylon, S. E.; Elimelech, M. Aggregation kinetics of alginate-coated hematite nanoparticles in monovalent and divalent electrolytes. *Environmental Science & Technology* **2006**, 40, 1516-1523.

(20) Dhawan, A.; Taurozzi, J. S.; Pandey, A. K.; Shan, W.; Miller, S. M.; Hashsham, S. A.; Tarabara, V. V. Stable Colloidal Dispersions of C60 Fullerenes in Water: Evidence for Genotoxicity. *Environmental Science & Technology* **2006**, 40, 7394-7401.

(21) Bouchard, D.; Ma, X.; Isaacson, C. Colloidal Properties of Aqueous Fullerenes: Isoelectric Points and Aggregation Kinetics of C60 and C60 Derivatives. *Environmental Science & Technology* **2009**, 43, 6597-6603.

(22) Labille, J.; Masion, A.; Ziarelli, F.; Rose, J.; Brant, J.; Villiéras, F.; Pelletier, M.; Borschneck, D.; Wiesner, M. R.; Bottero, J.-Y. Hydration and dispersion of C60 in aqueous systems: The nature of water−fullerene interactions. *Langmuir* **2009**, 25, 11232-11235.

(23) Zakharian, T. Y.; Seryshev, A.; Sitharaman, B.; Gilbert, B. E.; Knight, V.; Wilson, L. J. A fullerene-paclitaxel chemotherapeutic: synthesis, characterization, and study of biological activity in tissue culture. *Journal Of The American Chemical Society* **2005**, 14, 12508-12509.

(24) Becker, L.; Bada, J.; Winans, R.; Hunt, J.; Bunch, T.; French, B. Fullerenes in the 1.85-billion-year-old Sudbury impact structure. *Science* **1994**, 265, 642-645.

(25) Heymann, D.; Jenneskens, L. W.; Jehlicka, J.; Koper, C.; Vlietstra, E. Terrestrial and extraterrestrial fullerenes. *Fullerenes, Nanotubes and Carbon Nanostructures* **2003**, 11, 333-370.

(26) Daniel, M.-C.; Astruc, D. Gold Nanoparticles: Assembly, supramolecular chemistry, quantum-size-related Properties, and qpplications toward biology, catalysis, and nanotechnology. *Chemical Reviews* **2003**, 104, 293-346.

(27) Zhou, J.; Ralston, J.; Sedev, R.; Beattie, D. A. Functionalized gold nanoparticles: Synthesis, structure and colloid stability. *Journal of Colloid and Interface Science* **2009**, 331, 251-262.

(28) Navarro, E.; Piccapietra, F.; Wagner, B.; Marconi, F.; Kaegi, R.; Odzak, N.; Sigg, L.; Behra, R. Toxicity of Silver Nanoparticles to Chlamydomonas reinhardtii. *Environmental Science & Technology* **2008**, 42, 8959–8964.

(29) Zhang, W.-X. Nanoscale iron particles for environmental remediation: An overview. *Journal of Nanoparticle Research* **2003**, 5, 323-332.

(30) Aitken, R. J.; Chaudhry, M. Q.; Boxall, A. B. A.; Hull, M. Manufacture and use of nanomaterials: current status in the UK and global trends. *Occupational Medicine* **2006**, 56, 300-306.

(31) Ohno, T.; Sarukawa, K.; Tokieda, K.; Matsumura, M. Morphology of a TiO_2 photocatalyst (Degussa, P-25) consisting of anatase and rutile crystalline phases. *Journal of Catalysis* **2001**, 203, 82-86.

(32) Hurum, D. C.; Agrios, A. G.; Gray, K. A.; Rajh, T.; Thurnauer, M. C. Explaining the enhanced photocatalytic activity of Degussa P25 mixed-phase TiO_2 using EPR. *Journal of Physical Chemistry* **2003**, 107, 4545-4549.

(33) Alvarez, P. J. J.; Colvin, V.; Lead, J.; Stone, V. Research priorities to advance eco-responsible nanotechnology. *ACS Nano* **2009**, 3, 1616-1619.

(34) Lead, J. R.; Wilkinson, K. J. Aquatic colloids and nanoparticles. Current knowledge and future trends. *Environmental Chemistry* **2004**, 3, 159-171.

(35) Murr, L. E.; Esquivel, E. V.; Bang, J. J.; Rosa, G. d. l.; Gardea-Torresdey, J. L. Chemistry and nanoparticulate compositions of a 10.000 year-old ice core melt water. *Water Research* **2004**, 38, 4282-4296.

(36) Kaegi, R.; Ulrich, A.; Sinnet, B.; Vonbank, R.; Wichser, A.; Zuleeg, S.; Simmler, H.; Brunner, S.; Vonmont, H.; Burkhardt, M.; Boller, M. Synthetic TiO_2 nanoparticle emission from exterior facades into the aquatic environment. *Environmental Pollution* **2008**, 156, 233-239.

(37) Kiser, M. A.; Westerhoff, P.; Benn, T.; Wang, Y.; Pérez-Rivera, J.; Hristovski, K. Titanium nanomaterial removal and release from wastewater treatment plants. *Environmental Science & Technology* **2009**, 43, 6757-6763.

(38) Tungittiplakorn, W.; Lion, L. W.; Cohen, C.; Kim, J. Y. Engineered polymeric nanoparticles for soil remediation. *Environmental Science Technology* **2004**, 38, 1605-1610.

(39) Limbach, L. K.; Bereiter, R.; Müller, E.; Krebs, R.; Gälli, R.; Stark, W. J. Removal of oxide nanoparticles in a model wastewater treatment plant: influence of agglomeration and surfactants on clearing efficiency. *Environmental Science & Technology* **2008**, 42, 5828-5833

(40) Navarro, E.; Baun, A.; Behra, R.; Hartmann, N. B.; Filser, J.; Miao, A. J.; Quigg, A.; Santschi, P. H.; Sigg, L. Environmental behavior and ecotoxicity of engineered nanoparticles to algae, plants, and fungi. *Ecotoxicology* **2008**, 17, 372-386.

(41) Fang, J.; Shan, X.-q.; Wen, B.; Lin, J.-m.; Owens, G. Stability of titania nanoparticles in soil suspensions and transport in saturated homogeneous soil columns. *Environmental Pollution* **2009**, 125, 1101-1109.

(42) Hofmann, T.; von der Kammer, F. Estimating the relevance of engineered nanoparticle facilitated transport of hydrophobic organic contaminants in porous media. *Environmental Pollution* **2009**, 157, 1117-1126.

(43) Waychunas, G. A.; Kim, C. S.; Banfield, J. F. Nanoparticulate iron oxide minerals in soils and sediments: Unique properties and contaminant scavenging mechanisms. *Journal of Nanoparticle Research* **2005**, 7, 409-433.

(44) Handy, R. D.; Henry, T. B.; Scown, T. M.; Johnston, B. D.; Tyler, C. R. Manufactured nanoparticles: their uptake and effects on fish-a mechanistic analysis. *Ecotoxicology* **2008**, 1.

(45) Klaine, S. J.; Alvarez, P. J. J.; Batley, G. E.; Fernandes, T. F.; Handy, R. D.; Lyon, D. Y.; Mahendra, S.; McLaughlin, M. J.; Lead, J. R. Nanomaterials in the environment: Behavior, fate, bioavailability, and effects. *Environmental Toxicology and Chemistry* **2008**, 27, 1825-1851.

(46) Birdi, K. S. (Ed.). **2009**. Handbook of surface and colloid chemistry. CRC Press LLC, London.

(47) Jiang, J.; Oberdörster, G.; Biswas, P. Characterization of size, surface charge, and agglomeration state of nanoparticle dispersions for toxicological studies. *J Nanopart Res* **2009**, 11, 77-89.

(48) Handy, R. D.; Owen, R.; Valsami-Jones, E. The ecotoxicology of nanoparticles and nanomaterials: current status, knowledge gaps, challenges, and future needs. *Ecotoxicology* **2008**, 17, 315-325

(49) Phenrat, T.; Saleh, N.; Sirk, K.; Tilton, R. D.; Lowry, G. V. Aggregation and sedimentation of aqueous nanoscale zerovalent iron dispersions. *Environmental Science & Technology* **2007**, 41, 284-290.

(50) Elimelech, M.; Omelia, C. R. Effect of particle-size on collision efficiency in the deposition of Brownian particles with electrostatic energy barriers. *Langmuir* **1990**, 6, 1153-1163.

(51) Grasso, D.; Subramaniam, K.; Butkus, M.; Strevett, K.; Bergendahl, J. A review of non-DLVO interactions in environmental colloidal systems. *Re/Views in Environmental Science & Bio/Technology* **2002**, 1, 17-38.

(52) Chen, K. L.; Elimelech, M. Relating colloidal stability of fullerene (C60) nanoparticles to nanoparticle charge and electrokinetic properties. *Environmental Science & Technology* **2009**, 43, 7270-7276.

(53) Baalousha, M. Aggregation and disaggregation of iron oxide nanoparticles: influence of particles concentration, pH and natural organic matter. *Science of The Total Environment* **2009**, 407, 2093-2101.

(54) Chen, K. L.; Mylon, S. E.; Elimelech, M. Enhanced aggregation of alginate-coated iron oxide (hematite) nanoparticles in the presence of calcium, strontium, and barium cations. *Langmuir* **2007**, 23, 5920-5928.

(55) Handy, R. D.; von der Kammer, F.; Lead, J. R.; Hassellöv, M.; Owen, R.; Crane, M. The ecotoxicology and chemistry of manufactured nanoparticles. *Ecotoxicology* **2008**, 17, 287-314.

(56) Kretzschmar, R.; Holthoff, H.; Sticher, H. Influence of pH and humic acid on coagulation kinetics of kaolinite: A dynamic light scattering study. *Journal of Colloid and Interface Science* **1998**, 202, 95-103.

(57) Imae, T.; Muto, K.; Ikeda, S. The pH dependence of dispersion of TiO_2 particles in aqueous surfactant solutions. *Colloid and Polymer Science* **1991**, 269, 43-48.

(58) Kosmulski, M. pH-dependent surface charging and points of zero charge III. Update. *Journal of Colloid and Interface Science* **2006**, 298, 730-741.

(59) Hyung, H.; Kim, J.-H. Natural organic matter (NOM) adsorption to multi-walled carbon nanotubes: Effect of NOM characteristics and water quality parameters. *Environmental Science & Technology* **2008**, 42, 4416-4421.

(60) Stumm, W.; Morgan, J. J. (Eds.). **1996**. Aquatic Chemistry. Chemical equilibria and rates in natural waters. JOhn Wiley & Sons, Inc. , New York.

(61) Harter, T.; Wagner, S.; Atwill, E. R. Colloid transport and filtration of cryptosporidium parvum in sandy soils and aquifer sediments. *Environmental Science & Technology* **1999**, 34, 62-70.

(62) Searcy, K. E.; Packman, A. I.; Atwill, E. R.; Harter, T. Deposition of cryptosporidium oocysts in streambeds. *Applied and Environmental Microbiology* **2006**, 72, 1810-1816.

(63) Searcy, K. E.; Packman, A. I.; Atwill, E. R.; Harter, T. Capture and retention of cryptosporidium parvum oocysts by pseudomonas aeruginosa biofilms. *Applied and Environmental Microbiology* **2006**, 72, 6242-6247.

(64) Flemming, H.-C. Sorption sites in biofilms. *Water Science and Technology* **1995**, 32, 27.

(65) Morales, C. F. L.; Strathmann, M.; Flemming, H.-C. Influence of biofilm on the movement of colloids in porous media: Implications for colloidal facilitated transport in subsurface environments. *Water Research* **2007**, 41, 2059-2068.

(66) Liu, Y.; Li, J. Role of pseudomonas aeruginosa biofilm in the initial adhesion, growth and detachment of escherichia coli in porous media. *Environmental Science & Technology* **2007**, 42, 443–449.

(67) Stolpe, B.; Hassellöv, M. Changes in size distribution of fresh water nanoscale colloidal matter and associated elements on mixing with seawater. *Geochimica et Cosmochimica Acta* **2007**, 71, 3292-3301.

(68) Maynard, A.; Baron, P.; Foley, M.; Shvedova, A.; Kisin, E.; Castranova, V. Exposure to carbon nanotube material: aerosol release during the handling of unrefined single-walled carbon nanotube material. *Journal of Toxicology and Environmental Health* **2004**, 67, 87-107.

(69) Oberdörster, G.; Ferin, J.; Gelein, R.; Soderholm, S. C.; Finkelstein, J. Role of the alveolar macrophage in lung injury: Studies with ultrafine particles. *Environmental Health Perspectives* **1992**, 97, 193-199.

(70) Lovern, S. B.; Klaper, R. Daphnia magna mortality when exposed to titanium dioxide and fullerene (C60) nanoparticles. *Environmental Toxicology and Chemistry* **2005**, 25, 1132-1137.

(71) Federici, G.; Shaw, B. J.; Handy, R. D. Toxicity of titanium dioxide nanoparticles to rainbow trout (oncorhynchus mykiss): Gill Injury, oxidative stress, and other physiological effects. *Aquatic Toxicology* **2007**, 84, 415-430.

(72) Wang, H.; Wick, R. L.; Xing, B. Toxicity of nanoparticulate and bulk ZnO, Al_2O_3 and TiO_2 to the nematode *Caenorhabditis elegans*. *Environmental Pollution* **2009**, 157, 1171-1177

(73) Yang, Y.; Hofmann, T.; Pies, C.; Grathwohl, P. Sorption of polycyclic aromatic hydrocarbons (PAHs) to carbonaceous materials in a river floodplain soil. *Environmental Pollution* **2008**, 156, 1357-1363.

(74) Yang, K.; Xing, B. Adsorption of fulvic acid by carbon nanotubes from water. *Environmental Pollution* **2009**, 157, 1095-1100

(75) Sun, H.; Zhang, X.; Niu, Q.; Chen, Y.; Crittenden, J. Enhanced Accumulation of Arsenate in Carp in the Presence of Titanium Dioxide Nanoparticles. *Water, Air, and Soil Pollution* **2007**, 178, 245.

(76) Baun, A.; Sørensen, S. N.; Rasmussen, R. F.; Hartmann, N. B.; Koch, C. B. Toxicity and bioaccumulation of xenobiotic organic compounds in the presence of aqueous suspensions of aggregates of nano-C60. *Aquatic Toxicology* **2008**, 86, 379-387.

(77) Hartmann, N.; von der Kammer, F.; Baalousha, M.; Ottofuelling, S.; Baun, A. Algal testing of titanium dioxide nanoparticles – testing considerations, inhibitory effects and modification of cadmium bioavailability. *Toxicology* **2009**, 269, 190-197.

(78) Mueller, N. C.; Nowack, B. Exposure modelling of engineered nanoparticles in the environment. *Environmental Science & Technology* **2008**, 42, 4447-4453.

(79) Brunet, L. n.; Lyon, D. Y.; Hotze, E. M.; Alvarez, P. J. J.; Wiesner, M. R. Comparative photoactivity and antibacterial properties of C60 fullerenes and titanium dioxide nanoparticles. *Environmental Science & Technology* **2009**, 43, 4355-4360.

(80) Kang, S.; Mauter, M. S.; Elimelech, M. Microbial cytotoxicity of carbon-based nanomaterials: Implications for river water and wastewater effluent. *Environmental Science & Technology* **2009**, 43, 2648-2653.

(81) Sayes, C. M.; Wahi, R.; Kurian, P. A.; Liu, Y.; West, J. L.; Ausman, K. D.; Warheit, D. B.; Colvin, V. L. Correlating nanoscale titania structure with toxicity: A cytotoxicity and inflammatory response study with human dermal fibroblasts and human lung epithelial cells. *Toxicological Sciences* **2006**, 92, 174-185.

(82) Warheit, D. B.; Webb, T. R.; Reed, K. L.; Frerichs, S.; Sayes, C. M. Pulmonary toxicity study in rats with three forms of ultrafine-TiO_2 particles: Differential responses related to surface properties. *Toxicology* **2007**, 230, 90-104

(83) Battin, T. J.; v d Kammer, F.; Weilhartner, A.; Ottofuelling, S.; Hofmann, T. Nanostructured TiO_2: transport behavior and effects on aquatic microbial communities under environmental conditions. *Environmental Science & Technology* **2009**, 43, 8098–8104.

(84) Farré, M.; Pérez, S.; Gajda-Schrantz, K.; Osorio, V.; Kantiani, L.; Ginebreda, A.; Barceló, D. First determination of C60 and C70 fullerenes and N-methylfulleropyrrolidine C60 on the suspended material of wastewater effluents by liquid chromatography hybrid quadrupole linear ion trap tandem mass spectrometry. *Journal of Hydrology* **2010**, 383, 44-51.

(85) Gottschalk, F.; Sonderer, T.; Scholz, R. W.; Nowack, B. Modeled environmental concentrations of engineered nanomaterials (TiO_2, ZnO, Ag, CNT, fullerenes) for different regions. *Environmental Science & Technology* **2009**, 43, 9216-9222.

(86) Koelmans, A. A.; Nowack, B.; Wiesner, M. R. Comparison of manufactured and black carbon nanoparticle concentrations in aquatic sediments. *Environmental Pollution* **2009**, 157, 1110-1116.

(87) Kretzschmar, R.; Borkovec, M.; Grolimund, D.; Elimelech, M. Mobile subsurface colloids and their role in contaminant transport. *Advances in Agronomy* **1999**, 66, 121-193

(88) Baalousha, M.; Lead, J. R.; v d Kammer, F.; Hofmann, T., **2009**. Natural colloids and nanoparticles in aquatic and terrestrial environments, in: Lead, J. R., Smith, E. (Eds.), Environmental and Human Health Impacts of Nanotechnology. John Wiley & Sons, pp. 109-161.

(89) French, R. A.; Jacobson, A. R.; Kim, B.; Isley, S. L.; Penn, R. L.; Baveye, P. C. Influence of ionic strength, pH, and cation valence on aggregation kinetics of titanium dioxide nanoparticles. *Environmental Science & Technology* **2009**, 43, 1354–1359.

(90) Gao, J.; Youn, S.; Hovsepyan, A.; Llaneza, V. n. L.; Wang, Y.; Bitton, G.; Bonzongo, J.-C. J. Dispersion and toxicity of selected manufactured nanomaterials in natural river water samples: Effects of water chemical composition. *Environmental Science & Technology* **2009**, 43, 3322-3328.

(91) Guzmán, D. K. A.; Finnegan, M. P.; Banfield, J. F. Influence of surface potential on aggregation and transport of titania nanoparticles. *Environmental Science & Technology* **2006**, 40, 7688-7693.

(92) Keller, A. A.; Wang, H.; Zhou, D.; Lenihan, H. S.; Cherr, G.; Cardinale, B. J.; Miller, R.; Ji, Z. Stability and aggregation of metal oxide nanoparticles in natural aqueous matrices. *Environmental Science & Technology* **2010**, 44, 1962–1967.

(93) Zhang, Y.; Chen, Y.; Westerhoff, P.; Crittenden, J. Impact of natural organic matter and divalent cations on the stability of aqueous nanoparticles. *Water Research* **2009**, 43, 4249-4257.

(94) Velzeboer, I.; Hendriks, A. J.; Ragas, A. M. J.; van de Meent, D. Aquatic ecotoxcicity tests of some nanomaterials. *Environmental Toxicology and Chemistry* **2008**, 27, 1942-1947.

(95) Domingos, R. F.; Peyrot, C.; Wilkinson, K. J. Aggregation of titanium dioxide nanoparticles: role of calcium and phosphate. *Environmental Chemistry* **2010**, 7, 61-66.

(96) Domingos, R. F.; Tufenkji, N.; Wilkinson, K. J. Aggregation of titanium dioxide nanoparticles: Role of a fulvic acid. *Environmental Science & Technology* **2009**, 43, 1282-1286.

(97) Chen, K. L.; Elimelech, M. Interaction of fullerene (C60) nanoparticles with humic acid and alginate coated silica surfaces: Measurements, mechanisms, and environmental implications. *Environmental Science and Technology* **2008**, 42, 7607-7614.

(98) Smith, B.; Wepasnick, K.; Schrote, K. E.; Bertele, A. R.; Ball, W. P.; O'Melia, C.; Fairbrother, D. H. Colloidal properties of aqueous suspensions of acid-treated, multi-walled carbon nanotubes. *Environmental Science & Technology* **2008**, 43, 819-825.

(99) Mukherjee, B.; Weaver, J. W. Aggregation and charge behavior of metallic and nonmetallic nanoparticles in the presence of competing similarly-charged inorganic ions. *Environmental Science & Technology* **2010**, 44, 3332–3338.

(100) Chen, K. L.; Smith, B. A.; Ball, W. P.; Fairbrother, D. H. Assessing the colloidal properties of engineered nanoparticles in water: case studies from fullerene C60 nanoparticles and carbon nanotubes. *Environmental Chemistry* **2010**, 7, 10-27.

(101) Ettlinger, M. Highly dispersed metal oxides produced by the AEROSIL process. Technical Bulletin Pigments Applied Technology Inorganic Products Division. **2006**.

(102) Sachtleben. Product Information Hombikat UV-100. Technical Information. **2005**.

(103) Colón, G.; Hidalgo, M. C.; Navío, J. A. Photocatalytic deactivation of commercial TiO_2 samples during simultaneous photoreduction of Cr(VI) and photooxidation of salicylic acid. *Journal of Photochemistry and Photobiology A: Chemistry* **2001**, 138, 79-81.

(104) Provencher, S. W. A constrained regularization method for inverting data represented by linear algebraic or integral equations. *Computer Physics Communications* **1982**, 27, 213-227.

(105) Schurtenberger, P.; Newman, M. E., **1993**. Characterization of biological and environmental particles using static and dynamic light scattering, in: Buffle, J., Leeuwen, H. P. v. (Eds.), Environmental Particles. Lewis Boca Raton.

(106) v.d. Kammer, F. v. d.; Baborowski, M.; Friese, K. Application of a high-performance liquid chromatography fluorescence detector as a nephelometric turbidity detector following Field-Flow Fractionation to analyse size distributions of environmental colloids. *Journal of Chromatography A* **2005**, 1110, 81-89.

(107) Dutta, P. K.; Pehkonen, S. O.; Sharma, V. K.; Ray, A. K. Photocatalytic oxidation of arsenic(III): Evidence of hydroxyl radicals. *Environmental Science & Technology* **2005**, 39, 1827-1834.

(108) Tipping, E.; Cooke, D. The effects of adsorbed humic substances on the surface charge of goethite (α-FeOOH) in freshwaters. *Geochimica et Cosmochimica Acta* **1982**, 46, 75-80.

(109) Amal, R.; Raper, J. A.; Waite, T. D. Effect of fulvic acid adsorption on the aggregation kinetics and structure of hematite particles. *Journal of Colloid and Interface Science* **1992**, 151, 244-257.

(110) Johnson, R. L.; Johnson, G. O. B.; Nurmi, J. T.; Tratnyek, P. G. Natural organic matter enhanced mobility of nano zerovalent iron. *Environmental Science & Technology* **2009**, 43, 5455-5460.

(111) Hyung, H.; Fortner, J. D.; Hughes, J. B.; Kim, J. H. Natural organic matter stabilizes carbon nanotubes in the aqueous phase. *Environmental Science & Technology* **2007**, 41, 179-184.

(112) Foppen, J. W.; Liem, Y.; Schijven, J. Effect of humic acid on the attachment of *Escherichia coli* in columns of goethite-coated sand. *Water Research* **2008**, 42, 211-219.

(113) Yang, X.; Flynn, R.; von der Kammer, F.; Hofmann, T. Quantifying the influence of humic acid adsorption on colloidal microsphere deposition onto iron-oxide-coated sand. *Environmental Pollution* **2010**, In Press, Corrected Proof.

(114) Hardy, W. B. A preliminary investigation of the conditions which determine the stability of irreversible hydrosols. *Journal of Physical Chemistry* **1899**, 4, 235-253.

(115) Elimelech, M.; J, G.; X, J.; A, W. R. **1995**. Particle deposition and aggregation: Measurements, modeling and simulation. Butterworth-Heinemann, Oxford.

(116) Fuerstenau, D. W.; Manmohan, D.; Raghavan, S., **1981**. The adsorption of alkaline-earth metal ions at the rutile/aqueous interface, in: Tewari, P. H. (Ed.), Adsorption from aqueous solutions. Plenum Press, New York, pp. 93-117.

(117) Filella, M.; Zhang, J.; Newman, M. E.; Buffle, J. Analytical applications of photon correlation spectroscopy for size distribution measurements of natural colloidal suspensions: capabilities and limitations. *Colloids and Surfaces A: Physicochemical and Engineering Aspects* **1997**, 120, 27-46.

(118) Fernandez-Nieves, A.; de las Nieves, F. J. The role of ζ potential in the colloidal stability of different TiO_2/electrolyte solution interfaces. *Colloids and Surfaces A: Physicochemical and Engineering Aspects* **1999**, 148, 231-243.

(119) Murdock, R. C.; Braydich-Stolle, L.; Schrand, A. M.; Schlager, J. J.; Hussain, S. M. Characterization of Nanomaterial Dispersion in Solution Prior to In Vitro Exposure Using Dynamic Light Scattering Technique. *Toxicol. Sci.* **2008**, 101, 239-253.

(120) Stone, V.; Nowack, B.; Baun, A.; van den Brink, N.; von der Kammer, F.; Dusinska, M.; Handy, R.; Hankin, S.; Hassellöv, M.; Joner, E.; Fernandes, T. F. Nanomaterials for environmental studies: Classification, reference material issues, and strategies for physico-chemical characterisation. *Science of The Total Environment* **2009**, In Press, Corrected Proof.

(121) Galletto, P.; Lin, W.; Borkovec, M. Measurement of heteroaggregation rate constants by simultaneous static and dynamic light scattering. *Physical Chemistry Chemical Physics* **2005**, 7, 1464-1471.

(122) Brar, S. K.; Verma, M.; Tyagi, R. D.; Surampalli, R. Y. Engineered nanoparticles in wastewater and wastewater sludge - Evidence and impacts. *Waste Management* **2010**, 30, 504-520.

(123) Ji, Z.; Jin, X.; George, S.; Xia, T.; Meng, H.; Wang, X.; Suarez, E.; Zhang, H.; Hoek, E. M. V.; Godwin, H.; Nel, A. E.; Zink, J. I. Dispersion and stability optimization of TiO_2 nanoparticles in cell culture media. *Environmental Science & Technology* **2010**, (in press).

(124) v.d. Kammer, F.; Ottofuelling, S.; Hofmann, T. Assessment of the pysico-chemical behavior of engineered nanoparticles in aqautic environments using multi-dimensional parameter testing. *Environmental Pollution* **2010**, (in press).

(125) Chen, K. L.; Elimelech, M. Aggregation and deposition kinetics of fullerene (C60) nanoparticles. *Langmuir* **2006**, 22, 10994-11001.

(126) Dunphy Guzmán, K. A.; Finnegan, M. P.; Banfield, J. F. Influence of surface potential on aggregation and transport of titania nanoparticles. *Environmental Science & Technology* **2006**, 40, 7688-7693.

(127) International Humic Substances Society. http://ihss.gatech.edu/ihss2/. **2008**.

(128) EPA. Short-term Methods for Estimating the Chronic Toxicity of Effluents and Receiving Waters to Freshwater Organisms. United States Environmental Protection Agency. **2002**. 335.

(129) Kosmulski, M.; Rosenholm, J. B. High ionic strength electrokinetics of anatase in the presence of multivalent inorganic ions. *Colloids and Surfaces A: Physicochemical and Engineering Aspects* **2004**, 248, 121.

(130) Kim, J.; Shan, W.; Davies, S. H. R.; Baumann, M. J.; Masten, S. J.; Tarabara, V. V. Interactions of aqueous NOM with nanoscale TiO_2: Implications for ceramic membrane filtration-ozonation hybrid process. *Environmental Science & Technology* **2009**, 43, 5488-5494.

(131) Weng, L. P.; VanRiemsdijk, W. H.; Koopal, L. K.; Hiemstra, T. Adsorption of humic substances on goethite: Comparison between humic acids and fulvic acids. *Environmental Science & Technology* **2006**, 40, 7494-7500.

(132) Lovern, S. B.; Strickler, J. R.; Klaper, R. Behavioral and physiological changes in daphnia magna when exposed to nanoparticle suspensions (Titanium Dioxide, Nano-C60, and C60HxC70Hx). *Environ. Sci. Technol.* **2007**, 41, 4465 -4470.

(133) Lyon, D. Y.; Adams, L. K.; Falkner, J. C.; Alvarez, P. J. J. Antibacterial activity of fullerene water suspensions: Effects of preparation method and particle size. *Environmental Science and Technology* **2006**, 40, 4360-4366.

(134) Zhu, X.; Zhu, L.; Chen, Y.; Tian, S. Acute toxicities of six manufactured nanomaterial suspensions to Daphnia magna. *Journal of Nanoparticle Research* **2009**, 11, 67.

(135) Domingos, R. F.; Baalousha, M. A.; Ju-Nam, Y.; Reid, M. M.; Tufenkji, N.; Lead, J. R.; Leppard, G. G.; Wilkinson, K. J. Characterizing manufactured nanoparticles in the environment: Multimethod determination of particle sizes. *Environmental Science & Technology* **2009**, 43, 7277-7284.

(136) Battin, T. J.; Kaplan, L. A.; Findlay, S.; Hopkinson, C. S.; Marti, E. M.; Packman, A. I.; Newbold, J. D.; Sabater, F. Biophysical controls on organic carbon fluxes in fluvial networks. *Nature Geoscience* **2008**, 1, 95-100.

(137) Liu, Y.; Li, J.; Qiu, X.; Burda, C. Bactericidal activity of nitrogen-doped metal oxide nanocatalysts and the influence of bacterial extracellular polymeric substances (EPS). *Journal of Photochemistry and Photobiology A* **2007**, 190, 94-100.

(138) Limbach, L. K.; Wick, P.; Manser, P.; Grass, R. N.; Bruinink, A.; Stark, W. J. Exposure of engineered nanoparticles to human lung epithelial cells: influence of chemical composition and catalytic activity on oxidative stress. *Environmental Science & Technology* **2007**, 41, 4158-4163.

(139) Matsunaga, T.; Okochi, M. TiO_2-mediated photochemical disinfection of escherichia coli using optical fibers. *Environmental Science & Technology* **1995**, 29, 501-505.

(140) Cho, M.; Chung, H.; Choi, W.; Yoon, J. Linear correlation between inactivation of E. coli and OH radical concentration in TiO_2 photocatalytic disinfection. *Water Research* **2004**, 38, 1069-1077.

(141) Cho, M.; Chung, H.; Choi, W.; Yoon, J. Different inactivation behaviours of MS-2 phage and Escherichia coli in TiO_2 photocatalytic disinfection. *Applied and Environmental Microbiology* **2005**, 71, 270-275.

(142) Gogniat, G.; Dukan, S. TiO_2 photocatalysis causes DNA damage via fenton reaction-generated hydroxyl radicals during the recovery period. *Applied and Environmental Microbiology* **2007**, 73, 7740-7743.

(143) Hund-Rinke, K.; Simon, M. Ecotoxic effect of photocatalytic active nanoparticles (TiO_2) on algae and daphnids. *Environmental Science and Pollution Research International* **2006**, 13, 225-232.

(144) Ibanez, J. A.; Litter, M. I.; Pizarro, R. A. Photocatalytic bactericidal effect of TiO_2 on *Enterobacter cloacae*. Comparative study with other Gram (-) bacteria. *Journal of Photochemistry and Photobiology A: Chemistry* **2003**, 157, 81-85.

(145) Kim, B.; Kim, D.; Cho, D.; Cho, S. Bactericidal effect of TiO_2 photocatalyst on selected food-borne pathogenic bacteria. *Chemosphere* **2003**, 52, 277-281.

(146) Lee, J.; Zoh, K.; Ko, G. Inactivation and UV disinfection of murine norovirus with TiO_2 under various environmental conditions. *Applied and Environmental Microbiology* **2008**, 74, 2111-2117.

(147) Maness, P.-C.; Smolinski, S.; Blake, D. M.; Huang, Z.; Wolfrum, E. J.; Jacoby, W. A. Bactericidal activity of photocatalytic TiO_2 reaction: toward an understanding of its killing mechanism. *Applied and Environmental Microbiology* **1999**, 65, 4094-4098.

(148) Rincon, A. G.; Pulgarin, C.; Adler, N.; Peringer, P. Interaction between E. coli inactivation and DBP-precursors - dihydroxybenzene isomers - in the photocatalytic process of drinking-water disinfection with TiO_2. *Journal of Photochemistry and Photobiology A: Chemistry* **2001**, 139, 233-241.

(149) Rincon, A. G.; Pulgarin, C. Bactericidal action of illuminated TiO_2 on pure *Escherichia coli* and natural bacterial consortia: Post-irradiation events in the dark and assessment of the effective disinfection time. *Applied Catalysis B: Environmental* **2004**, 49, 99-112.

(150) Rincón, A. G.; Pulgarin, C. Photocatalytical inactivation of E. coli: Effect of (continuous-intermittent) light intensity and of (suspended-fixed) TiO_2 concentration. *Applied Catalysis B* **2003**, 44, 263.

(151) Jensen, H.; Soloviev, A.; Li, Z.; Søgaard, E. G. XPS and FTIR investigation of the surface properties of different prepared titania nano-powders. *Applied Surface Science* **2005**, 246, 239-249.

(152) Dutta, P. K.; Ray, A. K.; Sharma, V. K.; Millero, F. J. Adsorption of arsenate and arsenite on titanium dioxide suspensions. *Journal of Colloid and Interface Science* **2004**, 278, 270.

(153) ISO/TS. Nanotechnologies -- Terminology and definitions for nano-objects. **2008**, 1-7.

(154) Jiang, X.; Wang, T. Influence of preparation method on morphology and photocatalysis activity of nanostructured TiO_2. *Environmental Science & Technology* **2007**, 41, 4441-4446.

(155) Mandzy, N.; Grulke, E.; Druffel, T. Breakage of TiO_2 agglomerates in electrostatically stabilized aqueous dispersions. *Powder Technol.* **2005**, 160, 121-126.

(156) Singer, G.; Besemer, K.; Hödl, I.; Chlup, A. K.; Hochedlinger, G.; Stadler, P.; Battin, T. J. Microcosm design and evaluation to study stream microbial biofilm. *Limnology and Oceanography: Methods* **2006**, 4, 436-447.

(157) Berney, M.; Weilenmann, H. U.; Egli, T. Flow-cytometric study of vital cellular functions in Escherichia coli during solar disinfection (SODIS). *Microbiology* **2006**, 152, 1719.

(158) Manini, E.; Danovaro, R. Synoptic determination of living/dead and active/dormant bacterial fractions in marine sediments. *FEMS Microbiology Ecology* **2006**, 55, 416-423.

(159) Shen, B.; Scaiano, J. C.; English, A. M. Zeolite encapsulation decreases TiO_2-photosensitized ROS generation in cultured human skin fibroblasts. *Photochemistry and Photobiology* **2006**, 82, 5-12.

(160) Boncagni, N. T.; Otaegui, J. M.; Warner, E.; Curran, T.; Ren, J.; Fidalgo de Cortalezzi, M. M. Exchange of TiO2 Nanoparticles between Streams and Streambeds. *Environmental Science & Technology* **2009**.

(161) Harrison, J. J.; Ceri, H.; Turner, R. J. Multimetal resistance and tolerance in microbial biofilms. *Nature Reviews Microbiology* **2007**, 5, 928-938.

(162) Gogniat, G.; Thyssen, M.; Denis, M.; Pulgarin, C.; Dukan, S. The bactericidal effect of TiO_2 photocatalysis involves adsorption onto catalysts and loss of membrane integrity. *FEMS Microbiology Letters* **2006**, 258, 18-24.

(163) Besemer, K.; Singer, G.; Limberger, R.; Chlup, A.-K.; Hochedlinger, G.; Hodl, I.; Baranyi, C.; Battin, T. J. Biophysical controls on community succession in stream biofilms. *Applied and Environmental Microbiology* **2007**, 73, 4966–4974.

(164) Berney, M.; Hammes, F.; Bosshard, F.; Weilenmann, H.-U.; Egli, T. Assessment and interpretation of bacterial viability by using the LIVE/DEAD BacLight Kit in combination with flow cytometry. *Applied and Environmental Microbiology* **2007**, 73, 3283-3290.

(165) Brayner, R.; Ferrari-Iliou, R.; Brivois, N.; Djediat, S.; Benedetti, M. F.; Fiévet, F. Toxicological impact studies based on escherchia coli bacteria in ultrafine ZnO nanoparticles colloidal medium. *Nano Letters* **2006**, 6, 866-870.

(166) Lyon, D. Y.; Brunet, L.; Hinkal, G. W.; Wiesner, M. R.; Alvarez, P. J. J. Antibacterial Activity of Fullerene Water Suspensions (nC60) Is Not Due to ROS-Mediated Damage. *Nano Letters* **2008**.

(167) Schumann, R.; Schiewer, U.; Karsten, U.; Rieling, T. Viability of bacteria from different aquatic habitats. II. Cellular fluorescent markers for membrane integrity and metabolic activity. *Aquatic Microbial Ecology* **2003**, 32, 137-150.

(168) Demchick, P.; Koch, A. L. The permeability of the wall fabric of Escherichia coli and Bacillus subtilis. *Journal of Bacteriology* **1996**, 178, 768-773.

(169) Nel, A.; Xia, T.; Mädler, L.; Li, N. Toxic potential of materials at the nanolevel. *Science* **2006**, 311, 622-627.

(170) Thill, A.; Zeyons, O.; Spalla, O.; Chauvat, F.; Rose, J.; Auffan, M.; Flank, A. M. Cytotoxicity of CeO_2 nanoparticles for escherchia coli. physico-chemical insight of the cytotoxicity mechanism. *Environmental Science & Technology* **2006**, 40, 6151-6156.

(171) Uchino, T.; Tokunaga, H.; Ando, M.; Utsumi, H. Quantitative determination of OH radical generation and its cytotoxicity induced by TiO_2-UVA treatment. *Toxicology in Vitro* **2002**, 16, 629-635

(172) Jiang, J.; Oberdörster, G.; Elder, A.; Gelein, R.; Mercer, P.; Biswas, P. Does nanoparticle activity depend upon size and crystal phase? *Nanotoxicology* **2008**, 2, 33-42.

(173) Senogles, P. J.; Scott, J. A.; Shaw, G.; Stratton, H. Photocatalytic degradation of the cyanotoxin cylindrospermopsin, using titanium dioxide and UV irradiation. *Water Research* **2001**, 35, 1245-1255.

(174) Boxall, A. B. A.; Chaudhry, Q.; Sinclair, C.; Jones, A.; Aitken, R.; Jefferson, B.; Watts, C. **2007**. Current and future predicted environmental exposure to engineered nanoparticles. Report by the Central Science Laboratory (CSL) York for the Department of the Environment and Rural Affairs (DEFRA), York.

(175) Gao, L.; Zhang, Q. Effects of amorphous contents and particle size on the photocatalytic properties of TiO_2 nanoparticles. *Scripta Materialia* **2001**, 44, 1195-1198.

(176) Minhua, X.; Jianmin, G.; Jianhua, G.; Zuhong, L. Photocatalytic TiO_2 nanoparticles damage to cellular membranes and genetic supramolecules. *Supramoleular Sciences* **1998**, 5, 511-513.

(177) Vileno, B.; Lekka, M.; Sienkiewicz, A.; Jeney, S.; Stoessel, G.; Lekki, J.; Forró, L.; Stachura, Z. Stiffness alterations of single cells induced by UV in the presence of NanoTiO_2. *Environmental Science and Technology* **2007**, 41, 5149-5153.

(178) Yeung, K. L.; Leung, W. K.; Yao, N.; Cao, S. Reactivity and antimicrobial properties of nanostructured titanium dioxide. *Catalysis Today* **2009**, 143, 218-224.

(179) Kim, S. C.; Lee, D. K. Preparation of TiO_2-coated hollow glass beads and their application to the control of algal growth in eutrophic water. *Microchemical Journal* **2005**, 80, 227-232.

(180) Griffitt, R. J.; Luo, J.; Gao, J.; Bonzongo, J.-C.; Barber, D. S. Effects of particle composition and species on toxicity of metallic nanomaterials in aquatic organisms. *Environmental Toxicology and Chemistry* **2008**, 27, 1972-1978.

(181) Aruoja, V.; Dubourguier, H.-C.; Kasemets, K.; Kahru, A. Toxicity of nanoparticles of CuO, ZnO and TiO_2 to microalgae *Pseudokirchneriella subcapitata*. *Science of The Total Environment* **2009**, 407, 1461-1468.

(182) Park, S.; Lee, Y. K.; Jung, M.; Kim, K. H.; Chung, N.; Ahn, E. K.; Lim, Y.; Lee, K. H. Cellular toxicity of various inhalable metal nanoparticles on human alveolar epithelial cells. *Inhalation Toxicology* **2007**, 19, 59-65.

(183) Moore, M. N. Do Nanoparticles present ecotoxicological risks for the health of the aquatic environment? *Environment International* **2006**, 32, 967-976.

(184) Chan, W. C. W.; Maxwell, D. J.; Gao, X.; Bailey, R. E.; Han, M.; Nie, S. Luminescent quantum dots for multiplexed biological detection and imaging. *Current Opinion in Biotechnology* **2002**, 13, 40-46.

(185) Singh, S.; Shi, T.; Duffin, R.; Albrecht, C.; van Berlo, D.; Höhr, D.; Fubini, B.; Martra, G.; Fenoglio, I.; Borm, P. J. A.; Schins, R. P. F. Endocytosis, oxidative stress and IL-8 expression in human lung epithelial cells upon treatment with fine and ultrafine TiO_2: Role of the specific surface area and of surface methylation of the particles. *Toxicology and Applied Pharmacology* **2007**, 222, 141-151.

(186) Knauer, K.; Sobek, A.; Bucheli, T. D. Reduced toxicity of diuron to the freshwater green alga Pseudokirchneriella subcapitata in the presence of black carbon. *Aquatic Toxicology* **2007**, 83, 143-148.

(187) Zhang, X.; Sun, H.; Zhang, Z.; Niu, Q.; Chen, Y.; Crittenden, J. C. Enhanced bioaccumulation of cadmium in carp in the presence of titanium dioxide nanoparticles. *Chemosphere* **2007**, 67, 160-166.

(188) Sachtleben. Product Information Hombitan LW-S. Technical Information. **2006**.

(189) Parkhurst, D. L.; Appelo, C. A. J. Users guide to PHREEQC (Version 2) – a computer program for speciation, batch-reaction, one-dimensional transport, and inverse geochemical calculations. U.S. Geological Survey Water-Resources. **1999**. 310.

(190) Arensberg, P.; Hemmingsen, V. H.; Nyholm, N. A miniscale algal toxicity test. *Chemosphere* **1995**, 30, 2103-2115.

(191) Mayer, P.; Cuhel, R.; Nyholm, N. A simple in vitro fluorescence method for biomass measurements in algal growth inhibition tests. *Water Research* **1997**, 31, 2525-2531.

(192) Christensen, E. R.; Kusk, K. O.; Nyholm, N. Dose-response regressions for algal growth and similar continuous endpoints: Calculation of effective concentrations. *Environmental Toxicology and Chemistry* **2009**, 28, 826-835.

(193) Brant, J.; Lecoanet, H.; Wiesner, M. R. Aggregation and Deposition Characteristics of Fullerene Nanoparticles in Aqueous Systems. *Journal of Nanoparticle Research* **2005**, 7, 545-553.

(194) Brain, P.; Cousens, R. An equation to describe dose responses where there is stimulation of growth at low doses. *Weed Research* **1989**, 29, 93-96.

(195) Cedergreen, N.; Ritz, C.; Streibig, J. C. Improved empirical models describing hormesis. *Environmental Toxicology and Chemistry* **2005**, 24, 3166-3172.

(196) Nielsen, H. D.; Berry, L. S.; Stone, V.; Burridge, T. R.; Fernandes, T. F. Interactions between carbon black nanoparticles and the brown algae Fucus serratus: Inhibition of fertilization and zygotic development. *Nanotoxicology* **2008**, 2, 88-97.

(197) Augustynski, J. The role of the surface intermediates in the photoelectrochemical behaviour of anatase and rutile TiO_2. *Electrochimica Acta* **1993**, 38, 43-46.

(198) Three Bond, C. L. **2004**. Titanium-Oxide Photocatalyst. Three Bond Technical News, pp. 1-8.

(199) Adams, L. K.; Lyon, D. Y.; Alvarez, P. J. J. Comparative eco-toxicity of nanoscale TiO_2, SiO_2, and ZnO water suspensions. *Water Research* **2006**, 40, 3527-3532

(200) Giammar, D. E.; Maus, C. J.; Xie, L. Effects of particle size and crystalline phase on lead adsorption to titanium dioxide nanoparticles. *Environmental Engineering Science* **2007**, 24, 85-95.

(201) Gao, Y.; Wahi, R.; Kan, A. T.; Falkner, J. C.; Colvin, V. L.; Tomson, M. B. Adsorption of cadmium on anatase nanoparticles-effect of crystal size and pH. *Langmuir* **2004**, 20, 9585-9593.

(202) Genter, R. B., **1996**. Ecotoxicology of inorganic chemical stress to algae, in: Stevenson, A. R. J.; Bothwell, M. L., Lowe, R. L. (Eds.), Algal Ecology. Academic Press, USA, San Diego, pp. 403-468.

8 Additional Study and Contribution

Preparation of gadolinium chelate coated HSA-lectin nanoparticles for magnetic resonance imaging

A. Kundu, S. Ottofuelling, M. Krssak, F. v.d. Kammer, T. Hofmann, T. H. Helbich, B. K. Keppler

To be submitted to Journal of Pharmaceutics (2010)

1 Abstract

Human serum albumin (HSA) derived nanoparticles represent promising systems for the development of diagnostic agents. Endothelial cell targeting lectins covalently conjugated to Gd-HSA combine magnetic resonance imaging (MRI) contrast enhancement with the advantages of tissue targeting. The present study reports the preparation of Gd(III) loaded albumin-lectin nanoparticles by different strategies for their potential exploration as targeted MRI contrast agents. As *in vivo* behaviour of nanoparticles strongly depends on particles dimension, the size as well as the polydispersity index has been evaluated for each preparation method. PCS measurements indicated a nanoparticles size range between 112 nm and 304 nm. Furthermore, the impact on the relaxation behaviour was determined by MRI experiments.

2 Introduction

Gadolinium based contrast agents have become a powerful imaging modality in magnetic resonance imaging (MRI). High spatial resolution images of soft tissues are provided by this non-invasive diagnostic technique (Caravan et al., 1999; Merbach and Toth, 2001). Nevertheless, free Gd(III) is known to be toxic and may cause damage to spleen, liver and bones and lead to nephrogenic systemic fibrosis (Sieber et al., 2008). Consequently, stable chelates are required. The use of polyaminocarboxylic acid ligands like the linear diethylenetriaminepentaacetic acid (DTPA), the macrocyclic 1,4,7,10-tetraazacyclododecane-*N,N',N'',N'''*-tetraacetic acid

(DOTA) or backbone modified derivatives thereof prevent the release of free Gd(III) and hence reduce the risk of the mentioned side effects (Hermann et al., 2008).

However, the use of low molecular weight contrast agents is limited due to their rapid clearance and diffusion from the vasculature into the interstitial space (Barrett et al., 2006). The attachment of low molecular weight contrast agents to nanospheres presents auspicious possibilities for improved biophysical and pharmacological properties. Increased rotational correlation time for enhanced relaxvity per gadolinium atom and the prolonged intravascular retention - leading to the increase of molar relaxivities from the vasculature over an extended period of time - provide the main advantages. Such macromolecular contrast media may define a blood-tissue barrier comparable to the existing barrier for large molecular endogenous substances in the blood like plasma proteins (Brasch and Daldrup-Link, 2003).

The most common approaches for the preparation of contrast enhancing nanoparticles include the conjugation of Gd(III) chelates to dextrans (Sirlin et al., 2004), dendrimers (Langereis et al., 2006; Xu et al., 2007a; Xu et al., 2007b; Kido et al., 2009), liposomes (Barrett et al., 2006), gold particles (Alric et al., 2008), polymers (Caravan et al., 1999) and albumins (Ogan et al., 1987; Barrett et al., 2006; Yan et al, 2006).

A remarkable perspective in MRI provides the introduction of a tissue specific targeting moiety to the contrast agent. High local concentration of contrast enhancing material at a particular site within the human body enables precise medical diagnosis and will become an essential tool in tracking the progress of therapies. Currently, great effort is invested in the development of such tissue specific contrast agents. The concept of liver targeting is realized by the introduction of lipophilic moieties to the contrast agent or alternatively, the encapsulation of Gd-DTPA or Gd-DOTA chelates into liposomal nanoparticles (Weinmann et al., 2003). Development of MRI contrast agents with the capability of seeking out tumors is approached by different strategies. One proposal is the non-covalent interaction of contrast agents bearing charged residues with charged groups of polyornithine and polyarginine. It is known, that positively charged polyaminoacids selectively bind to tumors as their charge is more negative than non-tumor cells (Aime et al., 2000). Receptor targeting through

monoclonal antibodies attached to contrast enhancing molecules is also widely investigated in this field of research. Monoclonal antibodies are an important category of targeting vectors and can be prepared to interact with a variety of receptor sites (Jaques and Desreux, 2002). Recently, the preparation and investigation of a peptide targeted contrast agent for molecular magnetic resonance imaging of fibronectin-fibrin complexes in tumor tissues was published (Ye et al., 2008). The ability of imaging and diagnosing atherosclerotic plaques is of considerable interest since atherosclerotic diseases are among the leading causes of death in developed countries. Investigated methods to face the challenge of imaging fatty deposits include the application of recombinant high density lipoprotein (HDL) like nanoparticles (Frias et al., 2004). Newly published investigations provide characterization of plaque in deep seated arteries using motexafin gadolinium (Brushett et al., 2008). MS 325, a gadolinium chelate that reversible binds to albumin in plasma has also been applied and areas of high signal intensity have been observed and were suggested not only to reflect the increased plaque vascularity but also the leakiness of the microvessels (Choudhury et al., 2002). In principle, also unspecific macromolecular or low molecular weight contrast agents suitable for imaging the blood pool bear the potential of indicating pathological alteration of the vasculature (Briley-Saebo et al., 2007).

A targeting group capable of binding to endothelial cells is the tomato derived lectin LEA (Lycopersicon esculentum agglutinin) (Porter et al., 1990; Mazzetti et al., 2004). The attachment of this lectin to gadolinium loaded nanoparticles has already shown to provide contrast media with the ability of imaging the blood vessel walls in high spatial resolution (Paschkunova-Martic et al., 2005).
Due to a considerably high number of functional groups albumin based nanoparticles represent promising systems for the development of MRI contrast enhancement and drug carriage facilities. Additionally, human serum albumin (HSA) derived nanospheres will be tolerated without side effects, since HSA is an integral component of plasma. The objective of this study was the preparation of Gd(III) loaded albumin-lectin nanoparticles for the exploration in targeted magnetic resonance imaging. For this purpose a bifunctional chelating agent was covalently attached to HSA and loaded with Gd(III). Different strategies were then explored to conjugate the modified albumin to LEA. Investigations of particle size and zeta

potential are also described. Finally, the relaxation behavior of the synthesized nanoparticles was evaluated.

3 Materials and Methods

3.1 Chemicals and reagents

Human serum albumin, Lectin (from Lycopersicon esculentum), phosphate buffered saline (1×PBS), glutaric dialdehyde (50 wt.% solution in water), glutaric anhydride as well as citric acid trisodium salt dihydrate and citric acid monohydrate for buffer preparation were purchased from Sigma-Aldrich. *N*-(3-dimethylaminopropyl)-*N´*-ethyl-carbodiimide hydrochloride (EDC), 2-aminoethanol and sodium bicarbonate were obtained from Fluka. Ethanol (LiChrosolve®, gradient grade for liquid chromatography) was purchased from Merk. Trisodium bis(nitrilotriacetate)gadolinate solution ($Na_3[Gd(NTA)_2]$) (Paschkunova-Martic et al., 2005) as well as 2-(*para*-aminobenzyl)-diethylenetriaminepentaacetic acid tetrahydrochloride (NH_2-Bn-DTPA·4 HCl) (Cummins et al., 1991) were prepared according to literature procedures. All water used was purified by a Millipore Synergy 185 UV Ultrapure Water System (Molsheim, France).

3.2 Preparation of Gd(III) loaded human serum albumin

Conjugation of the bifunctional chelating agent and subsequent complexation with Gd(III) was performed using a recently described method (Kundu et al. 2009). HSA (53 mg, 0.8×10^{-3} mmol) was dissolved in 0.1 M $NaHCO_3$ (10 ml) and cooled to 4°C. Glutaric anhydride (62 mg, 543.4×10^{-3} mmol) was added slowly in small portions while the pH of the mixture was maintained within a range of 7.8 - 8.2 by the addition of 0.6 M NaOH. Afterwards, the solution was stirred for 22 h at 4°C. To remove excess reagents the albumin-solution was concentrated by centrifugation (Vivaspin 20, MWCO: 30000, 2500×g, 19°C) and washed with water (three times). The purified glutarylated albumin solution was diluted with H_2O (7 ml) and NH_2-Bn-DTPA•4HCl (60 mg, 931×10^{-3} mmol) in H_2O (2 ml) were added at ambient temperature. During the addition, the pH was repeatedly adjusted to 6.8 - 7.2 by 0.3 M NaOH. EDC (8 mg) was added and the conjugation reaction proceeded for 2 h at room temperature. To separate non-conjugated bifunctional ligand and low molecular weight compounds the solution was concentrated by centrifugation (Vivaspin 20, MWCO: 30000, 2500×g,

19°C) and again washed with water (three times). For the purpose of complexation with Gd(III) the modified albumin was then dissolved in 0.1 M citric buffer (10 ml) (pH 6.5) and cooled to 4°C. 0.1 M $Gd(NTA)_2$ solution (2.5 ml, 0.25 mmol) was added and allowed to react for 19 h. Finally, the reaction mixture was concentrated by centrifugation (Vivaspin 20, MWCO: 30000, 2500×g, 19°C) and washed with water (three times) to give a purified aqueous solution (10 mg/ml) of the gadolinium loaded HSA.

3.3 Albumin determination

The protein concentration of purified gadolinium loaded albumin solutions was determined by the method of Bradford. A Bradford test kit from Bio-Rad Laboratories (Vienna, Austria) was used and adapted for usage in 96 - well plates. Optical densities at 595 nm were recorded on a microplate reader (Synergy HT, Biotek) 15 min. after the addition of Bradford solution.

3.4 Determination of the gadolinium content

Gadolinium content of purified loaded albumin solutions was determined by an ICP-MS (Inductively Coupled Plasma Mass Spectrometry) instrument (Agilent 7500ce, Waldbronn, Germany), equipped with a CETAC ASX-520 autosampler (Neuss, Germany), a Scott double pass spray chamber, and a MicroMist nebulizer.

3.5 Preparation of Gd-HSA-Lectin nanoparticles by the activation of HSA (method 1)

Gd-HSA solution (0.531 ml, 5.31 mg) was diluted in PBS (1 ml) and the pH was adjusted to 8 by the use of 0.01 M NaOH. Glutaraldehyde ((10 µl, 10% solution) was added and mixed by rotation (Multi Bio RS 24) for 5 h at 30 rpm. To remove excess glutaraldehyde the reaction liquid was concentrated by centrifugation (Vivaspin 20, MWCO: 30000, 2500×g, 19°C) and washed with water (three times). The activated Gd-albumin was diluted in PBS (3 ml) and LEA (2 mg) dissolved in H_2O (0.4 ml) was added. After 18 h of rotation (Multi Bio RS 24) at 30 rpm the reaction was quenched by the addition of aminoethanol (20 µl) and the suspension was rotated for one further hour. The resulting nanoparticles were purified by centrifugation (Vivaspin 20, MWCO: 30000, 2500×g, 19°C) and redispersion in water (three times).

3.6 Preparation of Gd-HSA-Lectin nanoparticles by desolvation (method 2)

The nanoparticles were prepared using a modification of a previously described technique (Weber et al., 2000; Langer et al., 2003). Gd-HSA solution (0.53 ml, 5.31 mg) was diluted in H_2O (1 ml) and LEA (2 mg) dissolved in H_2O (0.4 ml) was added. The pH was adjusted to 8.2 with 0.01 M NaOH. EtOH (1.6 ml) was added dropwise (1 ml/min) under constant stirring (1000 rpm) at room temperature. Subsequently, glutaraldehyde (8 µl, 10% solution) was added to crosslink the protein molecules. The reaction proceeded for 22 h under stirring. Unconverted glutaraldehyde was inactivated by the addition of aminoethanol (20 µl) and the suspension was stirred for a further hour. The resulting nanoparticles were purified by centrifugation (Vivaspin 20, MWCO: 30000, 2500×g, 19°C) and redispersion in water (three times).

3.7 Preparation of Gd-HSA-Lectin nanoparticles by simultaneous crosslinking (method 3)

At room temperature, Gd-HSA solution (0.53 ml, 5.31 mg) was diluted in H_2O (1 ml) and LEA (2 mg) dissolved in H_2O (0.4 ml) was added. The pH was adjusted to 8.2 with 0.01 M NaOH. To start the crosslinking reaction glutaraldehyde (8 µl, 10% solution) was added and the reaction was allowed to proceed for 22 h. Excess glutaraldehyde was inactivated by the addition of aminoethanol (20 µl) and the suspension was stirred for a further hour. The resulting nanoparticles were purified by centrifugation (Vivaspin 20, MWCO: 30000, 2500×g, 19°C) and redispersion in water (three times).

3.8 Preparation of Gd-HSA-Lectin nanoparticles by the activation of LEA (method 4)

LEA (2.5 mg) dissolved in H_2O (0.5 ml) was diluted in 0.1 M $NaHCO_3$ (4 ml) and cooled to 4°C. Glutaric anhydride (15 mg) was added in small portions and the pH was maintained between 7.8 and 8.2 by the addition of 0.1 M NaOH. The glutarylation was allowed to proceed for 2 h at 4°C. Thereafter, repeated centrifugation (Vivaspin 20, MWCO: 30000, 2500×g, 19°C) and washing with water removed small molecular weight compounds. The purified and concentrated glutarylated lectin solution was diluted with water (7 ml). Gd-HSA solution (0.7 ml, 7

mg) was added and the pH was adjusted to 6.7 by 0.1 M HCl. EDC (5 mg) was added and the conjugation reaction proceeded for 1 h. During this time the pH was permanently corrected to 6.7. The resulting nanoparticles were purified by centrifugation (Vivaspin 20, MWCO: 30000, 2500×g, 19°C) and redispersion in water (three times).

3.9 Measurement of particle size and zetapotential

Particle size distribution of the undiluted sample was measured by dynamic light scattering (DLS) at a 173° angle using a Zetasizer Nano ZS (Malvern Instruments, UK). We used the general purpose method for derivation of the average particle diameter (z-average) and polydispersivity index (PDI). The general purpose method provides a multimodal analysis using result transformation based on Mie theory. Cummulant analysis with a quadratic weighing scheme was used for size distributions. Each measurement consists of 3 individual runs of 10 sec. We used a refractive index of 1.45 and an absorption index of 0.001. The temperature of the dispersant (ultrapure water) was set to 21 °C with a viscosity of 0.9781 cP and a refractive index of 1.330. Each sample was transferred and capped into low volume disposable sizing cuvettes (PMMA) in a clean bench to prevent contamination (e.g. dust). The electrophoretic mobility of the particles was measured by laser Doppler velocimetry with the same instrument. We used folded capillary cells and injected the undiluted samples with a syringe to prevent encapsulation of air bubbles. The Smoluchowski approximation was used to calculate the zeta potentials and for better comparison we kept the voltage of 40 mV constant for all measurements. We calculated mean values and standard deviation out of three individual measurements.

3.10 Spin-Lattice and Spin-Spin Relaxivity measurements

Relaxivity measurements were performed on a 3 Tesla whole-body MRI scanner (TimTrio 3 T, Siemens Medical Solutions, Erlangen, Germany) using a whole body coil for excitation and standard head receiver coil for signal reception. Homogeneity of B_1-field was insured by test measurements before the actual measurements of relaxivity. For each agent four dilutions ranging from 1.25 mg/ml to 10 mg/ml in PBS with the volume of 0.25 ml were prepared. All probes were measured in standard PE-tubes with a diameter of 0.8 cm. The tubes were placed in the centre of a plastic box surrounded by water heated to 37°C.

For the determination of spin-lattice relaxation times T_1, spin echo inversion recovery (IR) sequences with inversion times from 0 to 3500 ms (TI = 0, 60, 80, 100, 150, 200, 250, 300, 400, 500, 750, 1000, 1250, 1500, 1750, 2000, 2500, 3500 ms) were used. An adiabatic pulse was applied for B1 insensitive inversion. The other parameters were: TR/TE = 5000/8.1 ms; flip angle 180°; 8 turbo factor 11; FOV read 180 × 180 mm; resolution matrix 192 × 192; bandwidth 260 Hz/pixel; and slice thickness 3 mm. The mean values of the signal intensities, the standard deviations, and pixel counts were determined by drawing regions of interest. The area assessed measured between 0.12 cm^2 and 0.14 cm^2; for each measurement series, the measured area was kept identical by copying and pasting the ROI. For all measurements, the relaxation rates (R_1) and the relaxivities (r_1) were calculated for each substance. The longitudinal relaxation rate (R_1) was calculated using the equation:

$$SI\ (TI) = A\left[1 - 2^{(-R_1 * TI) + (-R_1 * TR)}\right]$$

with *SI* being the signal intensity as a function of *TI*, *"A"* accounting for the thermal equilibrium magnetization M0, and *TI* being the inversion time in ms.

For the determination of individual spin-spin relaxation times (T_2), spin-echo sequence with multiple echoes (NE= 5) ranging from 13.8 ms to 69 ms was used. Repetition time was set to 2500 ms, FOV 160 × 160 mm, resolution matrix 128 × 128, bandwidth 260 Hz/pixel; and slice thickness 3 mm. The mean values of the signal intensities, the standard deviations, and pixel counts were determined by drawing regions of interest. The area assessed measured between 0.12 cm^2 and 0.14 cm^2; for each measurement series, the measured area was kept identical by copying and pasting the ROI. For all measurements, the relaxation rates (R_2) and the relaxivities (r_2) were calculated for each substance. The transversal relaxation rates (R_2) were calculated as the reciprocal value of the slope of semilogarithmic plot of signal intesities at individual echo times and respective echo times. The relaxivities (r_1, r_2) were calculated as the slope of linear regression of R_1 and R_2 as a function of contrast agent concentration.

4 Results and Discussion

The objective of this study was the evaluation of different parameters to characterize the prepared nanoparticles with regard to a possible application in MRI. The synthesis of Gd(III) loaded human serum albumin is based on a previously published technique (Kundu et al., 2009). The bifunctional chelating agent NH_2-Bn-DTPA was covalently attached to the albumin by a glutaric acid linker. Amide coupling to the primary amine functionalities of lysine residues as well as amide formation to the primary amine of the ligand provided stable conjugation. Gadolinium coordination exclusively to the DTPA derivative succeeded by the introduction of a $Gd(NTA)_2$ solution. Nitrilotriacetic acid was utilized for the reason of being a weak ligand for Gd(III) and therefore, to prevent nonspecific complexation to proteins which may result in the release of free Gd(III) (Spanoghe et al., 1992). The gadolinium:albumin ratio was determined by the measurement of protein concentration by the Bradford assay and the determination of the metal content by ICP-MS. The detected gadolinium amount was related to the protein concentration and indicated that 35 contrast enhancing Gd(III) ions were attached to each albumin molecule (Figure 46).

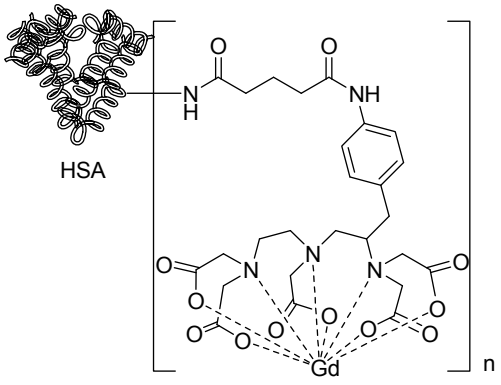

n= 35

Figure 46. Gd(III) loaded HSA.

Syntheses of nanoparticles were performed by four different strategies to indicate possible variations in size, zeta potential and relaxivity behavior. The homobifunctional reagent glutaraldehyde was chosen as crosscoupling reagent due to its convenient handling. The use of this probably most popular protein crosslinking reagent is well established in literature (Hermanson, 2008). After the reaction, remaining aldehyde functionalities were inactivated by the addition of aminoethanol. This procedure prevented further crosscoupling. Applied techniques covered the

activation of Gd-HSA with glutaric dialdehyde followed by subsequent addition of the lectin for conjugation (method 1). Furthermore, a preparation method utilizing a modification of a previously described desolvation technique (Weber et al., 2000; Langer et al., 2003) has been investigated (method 2). The simultaneous crosslinking of Gd-HSA and LEA by glutaraldehyde was examined as well (method 3). Finally, the crosslinking of Gd-HSA and LEA with prior activation of the lectin by glutaric anhydride has been performed (method 4). The choice of employing glutaric anhydride was made to evaluate possible differences in size or size distribution in contrast to nanoparticles derived from glutaraldehyde crosslinking.

Table 13. Detailed characterization of synthesized nanoparticles by dynamic light scattering (n=3, ± 1SD).

	z-average (nm)	peak 1 (nm) ± 1SD	peak 2 (nm) ± 1SD	peak 3 (nm) ± 1SD	PDI	Count rate (kcps)	Zeta potential (mV) ± 1SD
Method 1	11.8	11.8 ± 3.82	304 ± 172.6	-	0.61	114.9	-0.69 ± 0.03
Method 2	12.2	13.5 ± 4.79	186 ± 90.10	4090 ± 53	0.59	144.4	-0.32 ± 0.19
Method 3	13.6	14.0 ± 5.02	239 ± 121.3	-	0.65	185.9	-2.39 ± 0.36
Method 4	95.9	11.6 ± 2.88	112 ± 33.6	463 ± 162.2	0.19	151.8	1.24 ± 0.4
LEA	1842.0	15.7 ± 1.50	-	-	1.00	387.8	-

The particle size distribution of nanoparticles prepared by all four methods show multiple peaks. The first peak is mostly attributable to unconverted starting material (at around 10 nm). None of the methods described did completely polymerize the provided Gd-HSA and lectin molecules. Discrimination between Gd-HSA and LEA by PCS is not detectable as both have almost the same size. The high intensities of unpolymerized material do not necessarily indicate a higher amount of not conjugated proteins in comparison to crosslinked nanoparticles. The second peak indicates the polymerized Gd-loaded nanoparticles. Method 4 produced the smallest particles (112 nm) compared to the other methods (186 to 304 nm). This might be a consequence of the applied method of synthesis. Primary activation of LEA and subsequent conjugation to Gd-HSA through a glutaric acid linker give well defined structures of nanoparticles. This is also indicated by the low PDI (0.19). In contrast, preparation method 1-3 – conjugated by glutaraldehyde linkage - form Gd-HSA-LEA conjugates having increased size and a less narrow size distribution and higher PDI, indicating the heterogeneity of the sample (see also Table 13). These differences can

possibly be explained by the distinct properties of the linkers. Glutaric acid, bearing two acid functionalities, connects two macromolecules. Whereas, it is known that glutaraldehyde forms *α,β* - unsaturated polymers in aqueous solutions which are highly reactive towards primary amines. The polymer size and structure is unknown and may be influenced by the age of the glutaraldehyde solution (Hermanson, 2008). As the glutaraldehyde polymer provides more than just two reactive functionalities per molecule, it promotes further crosslinking leading to a broader distribution of formed nanoparticles. However, method 4 also shows a distinct peak at 463 nm which can be interpreted as a temporary reversible aggregation. Peaks above 1 µm can be defined as contamination through dust.

The discrepancy between nanoparticle diameter in Table 13 and Figure 47 are based on the CONTIN algorithm which is the underlying model for calculations in the zetasizer software. Here, the averaged particle diameter takes the larger agglomerates (> 1 µm) for the cummulant fit analysis into account and hence, overestimates the actual particle size distribution. The size distribution, however, is representing the actual measured data. The z-average is the average particle diameter of the overall size distribution and is depending on the PDI.

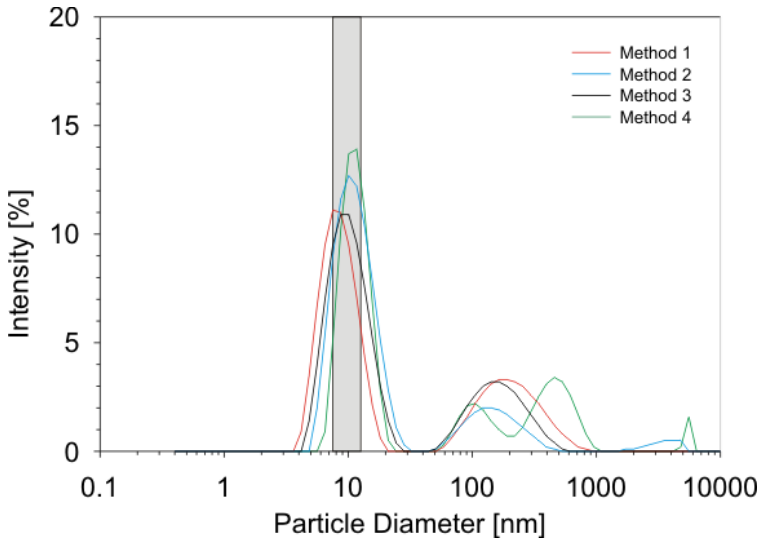

Figure 47. Particle size distribution (nm) by intensity (%) for nanoparticle synthesis method 1 to 4 as well as the range for Lectin (grey bar).

The ability of the Gd-HSA-LEA conjugates to modify the relaxation rate of water was evaluated at 37°C in PBS. Relaxation rates (R_1, R_2) and respective relaxivities (r_1, r_2) were measured at 3T and are displayed in Table 14.

Table 14. Relaxation behavior of the nanoparticles

Method	$c_{conjugate}$ (mg/ml)	$R_1(s^{-1})$	$r_1[s^{-1}*(mg/ml)^{-1}]$	$R_2(s^{-1})$	$r_2[s^{-1}*(mg/ml)^{-1}]$
Method 1	10	2.414	0.166	4.097	0.284
	5	1.669		2.989	
	2.5	1.389		2.350	
	1.25	0.826		1.389	
Method 2	10	4.108	0.354	8.130	0.686
	5	/		/	
	2.5	1.591		3.210	
	1.25	1.047		1.980	
Method 3	10	3.688	0.294	7.515	0.607
	5	3.044		6.295	
	2.5	1.699		3.431	
	1.25	1.053		2.964	
Method 4	10	4.902	0.445	11.336	1.023
	5	3.032		7.307	
	2.5	1.680		4.082	
	1.25	0.972		2.21	

As the accurate structure and molecular weight of the tomatoe lectin is still unclear (Oguri et al., 2008), the molecular weight of the prepared nanoparticles is hardly to determine. For that reason the relaxation rates and the relaxivities are given related to the amount of substance in mg. Two effects account for the differences in relaxivity. First, accessibility of the gadolinium ion for protons within the Gd-HSA-LEA conjugates prepared by diverse techniques and secondly, the variations in the tumbling rate of the nanoparticles. These properties impact the water exchange rate and hence, the relaxivity of the particles.

In conclusion, Gd-HSA-LEA nanoparticles were prepared by four different strategies. Size determination indicated a range between 112 and 304 nm depending on the preparation method. Additionally, the relaxation behavior was evaluated. In effort to develop contrast agents with the capability of targeting the vasculature, further investigations on the *in vivo* behavior like chelate stability, the degradability and the accumulation of these contrast enhancing conjugates at endothelial cells are required.

5 References

Aime, S., Botta, M., Garino, E., Crich, S. G., Giovenzana, G., Pagliarin, R., Palmisano, G., Sisti, M., 2000. Non-covalent Conjugates between Cationic Polyamino Acids and Gd (III) Chelates: A Route for Seeking Accumulation of MRI-Contrast Agents at Tumor Targeting Sites. *Chem. Eur. J.*, 6, 2609-2617.

Alric, C., Taleb, J., Le Duc, G., Mandon, C., Billotey, C., Le Meur-Herland, A., Brochard, T., Vocanson, F., Janier, M., Perriat, P., Roux, S., Tillemant, O., 2008. Gadolinium Chelate Coated Gold Nanoparticles As Contrast Agents for Both X-ray Computed Tomography and Magnetic Resonance Imaging. J. Am. Chem. Soc., 130, 5908-5915.

Barrett, T., Kobayashi, H., Brechbiel, M., Choyke, P. L., 2006. Macromolecular MRI contrast agents for imaging of tumor angiogenesis. *Eur. J. Radiol*., 60, 353-356.

Brasch, R. C., Daldrup-Link, H. E., 2003. Macromolecular contrast agents for MR mammography: current status. *Eur. Radiol.* 13, 354-365.

Briley-Saebo, K. C., Mulder, W. J. M., Mani, V., Hyafil, F., Amirbekian, V., Aguinaldo, J. G. S., Fisher, E. A., Fayad, Z. A., 2007. Magnetic Resonance Imaging of Vulnerable Atherosclerotic Plaques: Current Imaging Strategies and Molecular Imaging Probes. *J. Magn. Reson. Imaging,* 26, 460-479.

Brushett, C., Qiu, B., Atalar, E., Yang, X., 2008. High Resolution MRI of Deep Seated Atherosclerotic Arteries Using Motexafin Gadolinium. *J. Magn. Reson. Imaging*, 27, 246-250.

Caravan, P., Ellison, J. J., McMurry, T. J., Lauffer, R. B., 1999. Gadolinium (III) Chelates as MRI Contrast Agents: Structure, Dynamics, and Applications. Chem. Rev., 99, 2293-2352.

Choudhury, R. P., Fuster, V., Badimon, J. J., Fisher, E. A., Fayad, Z. A., 2002. MRI and Characterization of Atherosclerotic Plaque: Emerging Applications and Molecular Imaging. Arterioscler. Thromb. Vasc. Biol., 22, 1065-1074.

Cummins, C. H., Rutter, E. W., Fordyce, W. A., 1991. A Convenient Synthesis of Bifunctional Chelating Agents Based on Diethylenetriaminepentaacetic Acid and their Coordination Chemistry with Yttrium (III). Bioconjugate Chem. 2, 180-186.

Frias, J. C., Williams, K. J., Fisher, E. A., Fayad, Z. A., 2004. Recombinant HDL-Like Nanoparticles: A Specific Contrast Agent for MRI of Atherosclerotic Plaques. J. Am. Chem. Soc., 126, 16316-16317.

Hermann, P., Kotek, J., Kubíček, V., Lukeš, I., 2008. Gadolinium (III) complexes as MRI contrast agents: ligand design and properties of the complexes. Dalton Trans., 3027-3047.

Hermanson, G. T., 2008. Bioconjugate Techniques. 2nd Edition. Elsevier

Jaques, V., Desreux, J. F., 2002. New Classes of MRI Contrast Agents. Topics In Current Chemistry, 221, 123.164.

Kido, N., Xu, H., Regino, C. A. S., Bernardo, M., Ileva, L., Riffle, L., Wong, K. J., Brechbiel, M. W., 2009. A New Approach in the Preparation of Dendrimer-Based Bifunctional Diethylenetriaminepentaacetic Acid MR Contrast Agent Derivatives. Bioconjugate Chem., 20, 1412-1418.

Kundu, A., Peterlik, H., Krssak, M., Bytzek, A. K., Helbich, T. H., Keppler, B. K., 2009. Strategies for the covalent conjugation of a bifunctional chelating agent to albumin: synthesis and characterization of potential MRI contrast agents. (in preparation)

Langer, K., Balthasar, S., Vogel, V., Dinauer, N., von Briesen, H., Schubert, D., 2003. Optimization of the preparation process for human serum albumin (HSA) nanoparticles. Int. J. Pharm., 257, 169-180.

Langereis, S., de Lussanet, Q. G., van Genderen, M. H., Meijer, E. W., Beets-Tan, R. G., Griffioen, A. W., van Engelshoven, J. M., Backes, W. H., 2006. Evaluation of Gd (III) DTPA-terminated poly(propylene imine) dendrimers as contrast agents for MR imaging. NMR Biomed., 19, 133-141.

Mazzetti, S., Frigerio, S., Gelati, M., Salmaggi, A., Vitellaro-Zuccarello, L., 2004. Lycopersicon esculentum lectin: an effective and versatile endothelial marker of normal and tumoral blood vessels in the central nervous system. Eur. J. Histochem., 48, 423-428.

Merbach, A. E., Tóth, É., 2001. The Chemistry of Contrast Agents in Medical Magnetic Resonance Imaging. John Wiley & Sons, New York

Ogan, M. D., Schmiedl, U., Moseley, M. E., Grodd, W., Paanjanen, H., Brasch, R. C., 1987. Albumin labeled with Gd-DTPA. An intravascular contrast enhancing agent for magnetic resonance blood pool imaging: preparation and characterization. Invest. Radiol., 22, 665-671.

Oguri, S., Amano, K., Nakashita, H., Nagata, Y., Momonoki, Y. S., 2008. Molecular Structure and Properties of Lectin from Tomato Fruits. Biosci. Biotechnol. Biochem., 72, 2640-2650.

Paschkunova-Martic, I., Kremser, C., Mistlberger, K., Shcherbakova, N., Dietrich, H., Talasz, H., Zou, Y., Hugl, B., Galanski, M., Sölder E., Pfaller, K., Höliner, I., Buchberger, W., Keppler, B., Debbage, P., 2005. Design, synthesis, physical and chemical characterisation, and biological interactions of lectin-targeted latex nanoparticles bearing Gd-DTPA chelates: an exploration of magnetic resonance molecular imaging (MRMI). Histochem. Cell Biol., 123, 283-301.

Porter, G. A., Palade, G. E., Milici, A. J., 1990. Differential binding of the lectins Griffonia simplicifolia I and Lycopersicon esculentum to microvascular endothelium: organ-specific localization and partial glycoprotein characterization. Eur. J. Cell Biol., 51, 85-95.

Sieber, M.A., Pietsch, H., Walter, J., Haider, W., Frenzel, T:, Weinmann, H. J., 2008. A Preclinical Study to Investigate the Development of Nephrogenic Systemic Fibrosis: A Possible Role for Gadolinium-Based Contrast Media. Invest. Radiol., 43, 65-75.

Sirlin, C. B., Vera, D. R., Corbeil, J. A., Caballero, M. B., Buxton, R. B., Mattrey, R. F., 2004. Gadolinium-DTPA-dextran: a macromolecular MR blood pool contrast agent. Acad. Radiol., 11, 1361-1369.

Spanoghe, M., Lanens, D., Dommisse, R., Van der Linden, A., Alderweireldt, F., 1992. Proton Relaxation Enhancement By Means of Serum Albumin And Poly-L-Lysine Labeled With DTPA-Gd^{3+}: Relaxivities As A Function Of Molecular Weight And Conjugation Efficiency. MagneticResonance Imaging, 10, 913-917.

Weber, C., Kreuter, J., Langer, K., 2000. Desolvation process and surface characteristics of HSA-nanoparticles. Int. J. Pharm. 196, 197-200.

Weinmann, H. J., Ebert, W., Misselwitz, B., Schmitt-Willich, H., 2003. Tissue-specific MRI contrast agents. Eur. J. Radiol., 46, 33-44.

Xu, H., Regino, C. A. S., Bernardo, M., Koyama, Y., Kobayashi, H., Choyke, P. L., Brechbiel, M. W., 2007a. Towards Improved Syntheses of Dendrimer-Based Magnetic Resonance Imaging Contrast Agents: New Bifunctional Diethylenetriaminepentaacetic Acid Ligands and Nonaqueous Conjugation Chemistry. J. Med. Chem., 50, 3185-3193.

Xu, H., Regino, C. A. S., Koyama, Y., Hama, Y., Gunn, A. J., Bernardo, M., Kobayashi, H., Choyke, P. L., Brechbiel, M. W., 2007b. Preparation and preliminary evaluation of a biotin-targeted, lectin-targeted dendrimer-based probe for dual modality magnetic resonance and fluorescence imaging. Bioconjugate Chem., 18, 1474–1482.

Yan, G. P., Robinson, L., Hogg, P., 2007. Magnetic resonance imaging contrast agents: Overview and perspectives. Radiography, 13, 5-19.

Ye, F., Jeong, E. K., Jia, Z., Yang, T., Parker, D., Lu, Z. R., 2008. A Peptide Targeted Contrast Agent Specific to Fibrin-Fibronectin Complexes for Cancer Molecular Imaging with MRI. Bioconjugate Chem., 19, 2300-2303.

APPENDIX

List of Figures

List of Tables

Stephanie Ottofuelling, M.Sc. Marktgasse 49/15, 1090 Wien

email: s.ottofuelling@gmail.com Phone: +43 650 7811877

Curriculum Vitae

Stephanie Ottofülling, M.Sc.

Professional Experience

07.2010 to date	Technical Consultant at the Kommunalkredit Public Consulting GmbH, Vienna
01.2007 – 06.2010	Scientist at the University of Vienna, Department of Environmental Geosciences, Prof. Dr. Thilo Hofmann PhD. thesis: *Engineered Nanoparticles in the Environment* **Affiliated to international and national projects:** • *Transport of TiO_2 nanoparticles in freshwaters as a function of biofilm growth and adverse effects nano-TiO_2 on microorganisms* • *Detection, fate and uptake of engineered nanoparticles in aquatic systems* • *Development and optimization of multifunctional nanoparticles for clinical molecular imaging and therapy* **Additional experiences:** Project management, organizing international scientific conferences (2007, 2009), personal management, administration, teaching, professional presentations at scientific conferences, project acquisition, budgeting.
03. – 09.2006	Teaching Assistant at the Institute of Soil Sciences, University of Natural Resources and Applied Life Sciences (BOKU), Vienna (A): Prof. Dr. W. E. H. Blum
09.2002 – 06.2005	Research Assistant at the Institute of Geography, Ruhr-University Bochum (D), Prof. Dr. T. Mansfeldt, PD Dr. T. Rennert, Prof. Dr. M. Hassler

Education

01.2007 – 06.2010	PhD. candidate (Dr. rer. nat.), Geology
04.2004 – 09.2006	Ruhr-University Bochum (D): Master of Science (M.Sc.) in Geography.
	M.Sc.-Thesis: *Engineered Nanoparticles in the Environment - Stability*
	and Effects of Titanium Dioxide in Natural Waters
04. – 09.2006	University of Natural Resources and Applied Life Sciences (BOKU), Vienna (A): Master of Natural Resources Management and Ecological Engineering
06. – 12.2005	Auckland University (NZ): Postgraduate Diploma in Sciences in Geography
04.2002 – 03.2004	Ruhr-University Bochum (D): Bachelor of Science (B.Sc.) in Geography
10.1998 – 03.2002	University of Wuppertal (D): English Linguistics and Literature

Grants and Fellowships

09.2009	CSIRO Publishing Award at the 4th International Conference on Environmental Effects of Nanoparticles and Nanomaterials
03.2008	Stipend for young scientists at the Annual Conference of the Water Chemical Society
12.2007	Award for *"Successful Congress Organization"* for organizing the *"1st International Conference on Aquatic Nanoscience and Nanotechnology 2007"* by the Vienna Convention Bureau
06.2007	Research stipend from the University of Vienna §§63-67 StudFG (BGB1 Nr. 305/1992 idgF)
03.2007	Stipend for young scientists at the Annual Conference of the Water Chemical Society
05.2006	Stipend for participating at the workshop *„Polluted Soils and Landscape Restoration in Europe"* in Estonia, financed by the European Community

IT Proficiency

SPSS, SigmaPlot, OriginLab, Adobe Photoshop, TYPO3, Freehand, Corel Draw, ArcGIS

Stay Abroad

New Zealand 06. – 12.2005 (study)

Tanzania 02. – 09.2001 (social-economic development work)